Title
Design and Applications of Anti Albumin-Adduct Antibodies to Assess Human Exposure to Aromatic Hydrocarbons

Author
Chung, Ming Kei

Publication Date
2013

Peer reviewed|Thesis/dissertation

Design and Applications of Anti Albumin-Adduct Antibodies to Assess Human Exposure to Aromatic Hydrocarbons

By

Ming Kei Chung

A dissertation submitted in partial satisfaction of the

requirements for the degree of

Doctor of Philosophy

in

Environmental Health Sciences

in the

Graduate Division

of the

University of California, Berkeley

Committee in charge:

Professor Stephen M. Rappaport, Chair
Professor S. Katharine Hammond
Professor Alan Hubbard

Fall 2013

ABSTRACT

Design and Applications of Anti Albumin-Adduct Antibodies
to Assess Human Exposure to Aromatic Hydrocarbons

By

Ming Kei Chung

Doctor of Philosophy in Environmental Health Sciences

University of California, Berkeley

Professor Stephen M. Rappaport, Chair

Aromatic hydrocarbons are ubiquitous pollutants. Many of the hydrocarbons such as benzene and benzo[*a*]pyrene are genotoxic and are known risk factors for cancers. The genotoxicity comes from the metabolic activation of the parent compound to a reactive electrophilic form, which binds to the nucleophilic DNA and albumin to form stable adducts. Because adduct represents the biologically effective dose and albumin has relatively long half-life (~ 1 month) and is abundant in blood (~45 mg/ml), albumin adduct becomes a promising candidate to assess exposure to aromatic hydrocarbons in cancer epidemiology. This dissertation can be roughly divided into two parts. In the first part, an antibody was used to quantitatively assess benzo[*a*]pyrene exposure. A sandwich enzyme-linked immunosorbent assay (ELISA), using a commercially available antibody, was developed to measure benzo[*a*]pyrene diol epoxide - albumin adduct (BPDE-HSA). The assay is much simpler and faster to use and is 10 times more sensitive than the traditional competitive ELISA to detect BPDE-HSA. The method was further revised to be directly compatible with plasma, hence eliminated all the tedious HSA isolation and purification steps. Finally, the revised assay was validated with two different sets of archived plasma samples. In the second part, another antibody was used in an enrichment step for the albumin adductomics. To characterize albumin adducts with liquid chromatography - mass spectrometry, they have to be digested and detected as peptide adducts. Cysteine (Cys34) is a known nucleophilic hotspot on the albumin that scavenges reactive aromatic electrophiles in blood (such as benzoquinone and naphthoquinones), therefore a semi-targeting antibody was designed to capture all peptides with electrophiles bound on the Cys34 (T3 adducts). After incorporating the antibody enrichment step into the adductomic workflow, results shown that the antibody enrichment has huge potential to increase the detection rate of low abundant T3 adducts. The major significance from this study is that the innovations are applicable to the exposure to other reactive chemicals. With a suitable capture antibody, the sandwich ELISA can be used to assess other exposures such as aflatoxin (in form of aflatoxin albumin adduct), while the semi-

targeting antibody can be tailored to capture albumin peptide with a different locus of exposure significant, such as lysine.

TABLE OF CONTENTS

ACKNOWLEDGEMENTS

I want to express my deepest thanks to my advisor, Stephen Rappaport, for his inspiration, guidance and financial support during my time in Berkeley.

I am also grateful to all the helps received from Jacques Riby, He Li, Anthony Iavarone, Luca Giovanni Regazzoni and Hasmik Grigoryan. The dissertation would not finish without their technical supports and advice. In addition to my advisor Steve, I would also like to thank Katharine Hammond and Alan Hubbard to serve in my dissertation committee. They provided insightful comments to improve the quality of the dissertation.

This dissertation is done with the grant support from the U.S. National Institute for Environmental Health Sciences (NIEHS) through the trans-NIH Genes, Environment and Health Initiative (U54ES016115) and the Long-range Research Initiative of the American Chemistry Council.

Last but not least, I would like to thank my parents and my girlfriend Zoe, for their continuous support, love and immense patience. As the dissertation is complete, Zoe and I will soon get married and start our new chapter in life.

Chapter 1

Introduction

Albumin Adducts as Biomarkers to Assess Exposure

Exposure to Aromatic Hydrocarbons

Since the mid-19th century, rapid industrialization has produced a large quantity and a wide variety of chemicals. Every day people are exposed to myriad agents from the environment through ingestion, inhalation and dermal absorption. Co-exposures to trace levels of harmful substances with essential intake of oxygen, water and nutrients are unavoidable because of the ubiquitous nature of environmental pollutants and food contaminants.

One class of toxic pollutants is the set of aromatic hydrocarbons, which includes benzene and polycyclic aromatic hydrocarbons (PAHs). These latter molecules are comprised of two or more fused carbon rings ranging from naphthalene (2 rings) to coronene (7 rings) (*1*). The toxicity of these hydrocarbons is known to vary markedly. Using the toxicity equivalency factors (TEFs) which compare the carcinogenicity of PAHs to benzo[*a*]pyrene (TEF = 1), the TEFs for dibenzo[*a,e*]pyrene and coronene are 100 and 0.012 respectively, covering 4 orders of magnitude (*2*). Benzene, benzo[*a*]pyrene and several other PAHs are mutagenic and carcinogenic as classified by the International Agency for Research on Cancer (*3*, *4*). Exposures to hydrocarbon mixtures are risk factors for blood, lung and skin cancers in humans (*5*–*7*).

Depending upon their particular sources, these hydrocarbons can be broadly classified as phytogenic, petrogenic and pyrogenic (*8*–*10*). Phytogenic hydrocarbons are derived from plant materials, such as from peat, pine, and lignin; petrogenic hydrocarbons mainly come from petroleum products, such as engine oils, jet fuel and kerosene; and pyrogenic hydrocarbons arise from incomplete combustion, such as fire, burning of fuels, tobacco smoking and cooking. In the United States, more than half of hydrocarbon emissions to the environment is from firewood burning, followed by vehicle and wildfire emissions (*11*). It is estimated that the general population is exposed to hydrocarbons mainly through active/passive inhalation of tobacco smoke and wood smoke, contaminated air and consumption of grilled foods (*12*). In addition, exposures to hydrocarbons from drinking water and through skin contact with soot and tars is also possible (*12*).

Assessing Exposures

Because it is impossible to completely avoid exposures to pollutants, health researchers usually monitor pollutants in various media and advise policy makers to direct limited resources towards measurements representing a certain level of concern (i.e. greater than an acceptable level or standard). There are 2 major approaches for assessing exposures, namely indirect and direct methods (*13*, *14*). The indirect approach estimates human exposures from various proxies, such as using questionnaires and environmental modeling. In the direct approach, personal monitoring (e.g., measurement of individuals' breathing-zone air) and biomarker

measurement are typically involved. In terms of accuracy and precision, the direct approach (particularly involving biomarkers) is generally better, because individual-level measurements account for temporal and spatial variability in pollutant levels and biological measurements account for differences in physiological activity and physiology. Nonetheless, indirect methods are more often used, mainly because of cost considerations.

Since the aim of exposure assessment is to obtain relevant information in the most efficient way (*15*), defining the aim of the assessment and knowing the exposure pathways in advance of measurements are important factors. For example, to access tobacco smoke exposure in a group of smokers, use of a self-administered questionnaire recording the average number of cigarettes smoked per day would be appropriate (*16*). This is because the individuals are aware of their smoking habits and the exposure pathway (inhalation) is known. However, when assessing air pollutants exposures across the general population, direct measurement of breathing-zone air with personal monitors would be more appropriate (*17*) because individuals cannot provide information about the magnitude or even the sources of such exposures (e.g. indoor vs. outdoor sources).

The Use of Biomarkers

In cases where exposure pathways, durations and frequencies are uncertain, measuring biomarkers will be the most appropriate option. An exposure biomarker is an indicator found within an organism that integrates the total exposure from different routes over a period of time (*18*). Biomarkers are also able to reflect different kinds of dose information (Figure 1). For example, a drug biomarker measured in tissues tells how well a drug has been absorbed and distributed throughout the body, thus providing important information for ensuring drug efficacy. Apart from being an objective measurement for personal exposure, biomarkers can damp the day-to-day variation of exposure thereby permitting more precise measurements of long-term exposure (Figure 2).

Exposure biomarkers are not limited to the parent chemicals but also their metabolites and target responses. Upon exposure, chemicals are absorbed, distributed, metabolized, and then excreted from the body. Metabolism of xenobiotic chemicals involves multiple enzymes and pathways that are generally classified in two phases (*19*). Phase I metabolism generally increases reactivity of the parent compound by hydrolysis, reduction and/or oxidation, with cytochrome P450 oxidases often involved. Phase II metabolism increases the water solubility of metabolites to facilitate excretion, often by conjugation with polar molecules such as glutathione, sulfate or glucose. Because the levels of intermediates and the excreted metabolites are correlated with exposure to the parent compound, quantitative exposure biomarkers include the parent compounds as well as the resulting metabolites. For example, urinary PAHs and their metabolites have been used as biomarkers to assess PAH exposures in asphalt-paving workers (*20*, *21*). Table 1 shows a summary of some common exposure biomarkers.

Reactive Chemicals and Adduct Biomarkers

Many hydrocarbons are procarcinogens, meaning that they are metabolized to carcinogenic intermediates (*19*). These hydrocarbons are hazardous because, although the parent compounds are relatively stable and persistent in the environment they are

biotransformed to reactive electrophiles, which covalently bind to functional biological nucleophiles such as proteins and DNA (*22*). The formation of DNA adducts in critical genes could initiate the first step of carcinogenesis (*23*) and thus detection of adducts could be used as a marker for cancer risks (*24*).

Aromatic hydrocarbons such as naphthalene can be metabolized to quinones, e.g., naphthoquinones, which bind to Cys amino acid in human serum albumin (HSA) to form adducts (Figures 3 and 4)(*25*). Similar metabolism and reactions occur for other PAHs such as phenanthrene, pyrene and benzo[*a*]pyrene (*26*–*28*). In addition to the formation of quinones, mammalian metabolism of benzo[*a*]pyrene forms diol epoxides [(+)-anti-benzo[*a*]pyrene-7,8-diol-9,10-epoxide (BPDE-I)] that form BPDE-HSA with modification made on His and Asp instead of Cys amino acids (Figures 5 and 6)(*29*). These findings suggest that particular macromolecular adducts could be used to assess exposure to the hydrocarbons.

Reactive electrophiles are difficult to measure because of their short lifespan. Since adducts are much more stable than these electrophiles, molecular cancer epidemiologists regard these adducts as surrogates of the biologically effective exposures (or doses) (*30*–*34*). For example, a summaries of adduct biomarkers that have been used to characterize smoking are shown in Tables 2 and 3.

Albumin Adducts as Exposure Biomarkers

Although electrophiles bind to all available nucleophilic sites in biofluids and tissues (*35*–*39*), detection of an exposure-related adduct in blood indicates that the parent compound has been absorbed, bioactivated and distributed through the systemic circulation. Stable metabolites of toxic substances are also transported by the circulation and hence should be detectable with blood-based biomarkers. Finally, blood is collected with minimally invasive methods and is often obtained for diagnostic tests. For these reasons, blood is one of the most commonly collected types of biospecimens (Table 4)(*40*).

Researchers typically use DNA adducts (isolated from white blood cells, WBCs) or adducts of the blood proteins, HSA and hemoglobin. HSA has a number of properties that make HSA adducts more desirable than DNA adducts for assessing exposures to electrophiles (*41*–*44*). First, whereas peripheral WBCs have to be isolated from whole blood during initial processing in order to extract DNA, HSA is readily available in plasma, serum or whole blood. Second, HSA is much more abundant (~45 mg/ml) than DNA in blood. Third, whereas the turnover rate for HSA is known (*45*), it is difficult to estimate for DNA because WBCs contain many different cell types, each with a different half-life. Fourth, HSA adducts are more stable because they are not repaired (*46*). Fifth, HSA possesses numerous nucleophilic amino acids with a range of nucleophilicity in the order of Cys > Lys > His > Met > Tyr (*47*). And finally, the half-life of HSA (~1 month) allows practical application of HSA adducts in exposure assessment over intermediate time scales (*29*). Although HSA adduct has numerous advantages as a biomarker to assess chronic exposure, it may unable to reveal short-term but high-level exposures due to its damping characteristics and the time lag in metabolic activation. Such exposures can be better assessed through measuring the stable urinary metabolites.

Antibody 101

Because this dissertation described the use and design of antibodies to assess exposure to aromatic hydrocarbons, a section dedicate to the introduction of antibody is provided. Readers who are knowledgeable about antibody may skip the entire section.

Immunoglobulins

Immunoglobulins (Igs) are functional proteins produced by the immune system that comprise the class of antibodies (*48*). A particular Ig has the ability to recognize and bind to a specific antigen. There are 5 different classes of human antibodies, namely IgG, IgA, IgM, IgD and IgE, which are found in different parts of the body (*49*). They share a basic Y-shaped structure but can have different conformations, such a monomer or dimer (Figure 7). Each Ig has unique properties. IgG is found in most parts of the body and is the only Ig capable of crossing into the placenta. It is also the major antibody expressed in the secondary immune response and has the most active role to engage (opsonize) bacteria. Furthermore, IgG is the only human antibody with 4 more subclasses (Table 5); IgA is present in secretions such as tears and saliva, and hence mainly targets microorganisms attached to mucous membranes; IgM is the largest of the antibodies and is the first to respond to an initial antigen exposure. Because of its size, it is mainly found in blood; IgD is usually found on the cell surface of B cells and plays a role in removing those B cells that generate self-reactive auto-antibodies; similar to IgD, IgE is mostly located on cell surfaces (basophils and mast cells) and responds to parasitic infections and allergens. Further comparisons among Ig classes can be found in Table 6.

Structure of IgG

The broad appearance and high plasma concentration of IgG make it a special target deserving more attention. The basic structure of an IgG is comprised of 2 long chains and 2 short chains, which are connected by disulfide bridges (Figure 8)(*48*). Fragmentation nomenclature of IgG is shown in Figure 9 (*50*). These fragments do not exist in nature and are created by digesting IgG with enzymes such as pepsin. In an application such as drug design, fragmentation provides advantages over use of whole IgG in various situations. For example, removing the Fc region could reduce non-specific interaction with cells as many of them have Fc receptors; keeping only the active binding region(s) allows more efficient tissue penetration; also, the affinity of the antibody-antigen binding could be increased through reduction of steric hindrance.

Generation of IgG

The humoral adaptive immune system is responsible for the production of the highly selective IgGs (*48*). In brief, exogenous antigens enter the body through inhalation, ingestion or skin contact and are bound to B lymphocytes via the B-cell receptor (BCR), which is basically an Ig. The antibody complex is engulfed through endocytosis and digested. The epitopes (an epitope is a unique molecular structure on an antigen that is recognized by an antibody) are displayed with the class II major histocompatibility complex (MHC) on the cell surface. The T-helper cell interacts with the display and stimulates proliferation and differentiation of B cells into antibody-secreting plasma cells. Although a single plasma cell can produce a large amount of IgG, only one class recognizing a single epitope can be secreted. Large antigens (from 1000-

3000 Da onwards) usually possess more than 1 epitope and hence invoke production of numerous clones of plasma cells.

Specificity and Diversity of IgG

The heads of the "Ys" of Igs represent the antibody binding regions that recognize the epitopes of particular antigens (*48*). Such an antibody binding region is made up of a heavy chain variable domain (V_H) and a light chain variable domain (V_L). The parts of the chains that come into contact with the epitope are called the complementarity determining regions (CDRs) and are made up of variable loops of β-strands, 3 each on V_H and V_L. The ability to recognize a diverse collection of unknown epitopes is achieved by varying the amino acid composition in the CDRs through different mechanisms, such as gene rearrangements and point mutations. During this process, hazardous clones generating auto-antibodies are removed.

Utilizing IgG

With knowledge of antibody biology and mechanisms of secretion, it is possible to make use of the immune system to produce useful IgGs that can be used for molecular identification, measurement, purification, enrichment, and drug development. The typical workflow to produce a custom antibody for identification and measurement is outlined in Figure 10. It starts with defining the antigen of interest and thereby developing a particular immunogen suitable for administration to an animal host. The immunization step usually involves administration of the immunogen to small mammals, such as rabbits and mice. Depending on the severity of the immune response, the immunization process could take up to 20 weeks to complete. Blood antibodies are then isolated and purified. Optional steps such as conjugation to biotin or enzymes and fragmentation may be included. Finally, the activity of the antibody towards the antigen of interest is characterized and the antibody is ready for application.

Polyclonal and Monoclonal IgG

As explained above, an antigen could have more than 1 epitope. Applications such as protein enrichment and identification require different levels of antibody specificity, and thus there are 2 typical antibody production approaches: polyclonal and monoclonal. The goal of the former approach is to produce antibody binding to a specific antigen whereas the latter demands further isolation of a single antibody clone that binds only to a specific epitope. The polyclonal antibody production workflow is much like what is described in Figure 11. An immunogen is designed and prepared, animals are immunized, and the antibody is purified and characterized. It takes longer to develop a monoclonal antibody (up to 30 weeks) and hybridoma technology is used to aid the screening of antibody-secreting clones (Figure 12). In brief, after immunization, B cells are isolated from the host's spleen and fused with myeloma B cell to form hybridomas, which are immortalized antibody secreting cells. Different clones of hybridomas are then screened using the plate dilution method and the correct clone is identified. The production of monoclonal antibody could be scaled up by the ascites method which involves direct injection of the hybridoma into the host's peritoneal cavity. The scale-up step could also be done *in vitro* using tissue culture systems. Although production costs of a monoclonal antibody can be ~5 times more than the polyclonal antibody ($3800 vs $800) , once a hybridoma is established, it is possible to obtain a low cost (~$70/mouse), stable and

consistent source of monoclonal antibody, which is an essential property required in drug development and quantitative measurement in antibody-based assays.

Current Methodologies for Measuring Albumin Adducts

Overview

Many analytical methods have been reported to measure HSA adducts in human samples. These include enzyme-linked immunosorbent assays (ELISA), high performance liquid chromatography (HPLC) with fluorescence detection, gas chromatography-mass spectrometry (GC-MS) and liquid chromatography-mass spectrometry (LC-MS) (Table 7). ELISA is a low-cost-antibody assay that has the lowest sensitivity among the methods. For example, the detection limits of the BPDE-HSA adduct in competitive ELISA, HPLC and GC-MS are: 10, 0.04, and 0.01 fmol/mg protein respectively (*29*). GC-MS and LC-MS are powerful 2-dimensional instrumental methods that fractionate samples and measure the analytes differentiated by their molecular masses. Though powerful, highly trained personnel are required to operate the instruments and interpret the mass spectra. Measuring protein adducts with GC-MS is especially complicated because derivatization is needed to increase the volatility and ionization efficiency. In contrast, HPLC is a simpler instrumental method having characteristics between the ELISA and LC-MS. Epidemiologists who may be only interested in a few known HSA adducts usually prefer to use ELISA (*29*), while those working on partially characterized HSA adducts or as part of discovery-based studies prefer to use LC-MS (*51–54*).

Competitive ELISA for BPDE-Albumin Adducts

There are 3 common ELISA formats, namely direct, indirect and sandwich (Figure 13). Using an indirect format to measure adducts requires competitive binding between the adduct in a sample and a known amount of a specific antigen that is added to the sample; hence it is called a competitive ELISA. The typical workflow to measure BPDE-HSA adducts with competitive ELISA is shown in Figure 14. In this assay, the monoclonal capture antibody, 8E11, recognizes both BPDE-HSA and benzo[*a*]pyrene tetrahydrotetraols (short for "tetrols". Figure 6), but it has much higher affinity to the latter (*55*). Because tetrols can be detected with greater sensitivity, BPDE-HSA adducts are generally treated with reagents that convert them to tetrols that are then detected. A number of steps are required to obtain tetrols from plasma samples. First, HSA is isolated from 2-5 ml of plasma by salt precipitation, which recovers about half of the total HSA. Then tetrols are hydrolyzed [tetrols I-1, I-2, II-1, and II-2 (*56*)] from the BPDE-HSA by strong acid. Following another purification step, tetrols are ready for the competitive ELISA. Despite the inherent drawbacks of performing such an assay, it has been the only ELISA format used for measuring BPDE-HSA adducts for more than 20 years (*57–59*).

LC-MS for Albumin Adducts of Hydrocarbons

Mass spectrometry became a popular platform for measuring the proteome and protein adducts in the late 90s, mainly because of the commercialization of electrospray ionization (ESI), which allows structured ionization of peptides. Aromatic hydrocarbon-HSA adducts can be measured by LC-MS. Most such applications have focused upon adducts bound to the only available sulfhydryl group in HSA, namely, Cys34, because it is the strongest and most abundant

electrophile in serum (*60*, *61*). These applications will be illustrated with assays of hydrocarbon-quinone-HSA adducts of benzene and 2-ring and 3-ring PAHs (see section "Reactive Chemicals and Adducts"). Similar to the situation in competitive ELISA, there are some sample-preparation steps required before measurement of hydrocarbon-HSA adducts with LC-MS. These include isolating HSA from plasma, removing mercaptoalbumin (HSA with intact Cys34) and digestion with trypsin. Since the T3 peptide (ie. third largest tryptic peptide) (seq: ALVLIAFAQYLQQCPFEDHVK) in the HSA digest is the one possessing Cys34 adducts, LC-MS measurement of quinone adducts of benzene, naphthalene and other small PAHs is usually targeting the T3 adducts (*54*).

It is challenging to detect specific T3 adducts because of a number of factors. First plasma is a complex matrix and it is difficult to isolate HSA at high purity. Second, the nucleophilic Cys34 is a target of multiple reactive species in the serum. Third, the unmodified T3 peptide is always greatly in excess compared to those of T3 adducts. And finally, co-elution of other abundant peptides suppresses the ionization efficiency of T3 adducts (i.e. charge competition, MS measures the mass-to-charge ratio rather than the mass of analytes). To handle these complex factors, methods for measuring Cys34 adducts rely a series of crude and analytical fractionation steps. For example, after isolation of HSA from serum or plasma, and digestion with trypsin, reverse-phase LC can be used to separate peptides and purify T3 adducts in the digest. This technique uses an inert and non-polar stationary phase to retain and separate compounds mainly by differences in polarity. The stationary bed is typically pre-packed in a column and can cause problems such as sample-to-sample carryover and crack formation, which subsequently contribute to contamination and lower separation efficiency. Furthermore, co-elution of peptides is still observable in the chromatogram even with an elution profile that runs for 90 min per sample. This coelution of peptides increases the complexity of mass spectra and makes it difficult to detect minor adducts.

Theme for the Research and Chapter Objectives

As described above, current methodologies for measuring HSA adducts have numerous limitations that either discourage the use of HSA adducts as exposure biomarkers or limit the discovery of low abundant HSA-Cys34 adducts. Thus, the purpose of this study is to improve the popular ELISA and LC-MS based methods for detecting HSA adducts of reactive electrophiles. First, a sandwich ELISA is developed to replace the competitive ELISA which has been used for more than two decades to detect BPDE-HSA adducts. The new design is more sensitive and can measure intact the BPDE-HSA adduct directly in human plasma, eliminating all the tedious sample preparation steps. Second, a customized semi-targeting capture antibody for T3 adducts is produced and used in a magnetic enrichment step to prepare samples for LC-MS measurement. The high specificity of the anti-T3-adduct antibody is expected to concentrate only the T3 adducts in the HSA digest, thereby increasing the sensitivity of the MS for detecting adducts.

These new methods for detection of HSA adducts are described in three chapters as illustrated in Figure 15. The aims of the three chapters are summarized as follows:

Chapter 2: Development of a sandwich ELISA for measuring intact BPDE-HSA adducts.

A. Investigate the sensitivity of a sandwich design and determine the extent of improvement.
B. Explore the options to increase sensitivity of the sandwich ELISA. Characterize the performance of the final design.
C. Validate the prototype with archived samples (purified HSA) collected from populations with relatively high levels of PAH exposures.

Chapter 3: Development of a sandwich ELISA for measuring intact BPDE-HSA adducts directly in human plasma.

A. Test the prototype ELISA from chapter 2 with human plasma samples and identify areas that need improvement.
B. Revise the prototype ELISA and characterize the final assay format.
C. Validate the final sandwich format with two batches of archived plasma samples from prior studies of low-level PAH exposures.

Chapter 4: Development of a semi-targeting immunomagnetic enrichment method for measuring the HSA-Cys34 adductome by mass spectrometry.

A. Design an immunogen that can produce a polyclonal, high affinity. semi-targeting anti-T3-adduct antibody.
B. Characterize the compatibility of four types of magnetic bead and select the most promising bead for use in immunomagnetic enrichment (IME).
C. Test the performance of IME for enriching Cys34 adducts with plasma samples collected from volunteer subjects.

References

1. Albers, P. H. (1995) Petroleum and individual polycyclic aromatic hydrocarbons. In *Handbook of ecotoxicology*, pp 330–355, Lewis Publishers, Boca Raton, Fla.
2. Knafla, A., Phillipps, K. A., Brecher, R. W., Petrovic, S., and Richardson, M. (2006) Development of a dermal cancer slope factor for benzo[a]pyrene, *Regul. Toxicol. Pharmacol. 45*, 159–168.
3. Fitzgerald, D. J. (1999) An international literature survey of "IARC Group 1 carcinogens, *Food Chem. Toxicol. Int. J. Publ. Br. Ind. Biol. Res. Assoc. 37*, 265–266.
4. Luch, A. (2005) The Carcinogenic Effects of Polycyclic Aromatic Hydrocarbons, Imperial College Press.
5. Boffetta, P., Jourenkova, N., and Gustavsson, P. (1997) Cancer risk from occupational and environmental exposure to polycyclic aromatic hydrocarbons, *Cancer Causes Control Ccc 8*, 444–472.
6. Bosetti, C., Boffetta, P., and La Vecchia, C. (2007) Occupational exposures to polycyclic aromatic hydrocarbons, and respiratory and urinary tract cancers: a quantitative review to 2005, *Ann. Oncol. Off. J. Eur. Soc. Med. Oncol. Esmo 18*, 431–446.
7. Estey, E., and Döhner, H. (2006) Acute myeloid leukaemia, *The Lancet 368*, 1894–1907.
8. Page, D. S., Boehm, P. D., Douglas, G. S., Bence, A. E., Burns, W. A., and Mankiewicz, P. J. (1999) Pyrogenic Polycyclic Aromatic Hydrocarbons in Sediments Record Past Human Activity: A Case Study in Prince William Sound, Alaska, *Mar. Pollut. Bull. 38*, 247–260.
9. Eisler, R. (1987) Polycyclic aromatic hydrocarbon hazards to fish, wildlife, and invertebrates: A synoptic review, Fish and Wildlife Service, U.S. Dept. of the Interior.
10. McElroy, A. E., Farrington, J. W., and Teal, J. M. (1989) Bioavailability of PAH in the aquatic environment. In *Metabolism of polycyclic aromatic hydrocarbons in the aquatic environment*, pp 1–10, CRC Press, Boca Raton, Florida.
11. Shen, H., Huang, Y., Wang, R., Zhu, D., Li, W., Shen, G., Wang, B., Zhang, Y., Chen, Y., Lu, Y., Chen, H., Li, T., Sun, K., Li, B., Liu, W., Liu, J., and Tao, S. (2013) Global atmospheric emissions of polycyclic aromatic hydrocarbons from 1960 to 2008 and future predictions, *Environ. Sci. Technol.*
12. ATSDR - Toxicological Profile: Polycyclic Aromatic Hydrocarbons (PAHs).
13. Nieuwenhuijsen, M., Paustenbach, D., and Duarte-Davidson, R. (2006) New developments in exposure assessment: the impact on the practice of health risk assessment and epidemiological studies, *Environ. Int. 32*, 996–1009.
14. Nieuwenhuijsen, M. J. (Ed.). (2003) Exposure Assessment in Occupational and Environmental Epidemiology 1st ed., Oxford University Press, USA.
15. Armstrong, B. G. (1996) Optimizing power in allocating resources to exposure assessment in an epidemiologic study, *Am. J. Epidemiol. 144*, 192–197.
16. Etzel, R. A. (1997) Environmental tobacco smoke I: childhood diseases. In *Topics in environmental epidemiology*, pp 200–226, Oxford University Press, New York, USA.
17. Strak, M., Boogaard, H., Meliefste, K., Oldenwening, M., Zuurbier, M., Brunekreef, B., and Hoek, G. (2010) Respiratory health effects of ultrafine and fine particle exposure in cyclists, *Occup. Environ. Med. 67*, 118–124.
18. Fowler, B. A. (2012) Biomarkers in toxicology and risk assessment, *EXS 101*, 459–470.

19. Klaassen, C. (2007) Casarett & Doull's Toxicology: The Basic Science of Poisons, Seventh Edition 7th ed., McGraw-Hill Professional.
20. Sobus, J. R., McClean, M. D., Herrick, R. F., Waidyanatha, S., Onyemauwa, F., Kupper, L. L., and Rappaport, S. M. (2009) Investigation of PAH biomarkers in the urine of workers exposed to hot asphalt, *Ann. Occup. Hyg. 53*, 551–560.
21. McClean, M. D., Rinehart, R. D., Ngo, L., Eisen, E. A., Kelsey, K. T., Wiencke, J. K., and Herrick, R. F. (2004) Urinary 1-hydroxypyrene and polycyclic aromatic hydrocarbon exposure among asphalt paving workers, *Ann. Occup. Hyg. 48*, 565–578.
22. Vineis, P., and Perera, F. (2007) Molecular epidemiology and biomarkers in etiologic cancer research: the new in light of the old, *Cancer Epidemiol. Biomarkers Prev. Publ. Am. Assoc. Cancer Res. Cosponsored Am. Soc. Prev. Oncol. 16*, 1954–1965.
23. Baird, W. M., Hooven, L. A., and Mahadevan, B. (2005) Carcinogenic polycyclic aromatic hydrocarbon-DNA adducts and mechanism of action, *Environ. Mol. Mutagen. 45*, 106–114.
24. Peluso, M., Munnia, A., Hoek, G., Krzyzanowski, M., Veglia, F., Airoldi, L., Autrup, H., Dunning, A., Garte, S., Hainaut, P., Malaveille, C., Gormally, E., Matullo, G., Overvad, K., Raaschou-Nielsen, O., Clavel-Chapelon, F., Linseisen, J., Boeing, H., Trichopoulou, A., Trichopoulos, D., Kaladidi, A., Palli, D., Krogh, V., Tumino, R., Panico, S., Bueno-De-Mesquita, H. B., Peeters, P. H., Kumle, M., Gonzalez, C. A., Martinez, C., Dorronsoro, M., Barricarte, A., Navarro, C., Quiros, J. R., Berglund, G., Janzon, L., Jarvholm, B., Day, N. E., Key, T. J., Saracci, R., Kaaks, R., Riboli, E., and Vineis, P. (2005) DNA adducts and lung cancer risk: a prospective study, *Cancer Res. 65*, 8042–8048.
25. Waidyanatha, S., Zheng, Y., Serdar, B., and Rappaport, S. M. (2004) Albumin Adducts of Naphthalene Metabolites as Biomarkers of Exposure to Polycyclic Aromatic Hydrocarbons, *Cancer Epidemiol. Biomarkers Prev. 13*, 117–124.
26. Snyder, R., and Hedli, C. C. (1996) An overview of benzene metabolism, *Environ. Health Perspect. 104 Suppl 6*, 1165–1171.
27. Nordqvist, M., Thakker, D. R., Vyas, K. P., Yagi, H., Levin, W., Ryan, D. E., Thomas, P. E., Conney, A. H., and Jerina, D. M. (1981) Metabolism of chrysene and phenanthrene to bay-region diol epoxides by rat liver enzymes, *Mol. Pharmacol. 19*, 168–178.
28. Pathway Analysis, Systems Biology.
29. Käfferlein, H. U., Marczynski, B., Mensing, T., and Brüning, T. (2010) Albumin and hemoglobin adducts of benzo[a]pyrene in humans--analytical methods, exposure assessment, and recommendations for future directions, *Crit. Rev. Toxicol. 40*, 126–150.
30. Poirier, M. C. (2012) Chemical-induced DNA damage and human cancer risk, *Discov. Med. 14*, 283–288.
31. Leong, Y.-H., Rosma, A., Latiff, A. A., and Izzah, A. N. (2012) Associations of serum aflatoxin B1-lysine adduct level with socio-demographic factors and aflatoxins intake from nuts and related nut products in Malaysia, *Int. J. Hyg. Environ. Health 215*, 368–372.
32. Obuseh, F. A., Jolly, P. E., Jiang, Y., Shuaib, F. M. B., Waterbor, J., Ellis, W. O., Piyathilake, C. J., Desmond, R. A., Afriyie-Gyawu, E., and Phillips, T. D. (2010) Aflatoxin B1 albumin adducts in plasma and aflatoxin M1 in urine are associated with plasma concentrations of vitamins A and E, *Int. J. Vitam. Nutr. Res. Int. Z. Für Vitam.- Ernährungsforschung J. Int. Vitaminol. Nutr. 80*, 355–368.

33. Pan, J., Keffer, J., Emami, A., Ma, X., Lan, R., Goldman, R., and Chung, F.-L. (2009) Acrolein-derived DNA adduct formation in human colon cancer cells: its role in apoptosis induction by docosahexaenoic acid, *Chem. Res. Toxicol. 22*, 798–806.
34. Liu, M., Chen, L., Zhou, R., and Wang, J. (2013) Association between GSTM1 polymorphism and DNA adduct concentration in the occupational workers exposed to PAHs: a meta-analysis, *Gene 519*, 71–76.
35. Mahadevan, B., Luch, A., Bravo, C. F., Atkin, J., Steppan, L. B., Pereira, C., Kerkvliet, N. I., and Baird, W. M. (2005) Dibenzo[a,l]pyrene induced DNA adduct formation in lung tissue in vivo, *Cancer Lett. 227*, 25–32.
36. Mikeš, P., Sístek, V., Krouželka, J., Králík, A., Frantík, E., Mráz, J., and Linhart, I. (2013) 3-(3,4-Dihydroxyphenyl)adenine, a urinary DNA adduct formed in mice exposed to high concentrations of benzene, *J. Appl. Toxicol. Jat 33*, 516–520.
37. Pruthi, S., Yang, L., Sandhu, N. P., Ingle, J. N., Beseler, C. L., Suman, V. J., Cavalieri, E. L., and Rogan, E. G. (2012) Evaluation of serum estrogen-DNA adducts as potential biomarkers for breast cancer risk, *J. Steroid Biochem. Mol. Biol. 132*, 73–79.
38. Bryant, M. S., Vineis, P., Skipper, P. L., and Tannenbaum, S. R. (1988) Hemoglobin adducts of aromatic amines: associations with smoking status and type of tobacco, *Proc. Natl. Acad. Sci. U. S. A. 85*, 9788–9791.
39. Kang-Sickel, J.-C. C., Butler, M. A., Frame, L., Serdar, B., Chao, Y.-C. E., Egeghy, P., Rappaport, S. M., Toennis, C. A., Li, W., Borisova, T., French, J. E., and Nylander-French, L. A. (2011) The utility of naphthyl-keratin adducts as biomarkers for jet-fuel exposure, *Biomarkers Biochem. Indic. Expo. Response Susceptibility Chem. 16*, 590–599.
40. Paustenbach, D., and Galbraith, D. (2006) Biomonitoring and Biomarkers: Exposure Assessment Will Never Be the Same, *Environ. Health Perspect. 114*, 1143–1149.
41. Day, B. W., Skipper, P. L., Zaia, J., and Tannenbaum, S. R. (1991) Benzo[a]pyrene anti-diol epoxide covalently modifies human serum albumin carboxylate side chains and imidazole side chain of histidine(146), *J Am Chem Soc 113*, 8505–8509.
42. Day, B. W., Doxtader, M. M., Rich, R. H., Skipper, P. L., Singh, K., Dasari, R. R., and Tannenbaum, S. R. (1992) Human serum albumin-benzo[a]pyrene anti-diol epoxide adduct structure elucidation by fluorescence line narrowing spectroscopy, *Chem Res Toxicol 5*, 71–76.
43. Lee, B. M., Yin, B. Y., Herbert, R., Hemminki, K., Perera, F. P., and Santella, R. M. (1991) Immunologic measurement of polycyclic aromatic hydrocarbon-albumin adducts in foundry workers and roofers, *Scand J Work Env. Heal. 17*, 190–4.
44. Sherson, D., Sabro, P., Sigsgaard, T., Johansen, F., and Autrup, H. (1990) Biological monitoring of foundry workers exposed to polycyclic aromatic hydrocarbons, *Br J Ind Med 47*, 448–53.
45. Törnqvist, M., Fred, C., Haglund, J., Helleberg, H., Paulsson, B., and Rydberg, P. (2002) Protein adducts: quantitative and qualitative aspects of their formation, analysis and applications, *J. Chromatogr. B Analyt. Technol. Biomed. Life. Sci. 778*, 279–308.
46. Lin, Y. S., Kupper, L. L., and Rappaport, S. M. (2005) Air samples versus biomarkers for epidemiology, *Occup. Environ. Med. 62*, 750–760.

47. Liebler, D. C. (2002) Proteomic approaches to characterize protein modifications: new tools to study the effects of environmental exposures, *Environ. Health Perspect. 110 Suppl 1*, 3–9.
48. Murphy, K. (2011) Janeway's Immunobiology: The Immune System 8th ed., Garland Science.
49. Manz, R. A., Hauser, A. E., Hiepe, F., and Radbruch, A. (2005) Maintenance of serum antibody levels, *Annu. Rev. Immunol. 23*, 367–386.
50. Andrew, S. M., and Titus, J. A. (2001) Fragmentation of Immunoglobulin G. In *Current Protocols in Cell Biology*, John Wiley & Sons, Inc.
51. Chou, C.-H., Chuang, L.-Y., Tseng, W.-L., and Lu, C.-Y. (2012) Characterization of protein adducts formed by toxic alkaloids by nano-scale liquid chromatography with mass spectrometry, *J. Mass Spectrom. Jms 47*, 1303–1312.
52. Regazzoni, L., Del Vecchio, L., Altomare, A., Yeum, K.-J., Cusi, D., Locatelli, F., Carini, M., and Aldini, G. (2013) Human serum albumin cysteinylation is increased in end stage renal disease patients and reduced by hemodialysis: mass spectrometry studies, *Free Radic. Res. 47*, 172–180.
53. Grigoryan, H., Li, H., Iavarone, A. T., Williams, E. R., and Rappaport, S. M. (2012) Cys34 adducts of reactive oxygen species in human serum albumin, *Chem. Res. Toxicol. 25*, 1633–1642.
54. Li, H., Grigoryan, H., Funk, W. E., Lu, S. S., Rose, S., Williams, E. R., and Rappaport, S. M. (2011) Profiling Cys34 adducts of human serum albumin by fixed-step selected reaction monitoring, *Mol. Cell. Proteomics Mcp 10*, M110.004606.
55. Santella, R. M., Lin, C. D., and Dharmaraja, N. (1986) Monoclonal antibodies to a benzo[a]pyrene diolepoxide modified protein, *Carcinogenesis 7*, 441–444.
56. INCHEM. (1998) Polycyclic aromatic hydrocarbons, selected non-heterocyclic. http://www.inchem.org/documents/ehc/ehc/ehc202.htm.
57. Lee, B. M., and Santella, R. M. (1988) Quantitation of protein adducts as a marker of genotoxic exposure: immunologic detection of benzo[a]pyrene--globin adducts in mice, *Carcinogenesis 9*, 1773–1777.
58. Lee, B. M., Yin, B. Y., Herbert, R., Hemminki, K., Perera, F. P., and Santella, R. M. (1991) Immunologic measurement of polycyclic aromatic hydrocarbon-albumin adducts in foundry workers and roofers, *Scand. J. Work. Environ. Health 17*, 190–194.
59. Wu, H. C., Wang, Q., Wang, L. W., Yang, H. I., Ahsan, H., Tsai, W. Y., Wang, L. Y., Chen, S. Y., Chen, C. J., and Santella, R. M. (2007) Polycyclic aromatic hydrocarbon- and aflatoxin-albumin adducts, hepatitis B virus infection and hepatocellular carcinoma in Taiwan, *Cancer Lett. 252*, 104–114.
60. Aldini, G., Regazzoni, L., Orioli, M., Rimoldi, I., Facino, R. M., and Carini, M. (2008) A tandem MS precursor-ion scan approach to identify variable covalent modification of albumin Cys34: a new tool for studying vascular carbonylation, *J. Mass Spectrom. Jms 43*, 1470–1481.
61. Aldini, G., Vistoli, G., Regazzoni, L., Gamberoni, L., Facino, R. M., Yamaguchi, S., Uchida, K., and Carini, M. (2008) Albumin is the main nucleophilic target of human plasma: a protective role against pro-atherogenic electrophilic reactive carbonyl species?, *Chem. Res. Toxicol. 21*, 824–835.

62. Wild, C. P. (2009) Environmental exposure measurement in cancer epidemiology, *Mutagenesis 24*, 117–125.
63. Phillips, D. H., and Venitt, S. (2012) DNA and protein adducts in human tissues resulting from exposure to tobacco smoke, *Int. J. Cancer 131*, 2733–2753.
64. Wild, C., Vineis, P., and Garte, S. (2008) Molecular Epidemiology of Chronic Diseases 1st ed., Wiley.
65. Malik, V. S., and Lillehoj, E. P. (Eds.). (1994) Antibody Techniques 1st ed., Academic Press.
66. Leffell, M. S., Donnenberg, A. D., and Rose, N. R. (1997) Handbook of Human Immunology, CRC Press.

Tables

Table 1. Biomarkers used to characterize exposures or early biologic effects. (Table from (62))

Biomarker type	Biomarker category	Examples
Carcinogens and their metabolites	Internal dose	1-Hydroxypyrene, aflatoxins and tobacco-specific nitrosamines in urine; fecal *N*-nitroso compounds; organochlorines in serum and adipose tissue; metals in nails or hair
Nutrients	Internal dose	Urinary sugars and flavonoids; serum vitamins
Circulating antibodies	Internal dose	Antibodies to viruses (e.g. HBV); parasites (e.g. *Opisthorchis viverrini*); bacteria (e.g. *Helicobacter pylori*)
DNA adducts	Biologically effective dose	Urinary AFB1-N7-gua, bulky DNA adducts; DNA strand breaks (comet assay)
Protein adducts	Biologically effective dose	Aminobiphenyl-hemoglobin, aflatoxin–albumin
Genetic alternations	Biologically effective dose or early effect	Chromosomal aberrations, micronuclei, somatic cell mutations in reporter genes (HPRT, glycophorin A) or tumor suppressor genes (TP53 mutation spectra)
Circulating proteins	Biologically effective dose or early effect	Altered growth factors (e.g. IGF-1, IGFBPs) and cytokines (e.g. IL-6)
Altered gene expression	Biologically effective dose or early effect	Lymphocyte CYP1A1 expression; transcriptomics

Abbreviations: HBV, hepatitis B virus; HPRT, hypoxanthine-guanine phosphoribosyltransferase; IGF, insulin-like growth factor; IGFBPs, insulin-like growth factor binding proteins.

Table 2. DNA adducts known to be related to cigarette smoking. (Adapted from (63))

Adduct DNA adducts	Source	Methods of detection
Bulky adducts (aromatic adducts)	Nonspecific: PAHs, other bulky carcinogens	^{32}P-postlabelling
Benzo[*a*]pyrene diol-epoxide (BPDE)-DNA	Benzo[*a*]pyrene	HPLC-fluorescence; LC-MS
BPDE-DNA	Benzo[*a*]pyrene, PAHs	ELISA
4-Aminobiphenyl-dGuo (4-ABP-dGuo)	4-Aminobiphenyl	LC-MS; GC-MS; immunological
8-Oxo-dG	ROS	LC-MS/MS SRM
1,N^6-ethenoadenine; 3,N^4-ethenocytosine	ROS	Immunoenriched ^{32}P-postlabelling
Malondialdehyde (MDA)-DNA	Products of lipid peroxidation	Immunohistochemistry with specific MDA-DNA adduct monoclonal antibody; ^{32}P-postlabelling
N^6-hydroxymethyl-dAdo	Formaldehyde	LC-MS/MS
N^2-ethylidene-dGuo	Acetaldehyde	LC-ESI-MS/MS-SRM
1,N^2-propanodeoxy-guanosine	Acrolein	^{32}P-postlabelling; LC-ESI-MS
O^4-ethylthymidine	Unknown ethylating agent	Immunoenriched ^{32}P-postlabelling
7-Ethylguanine	Unknown ethylating agent	LC-NSI-HRMS/MS-SRM
HPB-releasing adducts	NNK, NNN	GC-NICI-MS

Abbreviations: GC, gas chromatography; LC, liquid chromatography; HPLC, high-performance liquid chromatography; MS, mass spectrometry; ESI, electrospray ionization; NSI-HRMS, nano-electrospray high-resolution mass spectrometry; NICI, negative ion chemical ionization; ELISA, enzyme-linked immunosorbent assay.

Table 3. Protein adducts known to be related to cigarette smoking. (Adapted from (63))

Adduct Protein adducts	Source	Methods of detection
Alkylvaline hemoglobin	Various alkylating agents	GC-MS
Methylvaline hemoglobin (MeVal-Hb)	e.g., NNK	GC-MS
Cyanoethylvaline hemoglobin (CyEtVal-Hb)	Acrylonitrile	GC-MS
Carbamoylethylvaline hemoglobin (AAVal-Hb)	Acrylamide	GC-MS; LC-MS
2-Hydroxy-2-carbamoyl-ethylvaline hemoglobin	Glycidamide	GC-MS; LC-MS
Hydroxyethylvaline hemoglobin (OHEtVal-Hb)	Ethylene, ethylene oxide	GC-MS; LC-MS
4-Aminobiphenyl hemoglobin (4-ABP-Hb)	4-Aminobiphenyl	GC-MS
BPDE hemoglobin (BPDE-Hb)	Benzo[*a*]pyrene	ELISA; GC-MS
BPDE albumin (BPDE-HSA)	Benzo[*a*]pyrene	ELISA; HPLC-fluorescence
HPB hemoglobin (HPB-Hb)	NNK, NNN	GC-MS
p-Benzoquinone albumin	*p*-Benzosemiquinone	Mass spectrometry (MALDI-TOF-TOF)

Abbreviations: GC, gas chromatography; LC, liquid chromatography; HPLC, high-performance liquid chromatography; MS, mass spectrometry; ESI, electrospray ionization; NSI-HRMS, nano-electrospray high-resolution mass spectrometry; NICI, negative ion chemical ionization; MALDI, matrix assisted laser desorption ionization; TOF, time of flight; SRM, selection reaction monitoring; ELISA, enzyme-linked immunosorbent assay.

Table 4. Biospecimens that can be used for molecular epidemiological studies. (Adapted from (64))

Method of collection	Biospecimens	Examples of biomarkers /biomaterials	Recommendation and condition for collection and storage
Invasive	Serum	Micronutrients (Vitamins and minerals)	Fasting for a maximum of 12 h
		Sex hormones	In females recording of day 1 of the ongoing and next menstrual cycle
		Lipids	Fasting for a maximum of 12 h
		Uric acid	Serum separation within the 32 h after venipuncture
		Glucose	Stabilized by sodium fluoride, separation within 3 h after venipuncture
		Metabonomics	Fasted subjects, clotting for 20-35 min on ice; avoid repeating freezing and thawing
	Plasma	Vitamin C	Stabilization with metaphosphoric acid, EDTA, perchloric acid or DTT
		DNA	Do not use heparin as an anticoagulant (inhibition of PCR); separate plasma within 2 h after venipuncture
	Tissue	Protein RNA	Freezing within 30 min after resection
			RNA later or snap-freezing in liquid nitrogen
Non-invasive	Urine	Erythropoietin	Immediate addition of complete protease inhibitor cocktail
		Fluoride, magnesium	24 h urine collection
	Buccal cells	DNA	Collection by cytobrush gives the best DNA yield and purity
	Cervical cells	RNA	Snap-freezing in liquid nitrogen
	Hair	DNA, drugs and metals	Sequential washing with detergent, water and organic solvent
	Nail	Metals	Hand-washed with distilled water and medicated soap devoid of metal contamination, nails cut with clean stainless stell scissors, nails washed sequentially with non-ionic detergent, acetone and water

Table 5. Properties of various human IgG subclasses. (Adapted from (65))

	IgG1	IgG2	IgG3	IgG4
Molecular weight (kDa)	146	146	170	146
Amino acids in hinge region	15	12	62	12
Inter-heavy chain disulfide bonds (in hinge region)	2	4	11	2
Susceptibility to proteolytic enzymes	++	+/-	+++	+
Number of allotypes	4	1	13	0
Serum level (mg/ml)	6.98	3.8	0.51	0.56
% of IgG	43-75	16-48	1.7-7.5	0.8-1.7

Table 6. Properties of various human immunoglobulin classes. (Adapted from (66))

	IgG	IgA	IgM	IgD	IgE
Concentration in serum (mg/ml)	12	3	1	0.1	0.001
% of Igs	77.8-71.8	12-18	10	0.2	0.004
Molecular weight (kDa)	150	180-500	950	175	200
Sedimentation coefficient(s)	7	7,10,13	18-20	7	8
Light chains	κ or λ	κ or λ	κ or λ	κ or λ	κ or λ
Heavy chains	γ	α	μ	δ	ε
Chain structure	L_2H_2	L_nH_n	$L_{10}H_{10}$	L_2H_2	L_2H_2
Tail piece	No	Yes	Yes	Yes	No
J chain	No	Yes/No	Yes	No	No
Carbohydrate % (average)	3-4	8-10	12-15	18	18
Number of oligosaccharides	1	2-3	5	NA	5

Table 7. Summary of methods to measure (+)-anti-benzo[a]pyrene-7,8-diol-9,10-epoxide (BPDE-I)-HSA adducts. (Adapted from (29))

Platforms	**Sample preparations**	Cost	Labor Time	Expertise	Untargeted
ELISA	Acidic hydrolysis (1 N HCl, 96°C, 3 h), solid phase extraction (C18)	Low	Short	Low	No
	Acidic hydrolysis (0.1 N HCl, 96°C, 3 h), liquid/liquid extraction (2×, isoamyl alcohol)				
HPLC-LIF	Enzymatic hydrolyses as described in Day *et al.* (1990), Addition of internal standard (Nπ-HBPDE),	Medium	Medium	Medium	Yes
HPLC-FLD	Similar as above				
GC-NCI-MS	Addition of internal standard (*cis*-BPDE-tetrol), enzymatic hydrolysis (pronase, 80°C, pH 11,2 h), solid phase extraction (C18), liquid/liquid extraction(2×, ethyl acetate), HPLC purification, liquid/liquid extraction (2×, ethyl acetate), derivatization (N,O-Bis(trimethylyilyl)acetamide and trimethylchlorosilane)	High	Long	High	Yes
HRGC-NCI-MS	Similar as above				
LC-ESI-MS-MS	Addition of internal standard, Isolation of protein, enrichment of protein, denature and digestion with trypsin for 6 h	High	Long	High	Yes
LC-ESI-HRMS-MS	Similar as above				

Abbreviations: HPLC-LIF, High-performance liquid chromatography and laser-induced fluorescence detection; GC-NCI-MS, gas chromatography and negative chemical ionization mass spectrometry; ELISA, enzyme-linked immunosorbent assay; HPLC-FLD, HPLC and fluorescence detection; LC-ESI-MS, liquid chromatography and electrospray ionization mass spectrometry; HRGC, high resolution gas chromatography; HRMS, high resolution mass spectrometry.

Figures

Figure 1. Different levels of dose and molecular events leading to diseases. (Adapted from PH220C, "health risk Assessment, regulation, and policy" class material)

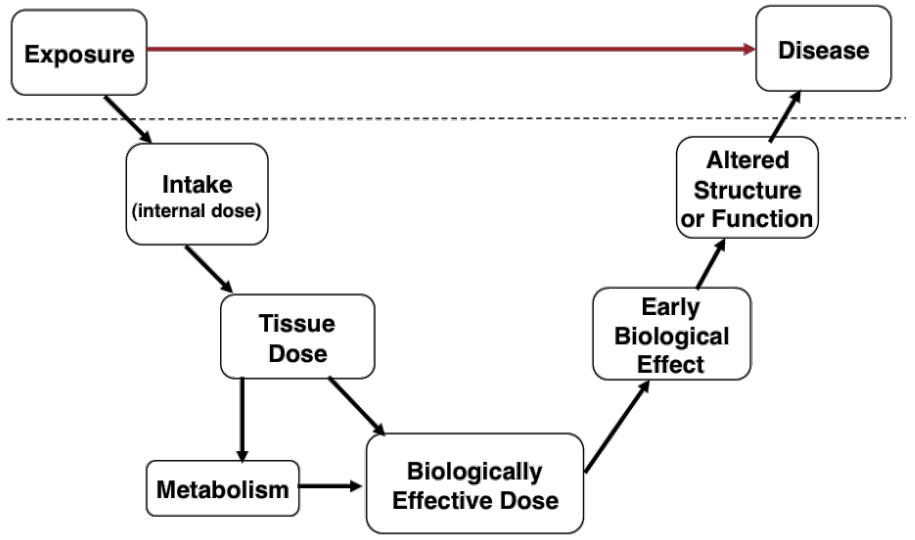

Figure 2. Interday variations of aflatoxin exposure as indicated by aflatoxin-HSA adducts, urinary-aflatoxin metabolites, and dietary aflatoxin. It can be observed that the degree of variation is in the decreasing order of dietary level > urinary metabolites > HSA adducts. (Adapted from (64))

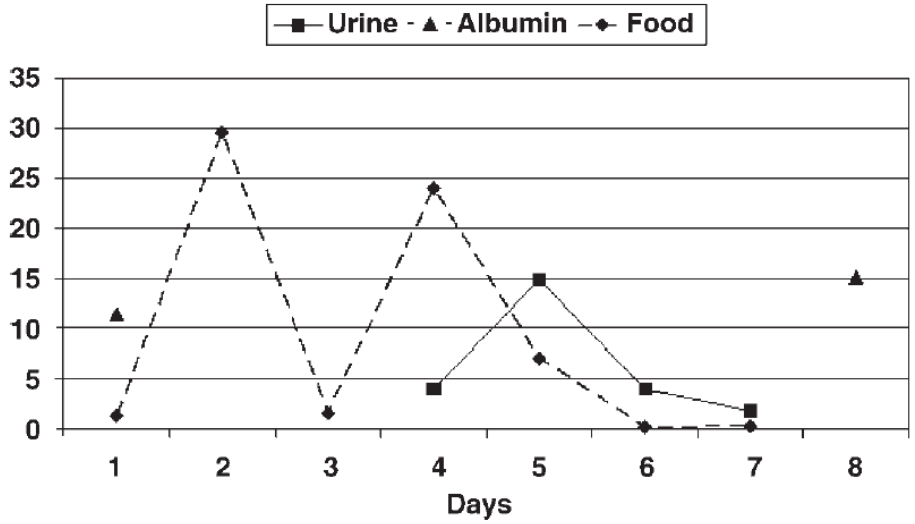

Units:
Dietary intake: µg/day
Urinary aflatoxin metabolites: ng/mg creatinine
Aflatoxin–albumin adducts (pg AFB_1–lysine equivalent/mg albumin)

Figure 3. Mammalian metabolic scheme for naphthalene. Naphthalene is first metabolized by the P450 enzymes to naphthalene-1,2-oxide, which is then oxidized to 1,2-dihydro-1,2-dihydroxy napthalene. Further oxidation leads to the formation of the reactive 1,2-naphthoquinone. (Figure from (25))

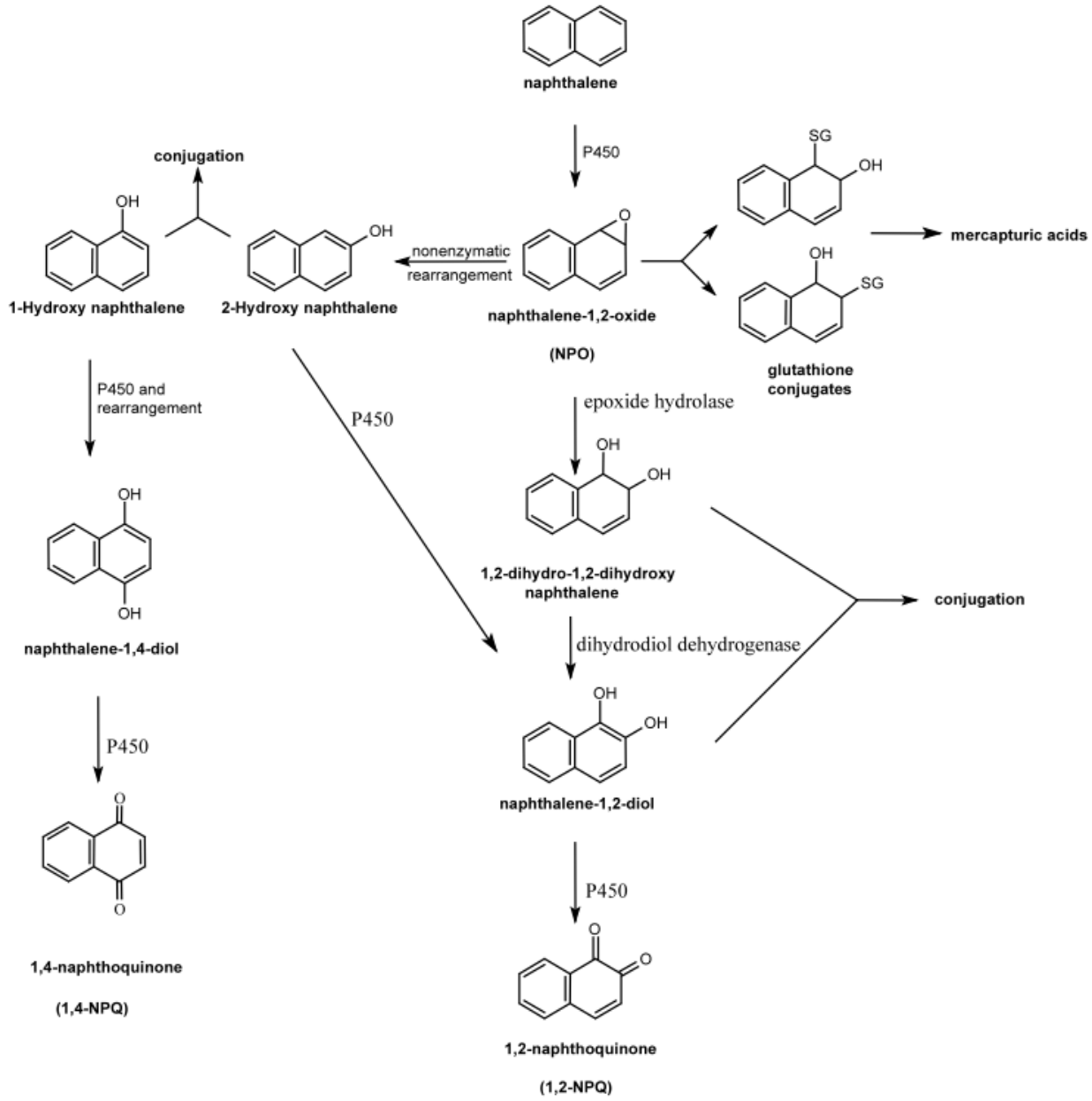

Figure 4. Formation of naphthoquinones-Cys adducts. Structures of the adducts are shown. (Adapted from (25))

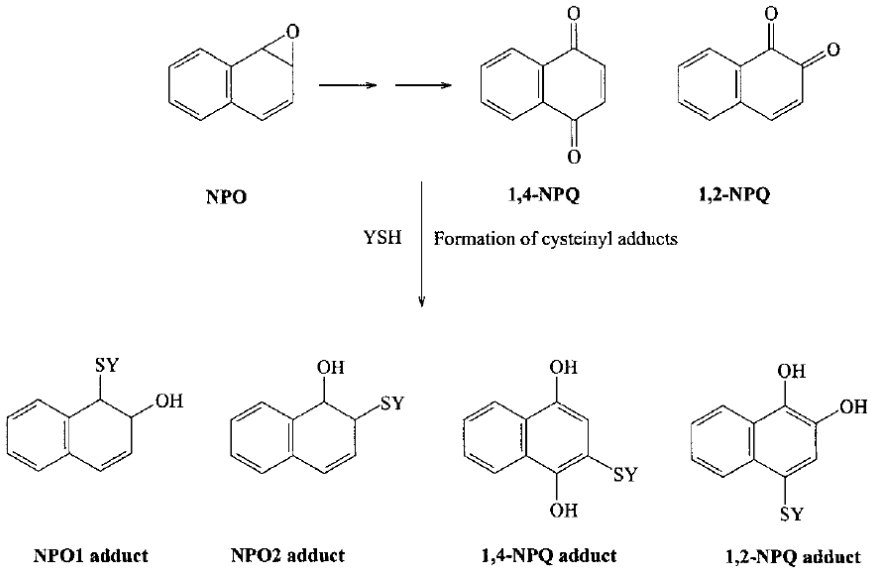

Figure 5. Metabolism of benzo[a]pyrene and the production of (+)-anti-benzo[a]pyrene-7,8-diol-9,10-epoxide (BPDE-I) and benzo[a]pyrene-7,8-quinone. The formation of BPDE-I and benzo[a]pyrene-7,8-quinone are through a series of oxidation steps. Noted that a reduction step on benzo[a]pyrene-7,8-dihydrodiols is essential to generate the quinone. (Figure from (29))

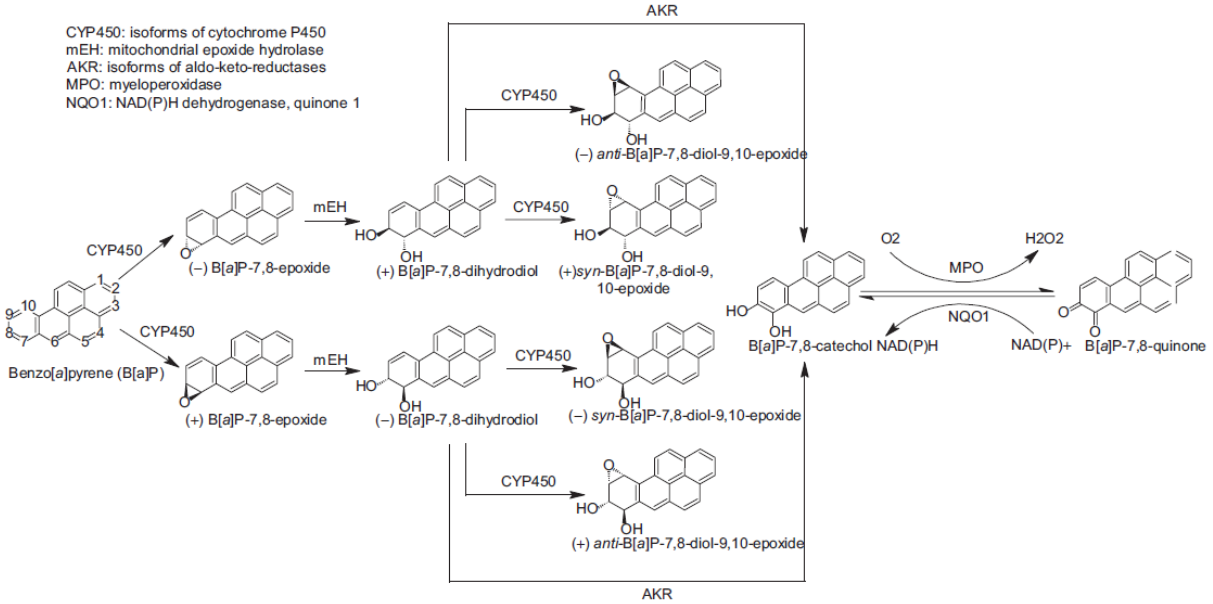

Figure 6. Formation of (+)-anti-benzo[a]pyrene-7,8-diol-9,10-epoxide-aspeartic acid adducts. Further hydrolysis of the esters leads to release of stable metabolites benzo[a]pyrene-r7,t8,t9,c10-tetrahydrotetrol (Tetrol I-1). (Figure adapted from (29))

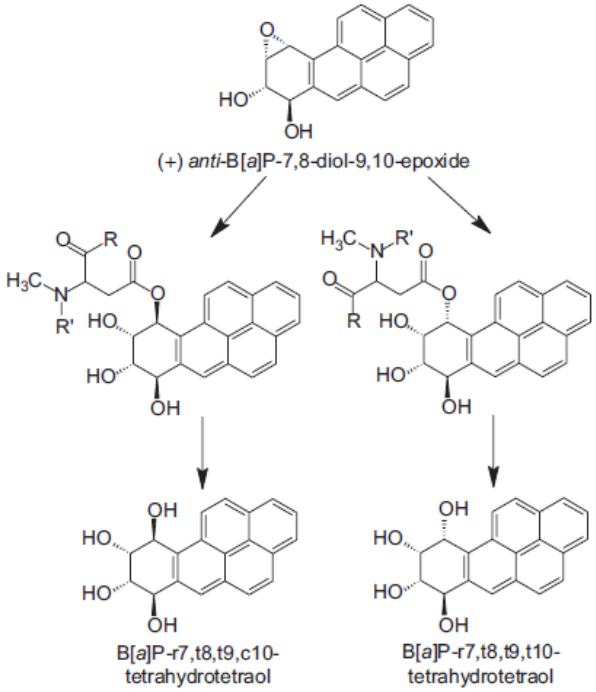

Figure 7. Classes of immunoglobulins. There are a total of five known classes in human, which are IgG, IgM, IgA, IgD and IgE.

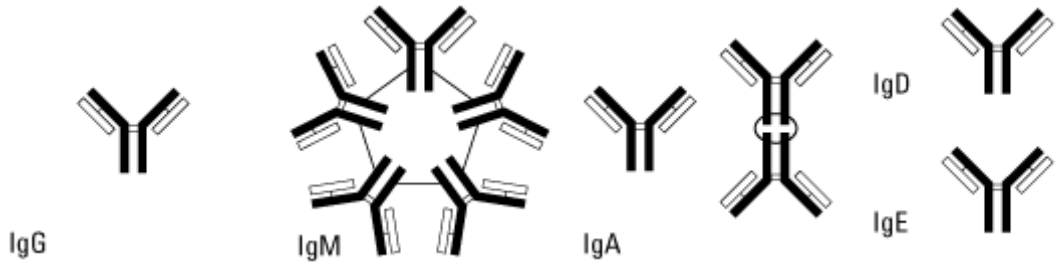

Monomer: IgG, IgA, IgD, IgE; Dimer: IgA; Pentamer: IgM

Figure from "Thermo scientific pierce antibody production and purification technical handbook, Thermo Scientific, (version 2)"

Figure 8. Structure and labeling sites of IgG. IgG is made up with two identical heavy chains and two identical light chains that overall arranged in a Y-shape. There are numerous labeling options such as reaction with the lysine residues.

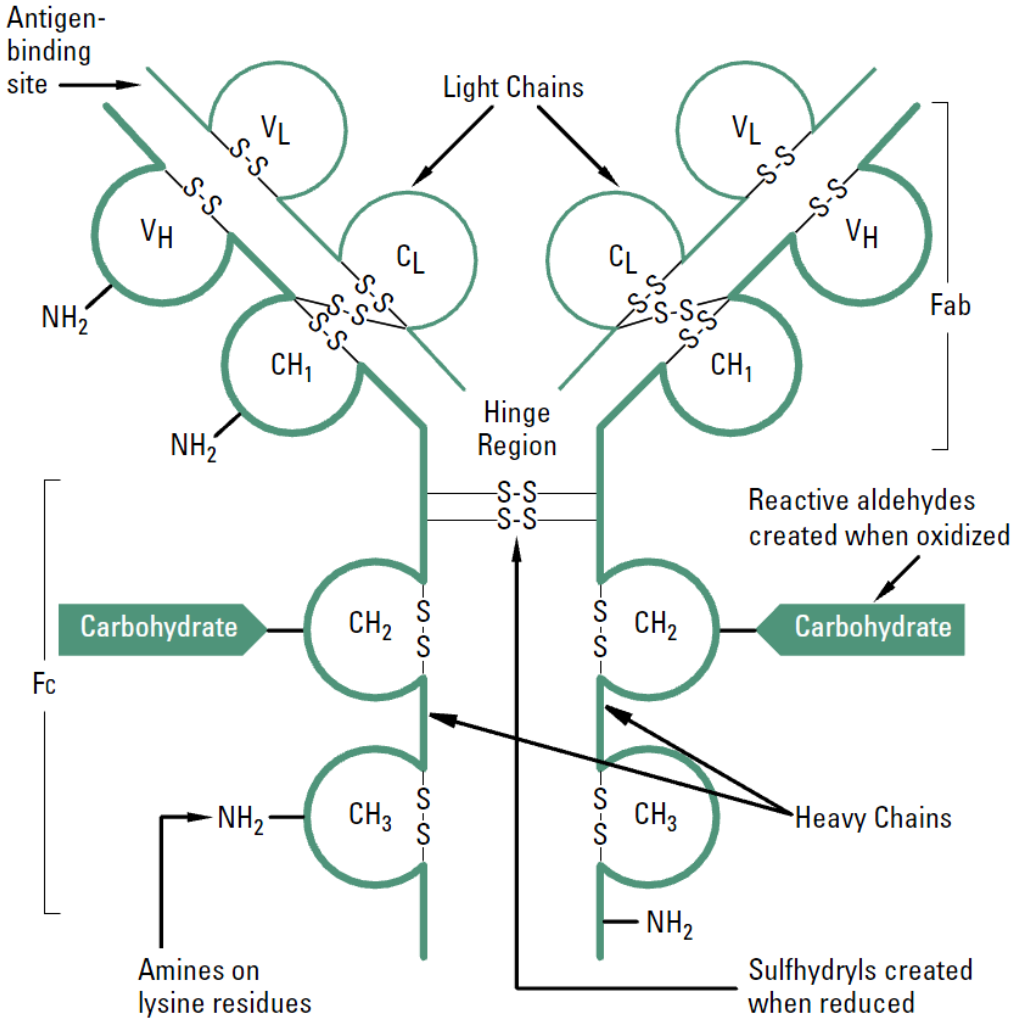

V_H, Variable domain of heavy chain; C_H, Constant domain of heavy chain; S-S, Disulfide bridge; NH_2, Primary amine; Fab, Fragment antigen-binding region; Fc, fragment crystallizable region

Figure from "Thermo scientific pierce antibody production and purification technical handbook, Thermo Scientific, (version 2)"

Figure 9. Fragment nomenclature of IgG.

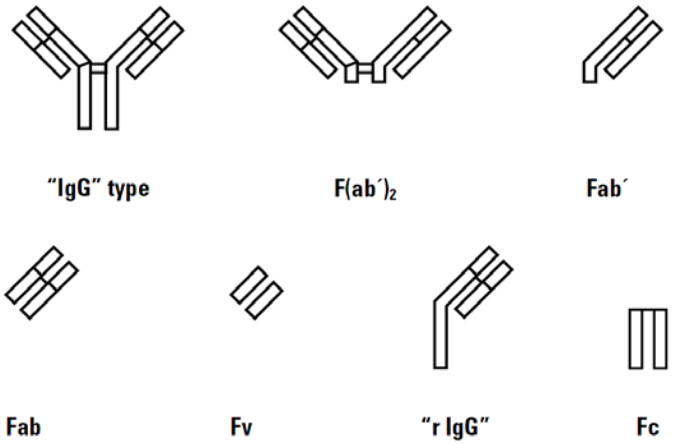

Figure from "Thermo scientific pierce antibody production and purification technical handbook, Thermo Scientific, (version 2)"

Figure 10. Overview of antibody production. With known antigen information, an immunogen is designed to maximize the immune response. Subsequently, the immunogen is injected into the animals at a specific interval before antibody is isolated. Optional modifications can be done after antibody is purified from the plasma. Finally, the antibody is characterized and can be applied in various situations.

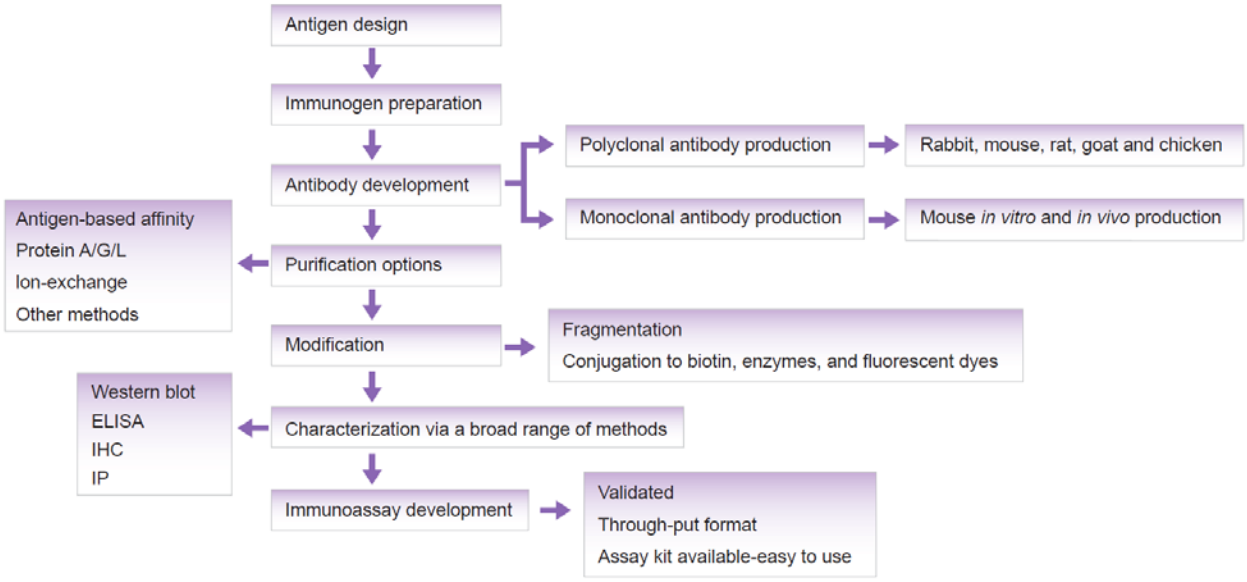

Adapted from "Biological service guide, GenScript. 2010-2011"

Figure 11. Production of a polyclonal antibody.

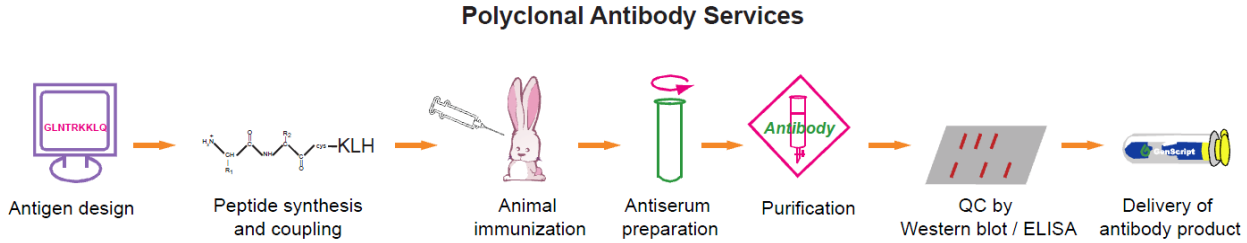

Figure from "Biological service guide, GenScript. 2010-2011"

Figure 12. Production of a monoclonal antibody.

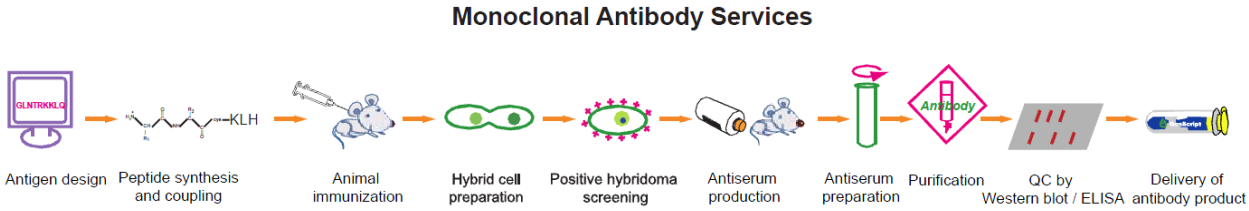

Figure from "Biological service guide, GenScript. 2010-2011"

Figure 13. Basic ELISA formats. In the direct assay, sample is loaded into the well of a 96-well plate. Antigen is coated on the surface and specific detection is done by a primary antibody that is conjugated to an enzyme. The indirect assay is similar to the direct assay, except that a primary capturing antibody is used and the detection antibody is made to recognize the primary antibody. In the sandwich ELISA, a specific capture antibody is coated to capture the antigen. Specificity to antigen is highest in this format because the antigen is recognized by a pair of antibodies.

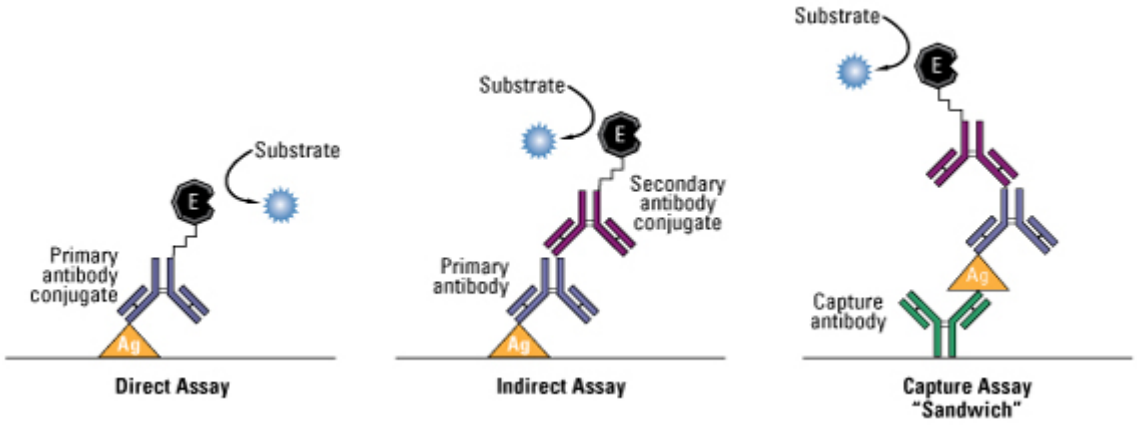

Figure from "Thermo scientific pierce assay development technical handbook, Thermo Scientific, (version 2)"

Figure 14. Workflow to measure (+)-anti-benzo[a]pyrene-7,8-diol-9,10-epoxide(BPDE-I)-HSA adducts in plasma with competitive ELISA. Starting with two ml of plasma, HSA is isolated by salt precipitation with at least a 50% loss. The HSA is then hydrolyzed by strong acid and benzo[a]pyrene-r7,t8,t9,c10-tetrahydrotetrol (Tetrol I-1) is released from the adduct. Tetrol is further purified by solid-phase extraction before measurement by competitive ELISA, which use BPDE-HSA as the plate-coating antigen.

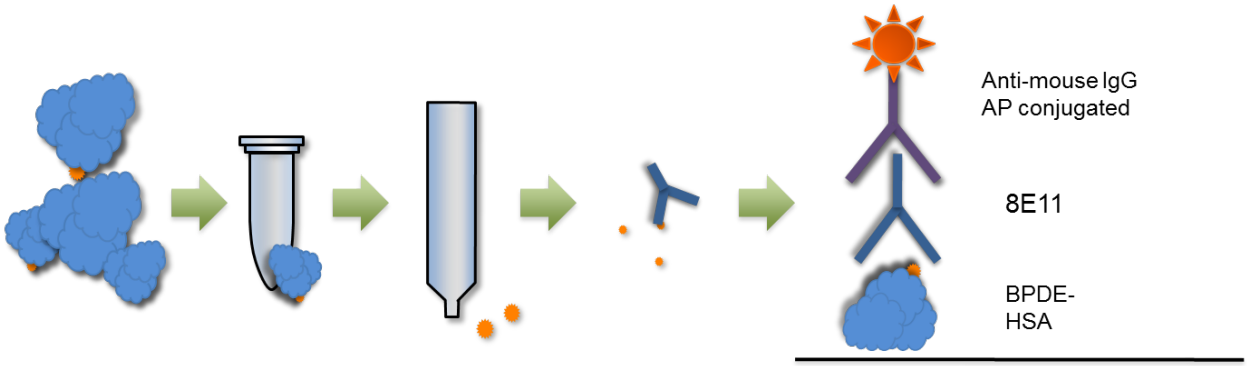

Figure 15. Overview of dissertation research.

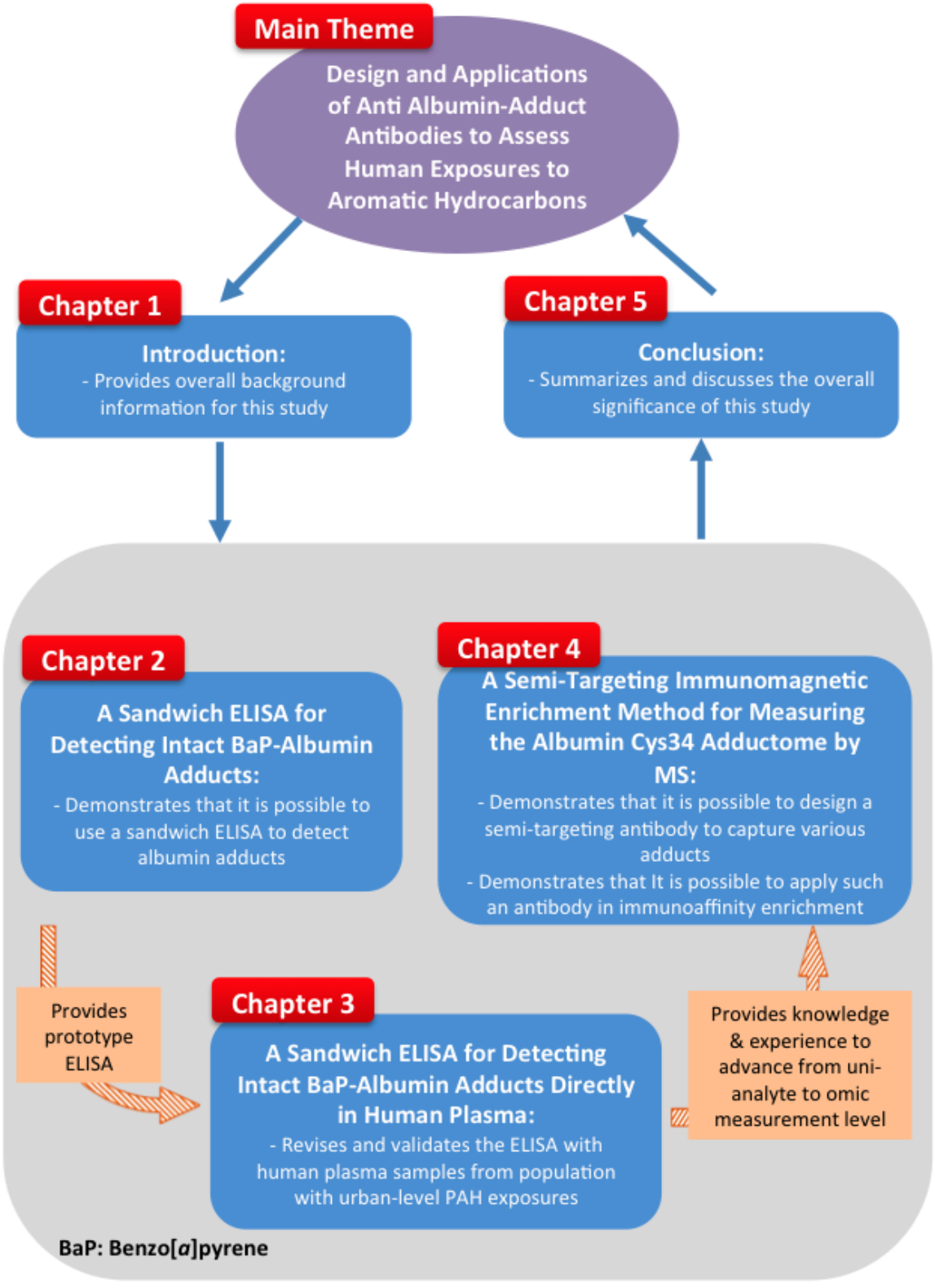

Chapter 2

A Sandwich ELISA for Measuring Intact Benzo[*a*]pyrene-Albumin Adducts

Introduction

Polycyclic aromatic hydrocarbons (PAHs) represent a class of ubiquitous pollutants arising from combustion of hydrocarbon fuels, fires, and cigarette smoke. Several PAHs are carcinogenic in humans and animals, notably benzo[*a*]pyrene (BaP) (*1*). The ultimate carcinogens derived from BaP metabolism are the isomeric benzo[*a*]pyrene-diol-epoxides (BPDEs) that bind to DNA, proteins, and other macromolecules to form adducts. Adducts of the BPDEs accumulate in blood and can be used as biomarkers of exposure to BaP and other PAHs from the same source (*2*).

Enzyme-linked immunosorbent assays (ELISAs) provide an efficient means for screening BPDE-human-serum-albumin (HSA) adducts in human studies. One such competitive assay, developed by Santella and coworkers, employs a monoclonal antibody 8E11, which was raised against BPDE-I-modified guanosine conjugated with bovine serum albumin but cross reacts with many other large PAHs (*3*). Because this assay involves hydrolysis of BPDE adducts to the corresponding BaP tetrols, it can be applied to essentially any hydrolysable BPDE adduct bound to proteins or DNA. As applied to HSA, the assay requires HSA to be isolated from blood, purified and hydrolyzed by treatment with enzymes or acid to generate BaP tetrols. The BaP tetrols are then purified and detected by competitive ELISA. Although each of these steps can result in losses of analyte and can introduce imprecision, this competitive ELISA has remained essentially unchanged for 20 years (*3*–*5*). Early attempts to use a direct ELISA with 8E11 to measure intact BPDE-HSA adducts, i.e., without hydrolysis to BaP tetrols, resulted in a 5-fold to 20-fold decrease in sensitivity (*4*, *6*).

The use of competitive ELISA to measure BaP exposure has usually been restricted to occupational scenarios (*3*, *7*–*9*) and not applied to large-scale epidemiological studies. This is largely because of the low sensitivity of the assay and the lengthy steps of sample preparation described above. This chapter describes development of a sandwich ELISA, which uses 8E11 to capture intact BPDE-HSA and an anti-HSA detection antibody. Although simpler to use, the assay is about 10 times more sensitive than the original competitive ELISA. Furthermore, it requires only 1 mg of isolated HSA, roughly equivalent to 20 µl of plasma. For validation, the assay was applied to samples of archived HSA from workers exposed to PAHs and from control subjects. In addition to assay development, a BPDE-HSA standard was characterized by MS.

Materials and Methods

Chemicals and Reagents

Benzo[*a*]pyrene-*r*-7,*t*-8-dihydrodiol-*t*-9,10-epoxides (±) [BPDE-I (±), MRI #477] were obtained from Midwest Research Institute, the NCI Chemical Carcinogen Repository (Kansas City, MO). Anhydrous tetrahydrofuran (THF, ≥ 99.9%), carbonate-bicarbonate buffer, Tween 20, human serum albumin (HSA, fraction V, 96-99%), triethylamine (TEA), diethanolamine (DEA, 99%) and para-nitrophenylphosphate (*p*NPP, >99%) were from Sigma-Aldrich (St. Louis, MO). Tris buffered saline (TBS) 10x, Tris base, acetonitrile (Fisher Optima grade, 99.9%), and formic acid (Pierce, 1 ml ampoules, 99+%) were from Fisher Scientific (Pittsburgh, PA). Non-fat dry milk (NFDM) was from Genesee Scientific (San Diego, CA). SuperBlock, ImmunoPure ABC (avidin-biotin complex) staining kits and 1-step ultra tetramethylbenzidine (TMB, the colorimetric substrate for HRP) were from Thermo Scientific (Rockford, IL). Goat anti-human albumin IgG [alkaline phosphatase (AP) conjugated] and rabbit anti-mouse IgG-Fc IgG were from Bethyl Laboratories (Montgomery, TX). Anti-HSA (rabbit IgG, biotin conjugated) and anti-BPDE monoclonal antibody clone 8E11 (mouse IgG) were obtained from Rockland Immunochemicals (Gibertsville, PA) and Trevigen, (Gaithersburg, MD), respectively. All antibodies were polyclonal except 8E11.

Archived HSA

Thirty archived specimens of HSA from both sexes were obtained from a study of PAH-exposed workers at a steel factory in Northern China (*10*) and a study of volunteer control subjects from North Carolina, U.S.A. (*11*). All blood samples had been obtained with informed consent after approval of protocols by Institutional Review Boards at the institutions where the initial investigations were conducted. The PAH-exposed subjects consisted of 10 top-side, coke-oven workers and 10 factory-control workers (both smokers and nonsmokers) from the same steel-making complex in Northern China; these workers had previously been shown to have high and intermediate levels of urinary PAH metabolites, respectively (*12*). The volunteer control subjects were nonsmokers. All HSA specimens had previously been isolated from plasma, dialyzed, lyophilized to constant weight, dissolved in distilled water (50 mg/ml) and stored at -80°C prior to analysis. For the current investigation, samples had been anonomyzed and included no personal information.

Fresh Human Plasma Samples

A fresh sample of human plasma was obtained by venipuncture from a laboratory volunteer. Ten ml of blood were collected and stored at 4°C for 30 min and then centrifuged at 200 g for 10 min to remove RBCs. Plasma was aliquoted into 1-ml portions and stored at -80°C prior to spiking with standard.

Synthesis of BPDE-HSA Standards

A BPDE stock solution was prepared by dissolving BPDE-I in THF with 5% TEA under nitrogen at a concentration of 3000 µg/ml. Commercial HSA (1 mg/ml in 0.01 M Tris buffer, pH 7.5) was mixed with BPDE stock in a molar ratio of 1:5 and gently shaken overnight in the dark at room temperature. The reaction mixture was applied to a 30 000 MW Microcon filter

(Millipore, MA), washed three times with 400 µl 0.01 M Tris buffer, and diluted to a concentration of 1 mg/ml with 0.01 M Tris buffer, pH 7.5.

Characterization of BPDE-HSA Adducts by MS

Samples of commercial HSA before and after reaction with BPDE were characterized with an Agilent 1200 series liquid chromatograph (LC) (Santa Clara, CA) that was connected in-line with an LTQ Orbitrap XL hybrid mass spectrometer (MS) equipped with an Ion Max electrospray ionization source (ESI; Thermo Fisher Scientific, Waltham, MA). The LC employed C8 guard (Poroshell 300SB-C8, 5 µm, 12.5 × 2.1 mm, Agilent) and analytical (75 × 0.5 mm) columns and a 100-µl sample loop. Solvent A was 0.1% formic acid in water and solvent B was 0.1% formic acid in acetonitrile (v/v). Following sample injection, analyte trapping was performed for 5 min with 99.5% A at a flow rate of 90 µl/min. The elution program consisted of a linear gradient from 25% to 95% B over 34 min, isocratic conditions at 95% B for 5 min, a linear gradient to 0.5% B over 1 min, and then isocratic conditions at 0.5% B for 14 min, at a flow rate of 90 µl/min. The column and sample compartments were maintained at 35ºC and 10ºC, respectively. The MS ESI source parameters were as follows: ion transfer capillary temperature 275°C, normalized sheath gas (nitrogen) flow rate 25%, ESI voltage 2.0 kV, ion transfer capillary voltage 33 V, and tube lens voltage 125 V. Positive ion mass spectra were recorded over the range m/z = 500 to 2,000 using the Orbitrap mass analyzer, in profile format, with full MS automatic gain control target settings of 3×10^4 and 5×10^5 charges for the linear ion trap and the Orbitrap, respectively, and an Orbitrap resolution setting of 6×10^4 (at m/z = 400, FWHM). ESI mass spectra were processed using Xcalibur software (version 4.1, Thermo) and charge state distributions were deconvoluted using ProMass software (version 2.5 SR-1, Novatia, Monmouth Junction, NJ), using the default “large protein” parameters and a background subtraction factor of 1.5.

Standard ELISA Procedures

Unless otherwise specified, these standard conditions were applied throughout the assays. To block the plate (MaxiSorp™, Nunc, NY), 250 µl/well of either 5% NFDM, Superblock, or 15% NFDM was used as indicated. To wash, the plate was briefly vortexed three times with 200 µl TBS-T (0.05% Tween in TBS) on a micro-plate mixer (Micromix 5, DPC, Flanders, NJ) before blotting with paper towel. The incubation time for each step was 1.5 h (45 min for the third sandwich design) at 37°C. All reagents, antibodies and HSA samples or standards were loaded at 100 µl/well.

First Sandwich Design

The first sandwich design is illustrated in Figure 1A. Monoclonal antibody 8E11 in 0.1 M carbonate-bicarbonate buffer (1:2000) was coated into a 96-well plate at 4°C overnight. Wells were blocked by 5% NFDM dissolved in TBS-T (0.05% Tween). After adding standards of BPDE-HSA adducts to the wells, goat anti-HSA IgG alkaline phosphatase (AP) was added (1:750) and the plates were incubated. After incubation, *p*NPP (1000 mg/l pNPP in 1 M DEA, pH 8.6) was added and readings were recorded after 12 h by a microplate spectrophotometer (ELx800, Bio-Tek, Winooski, VT) set at 405 nm.

Second Sandwich ELISA Design

This sandwich ELISA design is shown in Figure 1B. Anti-mouse IgG-Fc (rabbit IgG) at 5 µg/ml in 0.1 M carbonate-bicarbonate buffer was coated into the 96-well plate at 4°C overnight. After blocking with SuperBlock, monoclonal antibody 8E11 at 0.5 µg/ml was added and the plate was incubated. After loading standards of BPDE-HSA adducts into the wells and incubating, biotin-conjugated anti-HSA (rabbit IgG) at 1 µg/ml in blocking buffer was loaded and the plate was incubated again. ABC reagent, prepared in TBS-T, was added to the wells and the plate was incubated for 30 min at room temperature and then rinsed 5 times. A 1-step TMB solution was added and the reaction was stopped by addition of 100 µl/well of 2 M sulfuric acid. Colorimetric measurements were made at 450 nm using a microplate spectrophotometer.

Third Sandwich ELISA Design

The third design shares the basic components used in the second ELISA but the reagent volumes for most of the steps were reduced from 100 to 20 µl/well. After coating the 96-well plate (50 µl/well) with anti-mouse IgG-Fc (rabbit IgG) diluted to 1 µg/ml with 0.1 M carbonate-bicarbonate buffer, the plate was incubated at 4°C overnight. The plate was blocked with 15% NFDM dissolved in TBS-T and monoclonal antibody 8E11 at 3 µg/ml in blocking buffer was added. After incubating the plate, the BPDE-HSA-adduct sample or unmodified-HSA sample was loaded in a 20-µl volume and the plate was incubated for 1.5 h. The assay then proceeded as described above except that biotin conjugated antibody was prepared with SuperBlock, and 8.5 M acetic acid with 0.5 M sulfuric acid (10 µl) was used to stop the final reaction. Colorimetric measurements were made at 450 nm using a microplate spectrophotometer.

Validating the Third Sandwich ELISA

The third ELISA was used to measure BPDE-HSA adducts in samples of HSA from PAH-exposed workers and volunteer control subjects (in duplicate). Sample IDs were randomized and the analyst was blinded to the exposure status during measurement. Wells containing sample HSA without monoclonal antibody 8E11 were used as individual controls to monitor the background signal.

Signal Calibration

Since the archived samples of purified HSA contained 50 mg/ml HSA, the standard curve was prepared by dissolving various amount of BPDE-HSA in a 50 mg/ml HSA buffer solution (10 mM Tris, pH 7.5). This allowed background matching between samples and the standard curve, and hence permitted the signal to be calibrated accurately. The calibration curve was fitted by a variable slope sigmoid function,

$$y = min + \frac{max - min}{1 + 10^{[\log(IC50) - x]Hillslope}}$$

where *y* is the absorbance, *min* is the minimum response plateau, *max* is the maximum response plateau, log(*IC50*) is the log (base 10) of *IC50*, *Hillslope* is the slope of the curve, and *x* is the log (base 10) concentration of BPDE-HSA. The fitting was done with Qtiplot (v. 0.9.8.3, ProIndep Serv, Romania). Calculations were performed with Excel (v. 14, Microsoft Office 2010).

Detection Limit and Precision

Limits of detection (DL) and quantitation were defined, respectively, as the mean of 12 blank values obtained with BPDE-HSA standards plus either 3 times or 10 times the respective standard deviation (*13*). The detection and quantitation limits for the third ELISA design were found to be at 0.124 and 0.619 ng BPDE-HSA/well respectively.

To estimate the precision of the third ELISA design, duplicate reference standards were tested on 5 different days, and the coefficients of variations (CVs) were calculated from the one-way analysis of variance with Excel (v. 14, Microsoft Office 2010). For the 5 ng BPDE-HSA/well test, the intra- and inter-day CVs were 32.2% and 15% and for the 80 ng BPDE-HSA/well test, the intra and interday CVs were 8.71% and 10.7%, respectively.

Statistical Analyses

Values below the DL were imputed a value of half the detection limit for statistical analysis. Normality and homogeneity of variance were confirmed by Shapiro-Wilks and Bartlett's tests. Descriptive statistics and pairwise *t*-tests with Bonferroni correction were performed with STATA 12 (StataCorp, TX), using log-transformed (base *e*) data to satisfy normality assumptions (Table 1). Because of the small sample size, the *p*-values were double checked using permutation tests on the t-statistics to confirm the validity of the inferences. All statistical analyses are done with STATA 12 (StataCorp, TX).

Results and Discussion

Characterization of the BPDE-HSA Standard

The modification level of the BPDE-HSA standard by ESI MS of the intact proteins is quantified and illustrated in Figure 2. There was little overlap between deconvoluted mass spectra of commercial HSA (Figure 2A) and the BPDE-HSA standard obtained by reaction of commercial HSA with BPDE-I (Figure 2B), suggesting that the standard contained BPDE-HSA adducts in high yield. The most prominent mass in the spectrum of commercial HSA (Figure 2A) was 66 555 Da, representing the cysteinylated adduct at HSA-Cys34, whereas mercaptalbumin was represented by the smaller peak at 66 439 Da (*14*). In contrast, the mass spectrum of the BPDE-HSA standard was dominated by peaks at 66 863 Da and 67 177 Da, which are labeled in Figure 2B as cluster X and cluster Y, respectively. The mass differences between clusters X and Y and the prominent peak in commercial HSA were 308 Da (66 863 Da minus 66 555 Da) and 622 Da (67 177 Da minus control HSA at 66 555 Da), respectively. Because the theoretical mass change for addition of one mol of BPDE to one mol of HSA is 302.3 Da, it is concluded that cluster X most likely represents one BPDE adduct per HSA molecule and cluster Y most likely represents two BPDE adducts per HSA molecule. Based on the relative abundances of the corresponding ions in the raw spectra (not shown), roughly 80% of the BPDE-HSA standard contained a single BPDE modification and 20% contained two BPDE modifications. Thus, the average level of BPDE modification was about 1.2 mol of BPDE/mol HSA. Since stable covalent BPDE binding has been observed at His146 of HSA and relatively unstable ester adducts have been observed at Asp187 and Glu188 of HSA (*15*, *16*), it is reasonable to expect that more than one BPDE molecule could be bound to a single HSA molecule. Also, since repeated analysis of the BPDE-HSA standard showed that adducts were stable under prolonged periods of

laboratory storage (results not shown), it appears that most of the adducts in the standard represent the stable modification at His146 of HSA. Further determination of the specific binding sites of BPDE on HSA can be found in Chapter 3.

First Sandwich Design: From Competitive to Sandwich ELISA

Experiments involved three different ELISA designs. The first design was used to determine the feasibility of the sandwich ELISA for detecting BPDE-HSA adducts. Since the original competitive ELISA uses AP conjugated antibody and *p*NPP substrate to produce an optical signal (7), a sandwich ELISA with minimal modifications was evaluated (Figure 1A). The response curve for this assay is shown in Figure 3. Although absorbance changes were observable above 10 ng BPDE-HSA/well, the absolute absorbance was less than 0.5 even at 1000 ng BPDE-HSA/well. The detection limit for this design is about 10 ng BPDE-HSA/well and is 10 times higher than that of the original competitive ELISA (~ 1 ng BPDE-HSA/well equivalent) (*4*). Although this experiment showed that it is possible to use a sandwich ELISA measure intact BPDE-HSA adducts, the sensitivity is too low for any practical applications involving human samples.

Second Sandwich ELISA

The second sandwich ELISA (Figure 1B) incorporated several elements to enhance sensitivity. These include coating the wells with a spacer antibody, anti-mouse IgG-Fc (rabbit IgG), and substituting an ABC-horseradish peroxidase (HRP) detection system for the alkaline phosphatase (AP)-*p*NPP system. A spacer antibody was used to minimize denaturation and loss of specificity (*17*) and also to free the 8E11 capture antibody from any constraints that might be imposed by its direct attachment to the wells. Introduction of the ABC-HRP detection system to replace AP-*p*NPP should theoretically amplify the detection of BPDE-HSA adducts by a factor of 4 because one avidin molecule is capable of binding 4 biotin molecules. As shown in Figure 3, this ELISA design produced an absorbance of 0.76 O.D. units at 10 ng BPDE-HSA/well and the detection limit was estimated to be 0.1 ng BPDE-HSA/well.

Third Sandwich ELISA

Because adduct levels in human samples are about one molecule of BPDE-HSA per 10^6 HSA molecules, a high non-specific binding (NSB) of HSA to the internal well surfaces is expected. Since the detection antibody does not recognize adducts but only HSA, NSB of HSA can produce substantial background signals. This problem is worsened by the exceptional amplification capability of the ABC. To illustrate this effect, the second ELISA design was loaded with high concentrations of commercial HSA. As shown in Figure 4 the background signal was proportional to the level of HSA. Note that these data were obtained by stopping the colorimetric reaction at 8 min; otherwise only saturated signals would have been recorded. To solve this problem, a third ELISA design was developed. The signals were reduced by lowering the reagent volume from 100 µl to 20 µl, thereby reducing the effective surface area of each well, while also increasing the concentration of NFDM from 5% to 15% in the blocking buffer (to increase competition of NFDM with HSA for nonspecific binding). The third ELISA design was evaluated with 2 kinds of samples: BPDE-HSA spiked into a 50 mg/ml HSA solution and into human plasma. As seen in Figure 5, the signals from controls (without spiking) and the spikes

were not saturated even after 45 min of color development, which is the time needed for the assay to achieve full sensitivity. As with the second design, the detection limit was about 0.1 ng BPDE-HSA/well, which is about 10 times more sensitive than the conventional competitive ELISA (*5*, *18*).

Measuring BPDE-HSA Adducts in Human Samples

Having developed a practical sandwich ELISA for BPDE-HSA, the assay was validated with archived HSA from subjects exposed to high, medium, and low (control) levels of PAHs. Descriptive statistics are shown in Table 1 for the assays of PAH-exposed and control subjects. Adducts were detected in all 20 of the PAH-exposed workers (high-exposure and medium-exposure groups) and in 7 of 9 of the volunteer control subjects. Adduct levels spanned a 200-fold range across specimens of HSA from workers with high and medium exposure to PAHs (1.4 - 257 ng BPDE-HSA/mg HSA). Pairwise *t*-tests detected significant differences across the three groups ($p < 0.05$ for all pairwise tests and also the permutation tests).

It is informative to compare levels of BPDE-HSA adducts from the current investigation to those reported in previous studies which used the competitive ELISA to measure BPDE-HSA adducts in PAH-exposed workers and controls. Four such studies were found, namely, Kure *et al.* (*7*), who reported adduct levels in coke-oven workers and rural controls, Lee *et al.* (*3*), who reported adduct levels in foundry workers, roofers and controls, and Sherson *et al.* (*9*) and Omland *et al.* (*8*), who reported adduct levels in foundry workers and controls. Results from these studies and the current investigation are summarized in Table 2. For comparison, geometric mean (GM) or median adduct levels are shown with units given as fmol BPDE equivalents/mg HSA. For the Kure *et al.* and Lee *et al.* studies, GM concentrations were estimated from the reported mean and SD values according to the relationship, $GM = (mean)^2/sqrt(mean^2+SD^2)$ (*19*), which assumed normal distribution of the adduct concentration. Absolute adduct concentrations varied widely across the published studies, even in nonsmoking control subjects, where levels ranged from 28.9 fmol BPDE equivalents/mg HSA in the current study to 3280 fmol BPDE equivalents/mg HSA reported by Lee *et al*. (*3*) To reduce effects of inter-laboratory differences, Table 2 also shows fold ratios of BPDE-HSA levels measured in each group of exposed workers compared to those measured concurrently in control subjects. Using the sandwich assay, fold ratios of 35 for the coke-oven workers and 7.6 for the steel-factory control workers were found when compared to unexposed controls. While these fold ratios are considerably larger than those from the other studies, which used the competitive ELISA (fold-ratio range: 0.83-5.6), the results should be regarded as preliminary given the small numbers of subjects involved and difficulties in choosing control subjects for PAHs, which are ubiquitous contaminants of air, water, food, and tobacco smoke. It has been estimated that for general population, the average daily intake of PAHs is in the decreasing order of tobacco smoke (3 to 6 μg) > diet (0.16 to 1.6 μg) > air (0.207 μg) > soil (0.06 μg, accidental ingestion) > water (0.027 μg) (*20*, *21*). For most nonsmoker, dietary PAHs is the major source of PAH exposures (*22*) and thus environmental tobacco smoke would have a daily PAH intake value between 0.207 to 1.6 μg. Van Rooij *et al.* (*23*) found that the daily pyrene exposure in coke oven workers are between 4 to 34 μg. Thus, it is likely that the observed fold change is mainly due to occupational exposure. The combination of lower control levels of BPDE-HSA adducts

and higher fold ratios observed with the sandwich ELISA suggests that this assay would be useful for characterizing PAH exposures in epidemiologic investigations.

Relationship to Chapter 3

In this chapter, a prototype sandwich ELISA is described that is much simpler than the original competitive ELISA and is capable of detecting intact BPDE-HSA with good sensitivity (0.1 ng BPDE-HSA/well). The assay was validated with archived samples of HSA from high to low PAH exposed subjects. The next step is to apply the assay to detect BPDE-HSA adducts in plasma from subjects exposed to low levels of PAH from smoking and from outdoor pollutants. However, numerous unexpected issues arose when testing the prototype extensively with plasma samples. Surprisingly, assay variation was observed that was not only plasma specific, but also sample specific (i.e. personalized). Hence, the ELISA design and use protocol were revised in a number of important ways that will be elaborated in the next chapter.

References

1. ATSDR - Toxicological Profile: Polycyclic Aromatic Hydrocarbons (PAHs). 1995. http://www.atsdr.cdc.gov/toxprofiles/tp.asp?id=122&tid=25.
2. Tang, D., Phillips, D. H., Stampfer, M., Mooney, L. A., Hsu, Y., Cho, S., Tsai, W. Y., Ma, J., Cole, K. J., Shé, M. N., and Perera, F. P. (2001) Association between carcinogen-DNA adducts in white blood cells and lung cancer risk in the physicians health study, *Cancer Res. 61*, 6708–6712.
3. Lee, B. M., Yin, B. Y., Herbert, R., Hemminki, K., Perera, F. P., and Santella, R. M. (1991) Immunologic measurement of polycyclic aromatic hydrocarbon-albumin adducts in foundry workers and roofers, *Scand. J. Work. Environ. Health 17*, 190–194.
4. Lee, B. M., and Santella, R. M. (1988) Quantitation of protein adducts as a marker of genotoxic exposure: immunologic detection of benzo[a]pyrene--globin adducts in mice, *Carcinogenesis 9*, 1773–1777.
5. Wu, H. C., Wang, Q., Wang, L. W., Yang, H. I., Ahsan, H., Tsai, W. Y., Wang, L. Y., Chen, S. Y., Chen, C. J., and Santella, R. M. (2007) Polycyclic aromatic hydrocarbon- and aflatoxin-albumin adducts, hepatitis B virus infection and hepatocellular carcinoma in Taiwan, *Cancer Lett. 252*, 104–114.
6. Wild, C. P., Jiang, Y. Z., Sabbioni, G., Chapot, B., and Montesano, R. (1990) Evaluation of methods for quantitation of aflatoxin-albumin adducts and their application to human exposure assessment, *Cancer Res. 50*, 245–251.
7. Kure, E. H., Andreassen, A., Ovrebø, S., Grzybowska, E., Fiala, Z., Strózyk, M., Chorazy, M., and Haugen, A. (1997) Benzo(a)pyrene-albumin adducts in humans exposed to polycyclic aromatic hydrocarbons in an industrial area of Poland, *Occup. Environ. Med. 54*, 662–666.
8. Omland, O., Sherson, D., Hansen, A. M., Sigsgaard, T., Autrup, H., and Overgaard, E. (1994) Exposure of iron foundry workers to polycyclic aromatic hydrocarbons: benzo(a)pyrene-albumin adducts and 1-hydroxypyrene as biomarkers for exposure, *Occup. Environ. Med. 51*, 513–518.
9. Sherson, D., Sabro, P., Sigsgaard, T., Johansen, F., and Autrup, H. (1990) Biological monitoring of foundry workers exposed to polycyclic aromatic hydrocarbons, *Br. J. Ind. Med. 47*, 448–453.
10. Waidyanatha, S., Zheng, Y., and Rappaport, S. M. (2003) Determination of polycyclic aromatic hydrocarbons in urine of coke oven workers by headspace solid phase microextraction and gas chromatography-mass spectrometry, *Chem. Biol. Interact. 145*, 165–174.
11. Lin, Y. S., McKelvey, W., Waidyanatha, S., and Rappaport, S. M. (2006) Variability of albumin adducts of 1,4-benzoquinone, a toxic metabolite of benzene, in human volunteers, *Biomarkers Biochem. Indic. Expo. Response Susceptibility Chem. 11*, 14–27.
12. Serdar, B., Waidyanatha, S., Zheng, Y., and Rappaport, S. M. (2003) Simultaneous determination of urinary 1- and 2-naphthols, 3- and 9-phenanthrols, and 1-pyrenol in coke oven workers, *Biomarkers Biochem. Indic. Expo. Response Susceptibility Chem. 8*, 93–109.
13. Steiner, J. M., Williams, D. A., Moeller, E. M., and Melgarejo, T. (2000) Development and validation of an enzyme-linked immunosorbent assay for feline trypsin-like immunoreactivity, *Am. J. Vet. Res. 61*, 620–623.

14. Beck, J. L., Ambahera, S., Yong, S. R., Sheil, M. M., de Jersey, J., and Ralph, S. F. (2004) Direct observation of covalent adducts with Cys34 of human serum albumin using mass spectrometry, *Anal. Biochem. 325*, 326–336.
15. Day, B. W., Skipper, P. L., Zaia, J., Singh, K., and Tannenbaum, S. R. (1994) Enantiospecificity of covalent adduct formation by benzo[a]pyrene anti-diol epoxide with human serum albumin, *Chem. Res. Toxicol. 7*, 829–835.
16. Ozbal, C. C., Skipper, P. L., Yu, M. C., London, S. J., Dasari, R. R., and Tannenbaum, S. R. (2000) Quantification of (7S,8R)-dihydroxy-(9R,10S)-epoxy-7,8,9,10-tetrahydrobenzo[a]pyrene adducts in human serum albumin by laser-induced fluorescence: implications for the in vivo metabolism of benzo[a]pyrene, *Cancer Epidemiol. Biomarkers Prev. Publ. Am. Assoc. Cancer Res. Cosponsored Am. Soc. Prev. Oncol. 9*, 733–739.
17. Butler, J. E. (2000) Solid supports in enzyme-linked immunosorbent assay and other solid-phase immunoassays, *Methods San Diego Calif 22*, 4–23.
18. Santella, R. M., Perera, F. P., Young, T. L., Zhang, Y. J., Chiamprasert, S., Tang, D., Wang, L. W., Beachman, A., Lin, J. H., and DeLeo, V. A. (1995) Polycyclic aromatic hydrocarbon-DNA and protein adducts in coal tar treated patients and controls and their relationship to glutathione S-transferase genotype, *Mutat. Res. 334*, 117–124.
19. Rappaport, S. M., and Kupper, L. L. (2008) Quantitative Exposure Assessment, Lulu, El Cerrito, CA.
20. ATSDR - Toxicological Profile: Polycyclic Aromatic Hydrocarbons (PAHs). 5. Potential for Human Exposure.
21. Menzie, C. A., Potocki, B. B., and Santodonato, J. (1992) Exposure to carcinogenic PAHs in the environment, *Environ. Sci. Technol. 26*, 1278–1284.
22. Lioy, P. J., and Greenberg, A. (1990) Factors associated with human exposures to polycyclic aromatic hydrocarbons, *Toxicol. Ind. Health 6*, 209–223.
23. Van Rooij, J. G., Van Lieshout, E. M., Bodelier-Bade, M. M., and Jongeneelen, F. J. (1993) Effect of the reduction of skin contamination on the internal dose of creosote workers exposed to polycyclic aromatic hydrocarbons, *Scand. J. Work. Environ. Health 19*, 200–207.

Tables

Table 1. Concentrations of BPDE-HSA adducts in groups of PAH-exposed and unexposed persons from this study.

Exposure Group	PAH Exposure	*n*	ng BPDE-HSA/mg HSA (fmol BPDE equivalents/mg HSA)		
			Geometric Mean	Geometric SD	Range
Coke-oven workers	High	10	67.8* (1010)	1.99	22.4 - 257 (336 - 3800)
Steel-factory control workers	Medium	10	14.7* (220)	2.63	1.4 - 53.5 (21.0 - 801)
Unexposed controls[a]	Low	10	1.93* (28.9)	2.68	0.5 - 15.3 (7.5 - 229)

* *p*-value <0.05 versus both other groups. Comparisons were made by ANOVA of logged data using pairwise *t*-tests with Bonferroni correction. Same conclusion was drawn using permutation tests.

[a] Adducts not detected (< 1 ng/mg HSA) in two control subjects.

Table 2. Equivalent concentrations of BPDE-HSA adducts from this study and from previous studies of PAH-exposed workers and control subjects.

Study	ELISA	Exposure Group	Location	No. Subj.	BPDE Equivalents (fmol/mg HSA)[a]	Fold Ratio (Exposed: Controls)
Current	Sandwich	Coke-oven workers (smoking & nonsmoking)	China	10	1010 (GM[b])	35
	Sandwich	Steel-factory control workers (smoking & nonsmoking)	China	10	220 (GM)	7.6
	Sandwich	Unexposed controls (nonsmoking)	U.S.A.	10	28.9 (GM)	
Kure *et al.* (19)	Competitive	Coke-oven workers (smoking & nonsmoking)	Norway	38	3920 (GM)	1.5
	Competitive	Controls (smoking & nonsmoking)	Norway	45	2620 (GM)	
Lee *et al.* (3)	Competitive	Foundry workers (nonsmoking)	Finland	13	5020 (GM)	1.4
	Competitive	Controls (nonsmoking)	Finland	10	3600 (GM)	
	Competitive	Roofers (nonsmoking)	U.S.A.	12	4020 (GM)	1.5
	Competitive	Controls (nonsmoking)	U.S.A.	12	3280 (GM)	
Omland *et al.* (21)	Competitive	Foundry workers (nonsmoking)	Denmark	25	580 (median)	0.83
	Competitive	Controls (nonsmoking)	Denmark	26	700 (median)	
Sherson *et al.* (20)	Competitive	Foundry workers (nonsmoking)	Denmark	19	200 (median)	5.6
	Competitive	Controls (nonsmoking)	Denmark	19	35.9 (median)	

[a] Since the reporting unit in competitive ELISA is "fmol of BPDE", ng unit as reported in this study is converted to fmol BPDE equivalents by assuming that the molar ratio between BPDE and HSA in BPDE-HSA is 1:1 and molecular weight of BPDE-HSA is 67128 Da

[b] Geometric mean

Figures

Figure 1. Illustration of sandwich ELISA designs. A) First design. It is the simplest design with an alkaline phosphatase (AP) conjugated detection antibody. B) Second design. The design incorporates an anti-mouse-IgG-Fc to increase the effective concentration of 8E11. Signals are amplified with an avidin-biotin HRP complex. The third ELISA also employed the same general design as the second but used a reduced loading volume.

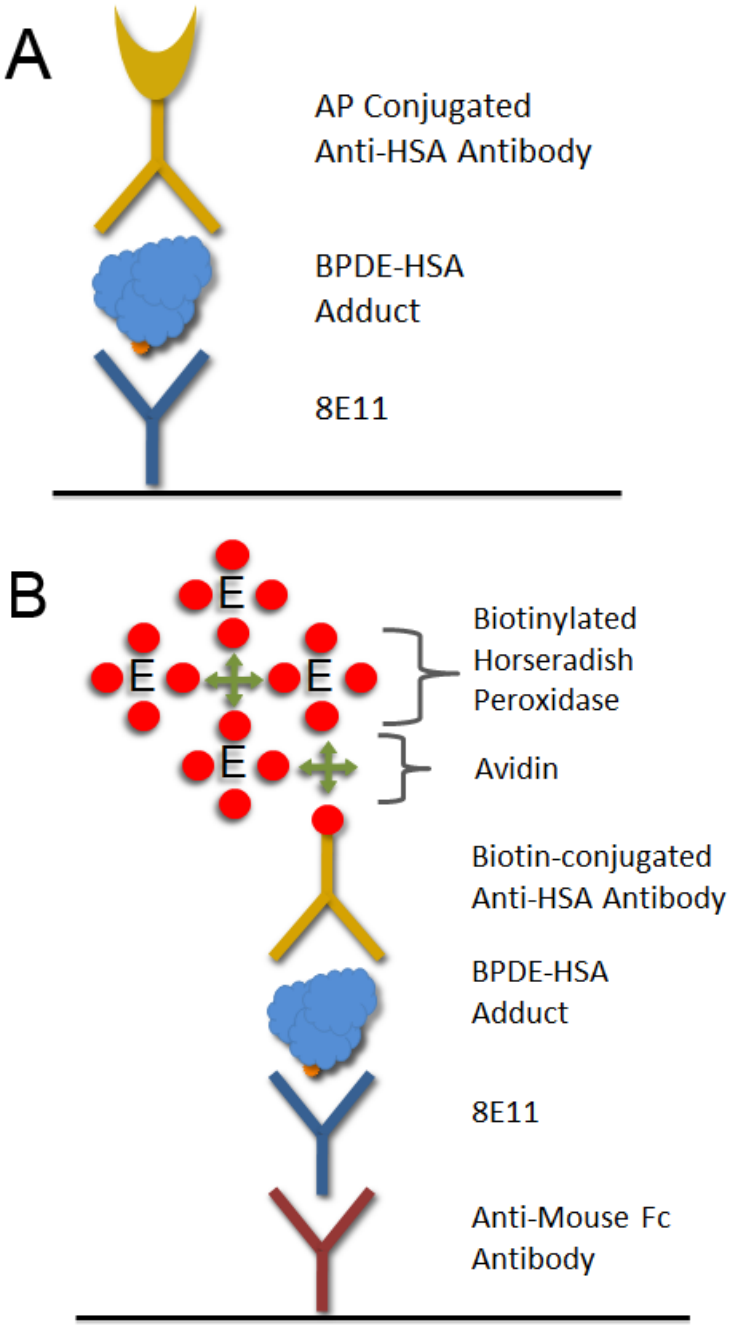

Figure 2. Deconvoluted mass spectra of commercial HSA (A) and the BPDE-HSA standard (B). Masses in (A) at 66 439 Da and 66 555 Da are mercaptalbumin and HSA which has been cysteinylated at HSA-Cys34. The mass difference between cluster X in (B) at 66 683 Da and cysteinylated HSA in (A) is 308 Da and between cluster Y in (B) at 67 177 Da and cysteinylated HSA is 622 Da. Since the theoretical mass change after addition of one mol of BPDE to one mol of HSA is 302.3 Da, clusters X and Y probably represent cysteinylated HSA which has been modified with one and two BPDE molecules, respectively.

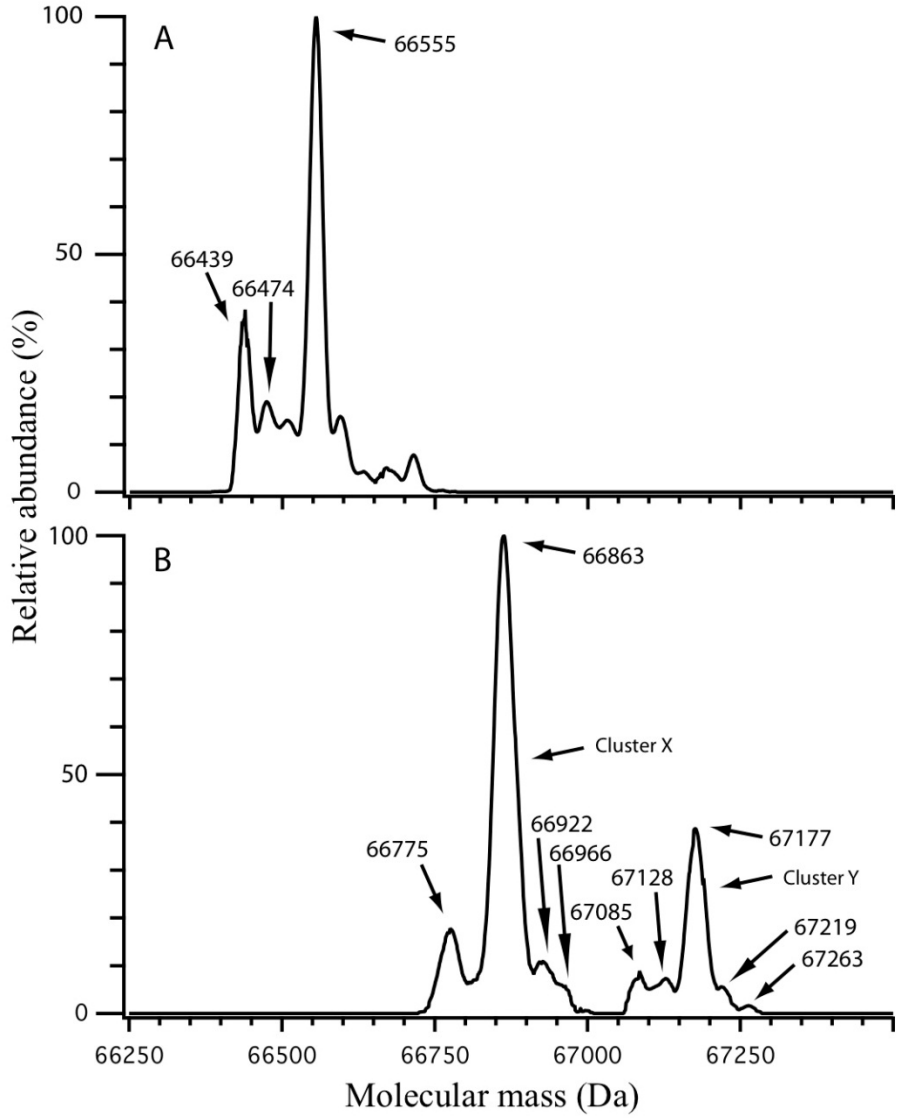

Figure 3. Standard curves obtained from the first (▲) and second (●) sandwich ELISA designs. The signals from the first and second designs were measured at 405 nm and 450 nm respectively. Error bars represent standard deviations of duplicate samples. Note that each well in the plate was filled with 100 µl of solution.

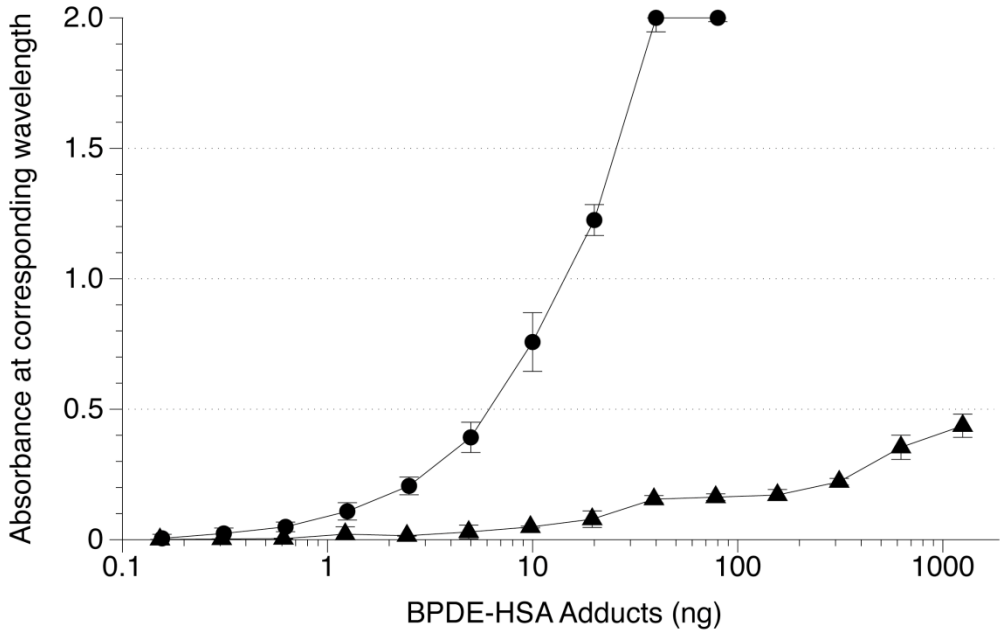

Figure 4. Relative background signals from non-specific binding of HSA in the second sandwich ELISA. Reaction was stopped at 8 min (rather than standard 45 min incubation) to avoid signal saturation.

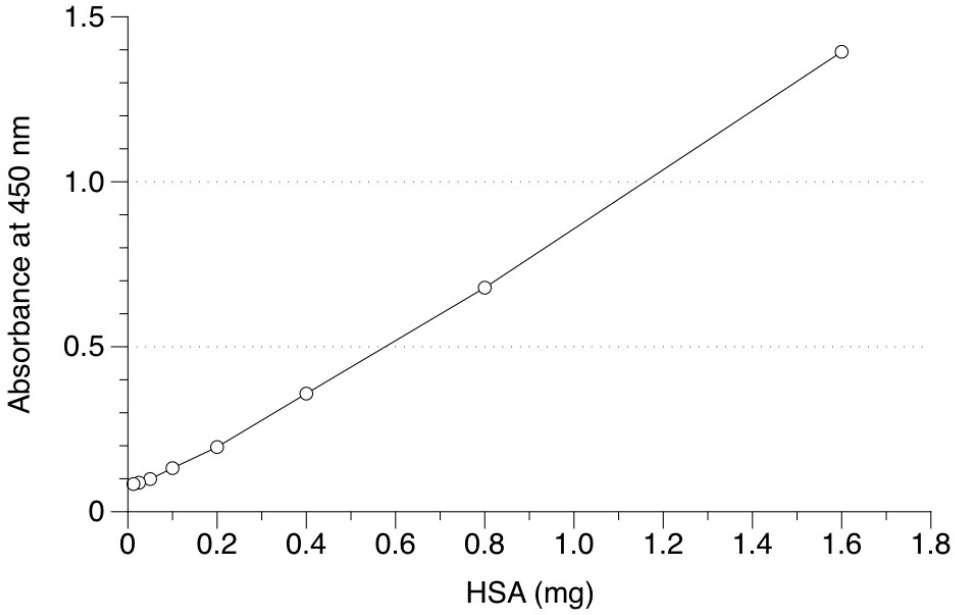

Figure 5. Response curves obtained from the third ELISA design. A) 50 mg/ml HSA spiked with BPDE-HSA. B) Human plasma spiked with BPDE-HSA. △ - BPDE-HSA spiked; □ - controls. Note that human plasma has an average of 45 mg/ml HSA. Error bars represent standard deviations of duplicates.

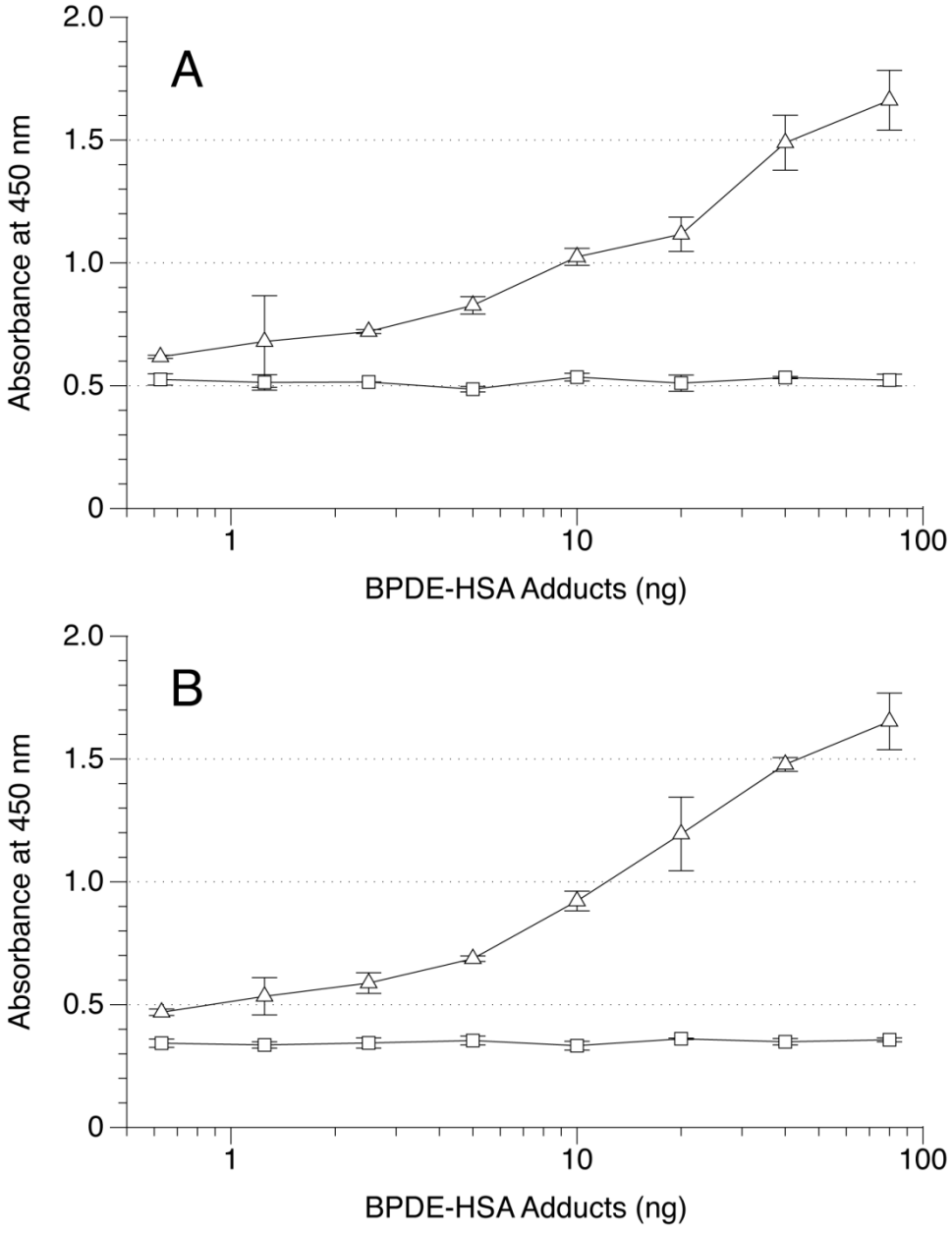

Chapter 3

A Sandwich ELISA for Measuring Intact Benzo[*a*]pyrene-Albumin Adducts Directly in Human Plasma

Introduction

Polycyclic aromatic hydrocarbons (PAHs) are ubiquitous pollutants produced by incomplete combustion of hydrocarbons and are constituents of cigarette smoke, engine exhausts, industrial effluents and grilled and smoked foods (*1*, *2*). The class of PAHs contains several hundred compounds with two or more fused aromatic rings. Exposures to PAHs cause human cancers, particularly of the lung, bladder and skin (*3–5*). Prenatal exposures to PAHs have been associated with low birth weight, premature delivery and a host of developmental problems in children (*6–9*).

Given the structural diversity of PAHs, the assessment of exposures to these toxic species has been challenging. Studies measuring dozens of PAHs in air, soil, water and dust (*10–13*) have been useful for apportioning sources of PAHs in environmental samples (*14*). However, because humans are simultaneously exposed to PAHs from air, water and food, measurement of all sources is impractical for investigations of PAH-related health effects. This diversity of exposure sources has motivated biomonitoring as an alternative to environmental monitoring for evaluating PAH exposures. Once absorbed in the body, PAHs are metabolized by cytochrome P450 enzymes to reactive molecules that either bind with macromolecules such as DNA and proteins to form adducts (*15*, *16*) or are hydrolyzed and excreted in urine and feces.

Applications of PAH-DNA adducts as biomarkers of exposure and early toxicity have been reported since the 1980s (*17*). Indeed, because PAH-DNA adducts can be detected with the ultra-sensitive ^{32}P-postlabeling assay (1 adduct per 10^{10} nucleotides), these adducts have been among the most popular biomarkers ever used by molecular epidemiologists (*18*). However, such applications of PAH-DNA adducts have inherent disadvantages. First, the only practical source of DNA in human biospecimens is peripheral blood mononuclear cells, which include many cell types having a hundred-fold range of life spans (*19*) and differential rates of DNA repair and adduct stability (*20*). Second, the ^{32}P-postlabeling assay is laborious and includes several steps that introduce significant variability (*18*, *21*, *22*), leading to inter-laboratory coefficients of variation (CV) as high as 108% (*22–24*). Third, the postlabeling assay detects all stable and bulky DNA modifications *en masse* and is, therefore, not specific for PAH generally or for quantifying particular PAHs of interest (*25*).

To simplify exposure assessment in epidemiologic research and health surveillance, benzo[*a*]pyrene (BaP) - a 5-ring PAH and a procarcinogen - has been used as a surrogate marker for PAHs in environmental samples. Mammalian metabolism converts BaP to the reactive benzo[*a*]pyrene diol epoxides (BPDEs), which form adducts with DNA and proteins (*17*) and is hydrolyzed to BPDE tetrols that are excreted. Although formation of DNA adducts (BPDE-DNA) has direct relevance to cancer development (*26*), the low abundance of DNA in blood plus the high turnover rate of DNA adducts (*27*) makes BPDE-DNA a less-than-optimal surrogate for BaP

exposure. As an alternative to BPDE-DNA, adducts of BPDE with human serum albumin (HSA) (BPDE-HSA) have been recommended for human biomonitoring (*28*–*31*). The concentration of HSA is more than a thousand-fold greater than that of DNA in human blood (45 mg HSA/ml vs. 28 μg DNA/ml) and, unlike DNA adducts, HSA adducts are not repaired. Thus BPDE-HSA should be a relatively stable biomarker of BaP exposure, with an estimated human half-life of 20 days that ensures integration of BaP exposures over about a month (*32*).

Several assays, including high-performance liquid chromatography (HPLC) with detection by fluorescence or mass spectrometry (MS) and competitive enzyme-linked immunosorbent assays (ELISA) have been used to measure BPDE-HSA in heavily modified samples (*32*). However, to permit detection of BPDE-HSA in humans exposed to PAHs in occupational and environmental settings, these adducts are usually hydrolyzed to BPDE tetrols that are then enriched prior to analysis (*31*–*34*). This is problematic because apart from the time-consuming preparation step, consistent and reliable quantitation of the BPDE tetrols depends on the particular hydrolysis conditions (*33*, *34*) that vary across studies (*32*, *35*). This need to precisely convert BPDE to tetrols hinders use of BPDE-HSA as a biomarker of PAH exposure in epidemiological studies.

In chapter 2, a highly sensitive sandwich ELISA was tested with intact BPDE-HSA in HSA isolated from plasma of steel-factory workers exposed to moderate and high levels of PAHs (*36*). Although this prototype ELISA was able to measure intact BPDE-HSA directly in plasma, numerous factors were discovered that affect accuracy and quantitation. These include highly varying intra- and inter-sample readings, which were ultimately related to the complexity of the plasma matrix.

In this chapter, enhancements to the sandwich ELISA are described for measuring intact BPDE-HSA adducts directly in plasma from subjects exposed to PAH at low levels. As shown in Figure 1, the major innovation involves parallel measurements of BPDE-HSA, with a tetrol-deactivated 8E11 as an internal control to adjust for background readings. These parallel measurements employ a novel sample-specific calibration (SSC) procedure to remove bias due to differences in interfering species across samples. Also, a set of decision rules was established to screen samples in order to minimize errors. The new assay design was validated with plasma samples from smokers and nonsmokers and from a group of highway workers exposed to low levels of PAHs from use of asphalt. Finally, since BPDE reacts with HSA at two loci as reported in Chapter 2, a follow-up proteomics analysis was performed to confirm the modification sites are at His146 and Lys195.

Materials and Methods

Chemicals and Reagents

The following chemicals and reagents were obtained from the indicated vendors: Fisher Scientific (Pittsburgh, PA): ThermalSeal® adhesive films, tris-buffered saline (TBS, 10x), acetic acid (glacial, ACS grade), sulfuric acid (ACS grade), dimethyl sulfoxide (DMSO), methanol (LCMS grade), TCEP, acetic acid (LCMS grade), formic acid (Optima®, LCMS Grade), acetonitrile (Optima grade, 99.9%); Sigma-Aldrich: carbonate-bicarbonate buffer, Tween 20, HSA (lyophilized powder, 97-99%), porcine trypsin, ammonium bicarbonate, sodium azide; Bethyl Lab, Inc.: goat anti-human albumin IgG, biotinylated; Thermo Scientific (Rockford, IL): SuperBlock®, ultra-sensitive ABC Peroxidase kits, one-step ultra TMB, goat anti-mouse IgG, Fc fragment specific (ImmunoPure®, min. cross-reactivity); Bethyl Laboratories, Inc. (Montgomery, TX): goat anti-human-albumin IgG, HRP conjugated (A80-129P); goat anti-human albumin IgG (A80-129A), TMB peroxidase substrate; Santa Cruz Biotech, Inc. (Santa Cruz, CA): 8E11; MRI Global (Kansas City, MO): tetrols powder (Benzo[*a*]pyrene-r-7,t-8,t-9,c-10-tetrahydrotetrol(+/-), MRI # 472); Genesee Scientific (San Diego, CA): nonfat dry milk (NFDM).

Human Plasma Samples

Archived plasma was obtained from two previous studies that had been conducted under human-subject protocols approved by institutional review boards at the University of North Carolina (*37*) and at Harvard University (*38*, *39*) between 1998 and 2000. The first sample was obtained from a group of 191 young healthy adult volunteers that had been recruited to investigate the variability of benzoquinone-HSA adducts in the general population. Since subjects had been equally divided between smokers and nonsmokers, the interest here was to determine whether levels of BPDE-HSA were associated with self-reported smoking status and intensity. Immediately after blood collection, red blood cells were removed by centrifugation and washed with an equal volume of phosphate-buffered saline (PBS), which was combined with the plasma. Samples of diluted plasma were stored at -80°C for 13 years prior to the current investigation. After thawing, specimens were pooled by combining aliquots of plasma from 4 or 5 subjects based on race (black or white), gender and self-reported smoking status; there were 35 pooled samples. Aliquoted samples were stored at -80°C for approximately three months prior to ELISA analysis and underwent two freeze-thaw cycles. Smoking intensity was quantified as the average number of cigarettes smoked per day for subjects in each pooled sample.

A second set of 80 plasma samples was selected from 203 specimens derived from 85 highway-paving and construction workers. The 80 plasma samples analyzed in the current investigation were obtained from 28 highway-paving workers who used asphalt (paver operators, screedmen and rakers) and 9 highway-construction workers who did not use asphalt. All of these workers were either white or Hispanic nonsmokers. Because the longitudinal study involved repeated blood collection, the 37 workers in the current sample had either 2 or 3 plasma samples (median = 2) collected during different seasons of the year. A Ficoll centrifugation procedure had been used to separate red blood cells, plasma and mononuclear white blood cells. Plasma was aliquoted and stored at -20°C for 6 years and at -80°C for an additional 6 years prior to the current investigation (one freeze-thaw cycle).

All plasma samples were assigned random numbers and the analyst was blinded as to exposure status and other characteristics of samples.

A fresh sample of human plasma was obtained as described in Chapter 2. It was used to make spiked samples for characterizing the SSC procedure.

Determination of BPDE-HSA Modification Sites by MS

A shotgun proteomics approach was used to identify the BPDE modification sites on HSA. A BPDE-HSA standard was prepared as described in Chapter 2. To start, a 50 µL aliquot containing 100 µg of BPDE-HSA standard was diluted 1:1 with 20% methanol in 100 mM ammonium bicarbonate. After adding TCEP to 5 mM, the solution was incubated at 37 °C for 15 min in the dark to reduce disulfide bonds. Then trypsin was added at a 1:10 (w:w) protease:protein ratio and digestion was performed at 37 °C with a pressurized system (Barocycler NEP2320, Pressure Biosciences Inc., South Easton, MA) that was programmed to generate 30 pressure cycles between ambient (15 s) and 1380 bar (45 s).

After diluting the tryptic digest 1:10 with water/acetonitrile/formic acid (94.9/5/0.1; v/v/v) in a clear glass HPLC vial (National Scientific, Rockwood, TN), the digest was stored at -80 °C prior to proteomics analysis. A 40-µl aliquot was injected into an HPLC (series 1200, Agilent, Santa Clara, CA, USA) coupled to a high-resolution MS (LTQ Orbitrap XL hybrid mass spectrometer with an Ion Max electrospray ionization (ESI) source (Thermo Fisher Scientific, Waltham, MA). Chromatographic separation was accomplished with a Zorbax 300SB C8 column (1.0×150 mm, 3.5-µm particle size) (Agilent, Santa Clara, CA) at a flow rate of 80 µl/min. The sample was loaded onto the column and cleared of the matrix with 98% buffer A (0.1% formic acid in water) and 2% buffer B (0.1% formic acid in acetonitrile) for 5 min and then programmed to 60% B over 60 minutes. After elution of peptides, the system was ramped to 95% B over 5 minutes to wash the column and then returned to initial conditions for 25 minutes.

The ESI source was operated at a spray voltage of 2.8 kV, a nebulizer gas (nitrogen) flow rate set at 15 (a.u.), a capillary temperature of 250° C and a capillary voltage of 20 V. The column and sample compartments were maintained at 35 and 4^{o}C, respectively. The MS performed scan cycles in data-dependent mode and acquired mass spectra using the Orbitrap with the following settings: positive-ion profile mode, full scan range 250–1,500 m/z, AGC target 5×10^{5}, 500 ms maximum inject time, microscan set to 1, resolving power 60,000 (FWHM at *m/z* 400). For each MS scan the three most intense ions exceeding a count of 2×10^{4} were selected for MS/MS analysis in the linear ion trap using both CID and ETD activation with the following settings: centroid mode, precursor ions isolation width of 3 m/z, AGC target 1×10^{4}, 100 ms maximum inject time, microscan set to 1. A normalized collision energy of 28 and an activation time of 30 ms were used for collision induced dissociation (CID). Electron transfer dissociation (ETD) was triggered by the fluoranthene anion using an activation time of 200 ms. Dynamic exclusion was enabled to reduce redundant MS/MS spectra acquisition as follows: 2 repeat counts, 30 s repeat duration, exclusion list size 500, 90 s of exclusion duration, relative exclusion mass ± 20 ppm. Charge state screening and monoisotopic precursor selection were enabled, singly and unassigned charged ions were not fragmented. A list of 7 background compounds reported by Keller *et al.* (*40*) were used as lock masses to provide a real time internal mass calibration during the analysis. Instrument control was provided by Xcalibur software (2.07, Thermo Fisher Scientific).

MassMatrix was used as the primary search engine for the identification of BPDE modification sites on HSA. According to the proposed mechanism by Day *et al.* (*29*), 302.094294 Da was used as the monoisotopic mass for BPDE modifications at Arg, His, Lys, Cys, Asp and Glu residues. UniProt entry P02768 was selected as the HSA sequence for mapping. 'Trypsin, no P rule' was selected for the *in silico* digestion and allowed for 2 maximum missed cleavages. Peptide and fragment ions tolerance were set to 10 ppm and 0.8 Da respectively. Other parameters were used as in the default profile for protein identification. Similar settings were also applied to the OMSSA Browser (v.2.1.1, National Library of Medicine), which was used as a secondary search engine to reduce false positive identification. All the precursor ion masses and the associated fragmentation patterns of the identified modifications from search engines were reviewed and cross-checked manually using the peptide sequence fragmentation modeling function available in Molecular Weight Calculator (v.6.49, Pacific Northwest National Laboratory, US Department of Energy).

Construction of a Molecular Model of BPDE-HSA

The spatial model of the BPDE-HSA was predicted by AutoDock Vina [v.1.1.2, (*41*)]. To start, 3D structures of HSA (PDB entry 1ao6) and BPDE (CID 41322) were downloaded from RCSB Protein Data Bank and NCBI Pubchem. The structure files were cleaned and prepared for use the AutoDockTools available in the MGLTools (v.1.5.4, The Scripps Research Institute). For HSA, the missing polar hydrogen atoms were added and the extra chain B was removed, while the torsion tree was automatically defined for BPDE. The grid box was placed close to the identified binding sites on HSA with the box size adjusted according to the space available. After searching by Vina, results were manually reviewed to select the best possible model representing the interaction between BPDE and HSA. Finally, Visual Molecular Dynamics (v.1.9.1) was used to create molecular representations of BPDE-HSA (*42*) and images were rendered with Tachyon (*43*) (Figure 2).

Revising the ELISA Prototype

As shown in Figure 1, the sandwich ELISA design has the same basic components as the prototype described in Chapter 2, namely, a spacer consisting of anti-mouse Fc antibody, 8E11 as capture antibody, biotinylated anti-HSA as detection antibody and an ABC amplification system. However, particular antibodies and reagents were changed to reduce background effects and to increase sensitivity. For example, use of an ultra-sensitive ABC staining kit increased sensitivity about 5-fold. The major change to the assay involves parallel ELISA measurements with and without BPDE tetrol-deactivated 8E11 to adjust for background effects due to non-specific binding of HSA and potential cross reactivity of antibodies.

Samples for the revised ELISA were prepared as follow: After thawing, 400 µl of plasma was centrifuged at 13 000 g for 10 min to remove potential interfering species. An aliquot of 335 µl was carefully withdrawn from the upper half of the plasma and made up to 15% NFDM and 0.02% sodium azide. Since readings are required with and without addition of BPDE tetrols, plasma was split into two portions at 30 µl/well, one diluted with a 3 000 ppm BPDE tetrol solution to a tetrol concentration of 60 ppm ('background' well in Figure 1) and the other diluted to an equivalent concentration of DMSO (0.034%) ('sample' well in Figure 1). All plasma samples were measured in quadruplicate (4 pairs of wells).

Unless otherwise mentioned, plates were incubated at 37°C for 45 min for each step. To minimize nonspecific binding of HSA, plates were rinsed between steps: three times with TBS-T (0.1% Tween) at 200 µl/well prior to sample incubation and five times after sample incubation. All reagents and samples were dissolved in 15% NFDM. In brief, goat anti-mouse IgG (Fc specific) was coated in the wells of a 96 well plate (MaxiSorp™, C type, Nunc, NY) at 10 µl/ml (in 0.1M carbonate-bicarbonate buffer, 30 µl/well) and incubated overnight at 4°C, followed by blocking with 15% NFDM (250 µl/well) and loading of 8E11 at 3.34 µg/ml (20 µl/well). Then, samples and standards were transferred to the plate at 30 µl/well in quadruplicate with 4 pairs of wells containing 8E11 and BPDE tetrol-deactivated 8E11, respectively. The detection antibody, biotinylated goat anti-HSA IgG prepared in SuperBlock®, was added at 1 µg/ml, 20 µl/well before the addition of ultra ABC (20 µl/well) and the mixture was allowed to stand for 30 min at room temperature. Then, ultra TMB was added (20 µl/well) and incubated for 30 min at room temperature in the dark. Finally, the reaction was stopped by adding 20 µl of a mixture of 8.5 M acetic acid and 0.5 M sulfuric acid. Color intensity was measured at 450 nm with a microplate spectrophotometer (ELx800, Bio-Tek, Winooski, VT).

Measurement of HSA

Because plasma samples contain varying level of HSA but not purified to 50 mg/ml HSA as the samples used in Chapter 2, the concentration of HSA in each specimen needs to be known in order to normalize and compare the BPDE-HSA data across samples. The HSA concentrations of plasma samples were measured by a sandwich ELISA with a dynamic range of 1 to 200 ng/ml. Plasma samples were assayed (in duplicate) at 3 consecutive 4-fold dilutions. Unless otherwise specified, plates were rinsed 3 times between incubations with 200 µl/well of TBS-T (0.05% Tween); all reagents, samples and antibodies were loaded at 50 µl/well with 5% NFDM; and plates were incubated at 37^{o}C for 45 min for each step. Goat anti-human-albumin IgG (0.5 µg/ml in 0.1 M carbonate-bicarbonate buffer) was coated on a 96-well plate (MaxiSorp™, C type, Nunc, NY) at 4^{o}C overnight. After blocking with 5% NFDM at 200 µl/well, diluted samples that should fall in into the range covered by the standard curve (3.1 to 200 ng/ml) were loaded. Then, goat anti-human-albumin IgG, conjugated HRP (0.2 µg/ml in 5% NFDM) was added and plates were incubated. Finally, TMB solution was loaded and plates were incubated for 25 min in the dark at room temperature. Color intensity was measured at 630 nm with a microplate spectrophotometer (ELx800, Bio-Tek, Winooski, VT). A calibration curve was fitted to a 4-parameter logistic function with Masterplex ReaderFit (v 2.0.0.76, Hitachi Solutions America, Ltd, San Francisco, CA).

Calibration of BPDE-HSA by SSC

The basic calibration curve was prepared from the BPDE-HSA standard. Since the calibration requires readings with and without BPDE tetrol-deactivated 8E11, standard solutions were split into two portions at 30 µl/well, one diluted with a solution of 3,000 ppm BPDE-tetrol in DMSO to a tetrol concentration of 60 ppm and the other diluted to an equivalent concentration of DMSO (0.034%). Standards were measured using the sandwich assay for BPDE-HSA described above at concentrations of 0.156, 0.313, 0.625, 1.25, 2.5, 5, 10, 20 ng BPDE-HSA/well.

Because the traditional calibration method for ELISA overestimates BPDE-HSA levels (mainly from the nonspecific binding of HSA to well surfaces), the BPDE-HSA concentration of each plasma sample was adjusted individually based on the associated background reading. As described above, pairs of ELISA readings were obtained for BPDE-HSA standards and a standard curve was constructed from the absorbance difference in each pair. Calibration involved fitting the BPDE-HSA standard curve with Qtiplot (v. 0.9.8.3, ProIndep Serv, Romania) with the following sigmoid function,

$$y = min + \frac{max - min}{1 + 10^{[\log(IC50) - x]Hillslope}}$$

where *min* and *y* are the minimum absorbance and total absorbance for a given standard pair, respectively, *max* is the maximum absorbance plateau from the calibration curve, log(*IC50*) is the log (base 10) of *IC50* from the calibration curve, *x* is the log (base 10) concentration of BPDE-HSA (ng/mg HSA), and *Hillslope* is the slope factor from the calibration curve. As shown in Figure 3, with SSC, a family of calibration curves is produced to adjust for background readings across plasma samples analyzed with a given set of standards. The core concept behind SSC is simple: In a standard curve, the slope of the tangent line of a point corresponding to an inputting signal is adjusted by a background signal characteristic of that particular plasma sample. Quantitation through SSC for a given sample involves substituting its absorbance readings from the background and sample wells for *min* and *y*, respectively, in the function and then solving for 10^x, which represents the BDE-HSA concentration. All calculations were performed with Excel (v. 14, Microsoft Office 2010).

Screening Samples for Valid Measurements

Some plasma samples were suspected to contain interfering substances that led to invalid detection of BPDE-HSA (i.e. *min* > *y,* which is uninterpretable in the sigmoid function) and, occasionally, to great intra-sample variability caused by an anomalously high reading in a replicate. To reduce potential errors from such interferences, a pair of screening rules was used to screen for invalid readings. A sample was designated as invalid if 3 of the 4 paired measurements had *min* > *y* absorbance readings or if BPDE-HSA levels differed by more than 10-fold across quadruplicate measurements. Invalid samples were re-assayed and the same criteria were applied. If the second determination was also invalid, then the sample was treated as a missing observation in statistical analyses.

Detection Limit, Accuracy and Precision

The detection limit (DL), defined as 3 times the background signal, was estimated at 0.2 ng BPDE-HSA/mg HSA (2.99 fmol BPDE equivalents/mg HSA). The precision and accuracy of the sandwich ELISA were assessed with samples of plasma containing known quantities of BPDE-HSA. A 1-ml aliquot of frozen plasma from a volunteer subject was thawed and 400 µl was centrifuged at 13 000 g for 10 min. An aliquot of 335 µl was carefully withdrawn from the upper half of the plasma and made up to 15% NFDM and 0.02% sodium azide. This plasma sample was spiked with BPDE-HSA at 10 ng/30 µl, aliquoted and stored at -80 ^{o}C prior to use. After thawing, a spiked plasma sample was diluted 5x and 25x with TBS to give three concentrations of 10 ng/30 µl, 2 ng/30 µl and 0.4 ng/30 µl, respectively, representing the useful range of the calibration curve. Data pairs were calibrated using SSC, as described above, in

triplicate on 13 different days to investigate intraday and interday sources of variation. Coefficients of variations (CVs) representing intra-day and interday variances were estimated via one-way analysis of variance with Excel (v. 14, Microsoft Office 2010).

Statistical Analyses

BPDE-HSA concentrations in plasma were normalized by the corresponding HSA content with units of ng BPDE-HSA/mg HSA. Since BPDE-HSA concentrations in both sets of validation samples covered large ranges and were right skewed, natural logarithmic transformation was applied to satisfy normality assumptions for statistical testing. Samples with measurements below the DL were imputed a value of half the DL for statistical analysis.

For the smoker/nonsmoker data, paired *t* test was used to distinguish between smoker and nonsmoker groups. Linear regressions were done through the generalized linear models (GLMs) to determine the effects of smoking, gender and their interaction on BPDE-HSA levels. Because each smoker/nonsmoker sample had been pooled from 4 or 5 subjects, simple linear regression of logged BPDE-HSA levels on smoking intensity employed the average number of cigarettes smoked per day in each pool.

The data from highway workers included repeated measurements from individual subjects during different seasons of the year. Thus, GLMs were estimated using gee and the exchangeable correlation matrix and robust option were applied. The effects of job types, working seasons and working tasks on BPDE-HSA levels were investigated. Model parameters of the categorical variables were further analyzed with a Wald test.

Because of the small sample size, tests returned significant *p*-values (<0.05) were double checked using permutation tests on the regression parameters, t- or F-statistics to confirm the validity of the inferences. All statistical analyses are done with STATA 12 (StataCorp, TX).

Results and Discussion

BPDE Modification Sites on HSA

Day *et al.* (*29*, *44*) suggested that His146, Asp187 and Glu188 were likely sites for BPDE modification of HSA but did not provide confirmatory data. In Chapter 2, it was found that about 80% of modified HSA contained one BPDE modification and about 20% contained 2 BPDE modifications, indicating that at least 2 modification sites were involved. Here with the proteomics analysis of a tryptic digest of the BPDE-HSA standard, it was possible to pinpoint the exact binding sites. Figure 4 shows ETD and CID MS/MS spectra of 2 modified peptides, RHPYFYAPELLFFAK (seq. # 145-159) and ASSAKQR (seq. # 191-197). These host peptides exhibit a monoisotopic mass increase of 302.094294 Da ± 5 ppm and were miscleaved at Arg145 and Lys195, probably due to steric hindrance imposed by the BPDE modification in the vicinity of the cleavage sites.

The CID MS/MS spectrum of the triply charged ion of modified peptide RHPYFYAPELLFFAK (734.7 *m/z*) shows a poor fragmentation pattern with the one charge-reduced native peptide (doubly charged ion at 950.3 *m/z*) and three ions at 303, 285 and 257 *m/z* (Figure 4c). This fragmentation pattern was reported by Day *et al.* (*29*) as the typical CID fragmentation pattern of BPDE. The same behavior was observed for the doubly charged ion (525.3 *m/z*) of modified peptide ASSAKQR (Figure 4d) and confirms that both peptides were modified by BPDE, but gives no information about the location of the covalent bond. However, the ETD MS/MS spectra of the same precursor ions retain more structural information and allow His146 and Lys195 to be confirmed as the modified sites. Specifically, for the peptide RHPYFYAPELLFFAK, the series of unmodified z ions and modified c ions, along with the unmodified c_1 fragment, leads to unequivocal assignment of His146 as a modification site (Figure 4a). For Lys195 the identification is not as straightforward because the low charge state of the precursor ion hinders the ETD fragmentation (no other charge state precursor ions for peptide ASSAKQR were detected). The spectrum shows the modified z ion series plus some unmodified z ions (Figure 4b), confirming that the BPDE modification of this peptide is very labile. The presence of modified c_8 and z_3 fragments confirm that the modification occurred at Gln196 or Lys195. The non-nucleophilicity of Gln plus the missed cleavage in correspondence with Lys195 makes the modification of Lys195 much more likely. Since there was greater than a 5-fold difference in signal intensities between the two modified peptides, it is likely that His146 is the major binding site.

Molecular Model of BPDE-HSA

Given the fact that there are2 apparent BPDE binding sites in HSA, and there are 4 possible modification locations, a molecular model of BPDE-HSA was constructed, to help clarify some of the questions on binding preferences (Figure 2). The auto fitting results from Vina provides one of the possible spatial fittings between BPDE and identified modification sites. Asp187, Glu188 and Lys195 are closely located to each other and adducts are likely to be located at the interface among HSA domains. While Lys195 is buried deep inside the structure of HSA, the 3 other potential modification sites are surrounded by partially opened structures. The relative bulky size of BPDE and the limited sharing space at the interface between domains may allow only 1 BPDE molecules at a time, and further explains why only 2 simultaneous bindings were

found in Chapter 2. The partial hindering structure around His146 and Lys195 could play a role regarding the low affinity of the 8E11 antibody toward the intact BPDE-HSA adduct, compared with free-tetrol antigens, which has a 20-fold greater affinity (*33*). This affinity difference could also explain why the tetrol-based competitive ELISA have been used so frequently in the past 20 years.

Although esters formed by reactions between BPDE and carboxylic acid side chains of Asp187 and Glu188 were not detected (*29*), it is possible that the ester adducts are labile and could have been hydrolyzed under the digestion conditions used in this study.

Revised Sandwich ELISA

Despite a 5-fold reduction in the DL (from 1 ng BPDE/mg HSA to 0.2 ng BPDE/mg HSA), difficulties were encountered when measuring BPDE-HSA directly in plasma with the prototype design. High intra-sample variability and inter-sample variability were observed in apparent BPDE-HSA levels across sets of plasma that, given their sources, could not be attributed to BaP exposure. Rather, it appeared that some unknown interfering species in the plasma were the causes. It was found that centrifugation of the plasma at 13 000 g for 10 min greatly reduced the intra variability in some samples.

Since all human plasma contains μM concentrations of HSA, small amounts of unadducted HSA can be adsorbed by well surfaces and subsequently detected (at fM concentrations) by the anti-HSA antibody. Yet, the extent of nonspecific HSA binding reflects the particular milieu of serum proteins in a plasma specimen and is thus sample specific. The ELISA was also sensitive to unknown interfering species that varied within and between sets of samples. The characteristics of interferences match descriptions of heterophilic antibodies that can bind to more than one antigen and to other species' immunoglobulins (*45*–*48*). In any case, the anti-HSA detection antibody is susceptible to cross reactivity with features that are also sample specific. And finally, the slope of the tangent line of a given point on the sigmoid calibration curve is correlated with the background level in a plasma specimen and is, again, sample specific.

Since the above combination of sample-specific factors effectively precludes a global background-matching scheme as used in Chapter 2, the prototype was redesigned by splitting each plasma specimen into background and sample pairs (Figure 1), blocking the activity of the 8E11 capture antibody with BPDE tetrols in the background well to provide a perfectly matched control to 8E11, and applying a SSC calibration procedure that adjusted for sample-specific background readings (Figure 3). This is apparently the first application of ELISA that systematically addresses such a combination of sample-specific factors.

The magnitudes of the background effects can be gauged by the first two rows of Table 1, which show absorbance of measurements with and without addition of BPDE tetrols to the control wells of BPDE-HSA standards at 0.4, 2 and 10 ng. Addition of BPDE tetrols reduced the absorbance by 28% at 0.4 ng, 54% at 2 ng and 71% at 10 ng. The positive biases associated with these background effects was about 60% to 70% over the dynamic range of the assay as indicated by the recoveries of standards listed in Table 1 with and without SSC.

The precision of the ELISA is indicated by the CVs given in Table 1 for three sets of triplicate standards at 0.4, 2 and 10 ng BPDE-HSA per well. With SSC, CVs varied between 5.05% and 17.2% and were comparable for both intra- and interday components of variation.

Screening Samples to Improve Accuracy

Immunoassays are prone to interferences and matrix effects when used for measuring exposure or diagnostic biomarkers in blood (*49*, *50*) and can result in either positive or negative biases. Although diluting samples and increasing the sample number can reduce the magnitudes of biases, these workarounds become problematic when analyte concentrations are very low, as is the case for BPDE-HSA in the general population.

The redesigned ELISA for BPDE-HSA includes sample-specific adjustments to reduce measurement errors, and is capable of measuring adducts with high accuracy and precision with spiked plasma samples (Table 1). However, the low quality of the samples (archived for > 10 years) amplifies the matrix effects. For example, within a set of plasma samples, data pairs were occasionally observed where the background reading (*min*) was greater than the experimental reading (*y*) and replicates of a given plasma sample occasionally differed by several fold.

To minimize the introduction of erroneous data into statistical analysis, all samples were measured in quadruplicate. Based on this design, a data screening step was formulated to flag samples where either the background reading exceeded the experimental reading or at least 10-fold variation was observed across replicates. Such samples were retested and, if flagged a second time, were excluded from statistical analysis (Figure 1). Results from the 115 validation samples (35 smokers/nonsmokers and 80 highway workers) flagged 32% of samples for retesting and excluded 10% from statistical analysis (Tables 2 and 3).

Validation with Plasma from Smokers and Nonsmokers

Since smoking is an important source of BaP exposure in the general population, BPDE-HSA in 35 samples of pooled plasma from 191 young healthy volunteer subjects (*37*) should be detectable by the revised ELISA (18 pooled samples from males and 17 from females). After applying the screening rules, 3 plasma samples were excluded from statistical analysis (all females).

Figure 5 shows a plot of the adduct levels in a group of smoker and nonsmoker. A marginally higher level of BPDE-HSA was found in smokers ($p = 0.0964$). Summary statistics are shown in Table 2 for adduct levels stratified by sex and smoking status (preliminary analysis showed no effect of race on BPDE-HSA levels). A model containing effects for smoking, sex and their interaction was also marginally significant ($p = 0.071$, $R^2 = 0.218$, $n = 32$) and showed a significant effect of the sex*smoking interaction. Subset analysis showed that smoking had a significant effect on logged adduct levels among males ($p = 0.035$, $R^2 = 0.249$, $n = 18$. $p = 0.034$ from permutation test) but not females ($p = 0.342$, $R^2 = 0.075$, $n = 14$).

The effect of smoking intensity on BPDE-HSA adducts was tested using the number of cigarettes smoked/day (as the average for subjects within each pool) as predictor variable (Figure 6) and was found to be significant ($p = 0.044$, $R^2 = 0.129$, $n = 32$. $p = 0.042$ from permutation test). Further stratification indicated that smoking intensity was a significant predictor of logged adduct levels for males ($p = 0.016$, $R^2 = 0.310$, $n = 18$. $p = 0.015$ from permutation test) but not for females ($p = 0.782$, $R^2 = 0.007$, $n = 14$).

The results provide evidence that cigarette smoking increases levels of BPDE-HSA - as measured by ELISA - in pooled plasma from male subjects. Although it is unclear why a similar effect was not observed in the female subjects, it is possible that female plasma contains more

interfering species than male plasma. In fact, the screening rule excluded only 3 of the 35 pooled plasma samples from statistical analysis of smokers/nonsmokers, all of which were from female subjects (one from nonsmokers and two from smokers). The lack of association between smoking and BPDE-HSA levels among females could also reflect the small sample size in this study (n = 17). Also, pooled samples are used and the observed difference is small. Therefore, a sample misclassification of smoking status within a pool could affect the results. Two previous studies used competitive ELISA with purified HSA to detect marginal-to-significant differences in levels of BPDE tetrols between smoking and nonsmoking mothers with 75 (p < 0.05) and 128 (p = 0.108) subjects, respectively (*51*, *52*).

It has been reported that in the lung cancer patients, the CYP1A1 and GSTM1 genotypes affect the BPDE-DNA adduct levels in the lung tissue (*53*). Looking at smoking-related bulky DNA adducts, an association between CYP1A1 gene expression and susceptibility to lung cancer was found in women (*54–56*). However, similar to the finding presented in Table 2, a difference in BPDE-DNA adduct levels in the peripheral lymphocytes from healthy male smokers and nonsmokers was found (*57*). These results suggested that the types of the samples and other genes such as the aryl hydrocarbon receptor gene expression (*55*) are factors affecting the change in BPDE-HSA observed between smokers and nonsmokers in male but not female.

Validation with Plasma from Highway Workers

A total of 80 archive plasma samples from a previous study of highway workers that had investigated lymphocytic DNA adducts (*39*) and urinary 1-hydroxypyrene (*38*) as potential biomarkers of asphalt exposure were analyzed. All of the samples used in the current were taken from workers who were nonsmokers. Box-plots of ln BPDE-HSA in this population are shown in Figures 7 and 8. Results of these analyses are shown in Table 3. Since the 80 plasma specimens had been collected from 37 workers (28 paving and 9 construction workers) during either 2 or 3 seasons of the year, GLM models with gee were used to estimate effects of job, task and season of the year on logged BPDE-HSA levels.

When all valid samples were included in the model (n = 68), no difference was observed in geometric mean (GM) adduct concentrations between the paving workers exposed to hot asphalt (GM = 1.55 ng BPDE-HSA/mg HSA) and the highway construction workers who were not exposed to asphalt emissions (GM = 1.53 ng BPDE-HSA/mg HSA).

When valid samples were investigated across seasons of the year, however, BPDE-HSA levels were found to be 2-fold higher in the winter (GM = 2.39 ng BPDE-HSA/mg HSA) than in the other seasons (GM = 1.15-1.37 ng BPDE-HSA/mg HSA) (p = 0.041. p = 0.021 from permutation test). This is interesting because a significant effect of the winter season on DNA-adduct levels had been observed in the original study (*39*). Since these highway workers did not work during the winter season, this suggests that the major BaP exposure experienced by this population did not arise from use of hot asphalt but rather from non-occupational sources that were more pronounced during the winter. Since these highway workers did not work during the winter season, this suggests that the major BaP exposure experienced by this population did not arise from use of hot asphalt but rather from non-occupational sources that were more pronounced during the winter.

The seasonal effect can be explained by an increased exposure to PAHs from indoor burning. In the 80s, it was estimated that 41% of PAHs emitted to the atmosphere in the US

was coming from the industrial processes. Mobile sources and residential heating attributed to another 25 and 16% respectively (*58*). Recently study shown that the PAH source profile has changed markedly, with over 57% of the PAHs is coming from residential heating (*59*). The second and third major contributing sources are mobile sources (17%) and industrial processes (12%) respectively. The changes are likely due to the growing influence of renewable energy and green chemistry concept, which reduce the consumption of fossil fuel and encourage more efficient industrial processes.

To investigate the contributions of occupational factors *per se*, samples collected during the winter were excluded and the remaining samples were tested for differences in adduct levels across the job tasks (n = 58). As shown in Table 3, the estimated GM concentration of BPDE-HSA (ng/mg HSA) increased in the following order: construction worker (1.18) < paver operator (1.20) < raker (1.29) < screedman (1.55); only the screedman was significantly different from construction (p = 0.037. p = 0.035 from permutation test). Interestingly, screedmen had also been identified as the most heavily PAH-exposed subjects in the original study, based upon both PAH-DNA adducts (*39*) and urinary 1-hydroxypyrene (*38*). Thus, ELISA measurements of BPDE-HSA in this subset of plasma samples are concordant with the results from the more extensive sets of measurements originally reported.

Relationship to Chapter 4

In this chapter, the prototype sandwich ELISA developed in Chapter 2 was successfully revised and applied to measure intact BPDE-HSA directly in human plasma samples. In the next chapter, the design of a semi-targeting antibody is described that can capture a range of known and unknown HSA peptide adducts. This antibody will be used to demonstrate a novel semi-targeting-enrichment methodology that can be used for characterizing the HSA Cys34 sub-adductome.

References

1. Khalili, N. R., Scheff, P. A., and Holsen, T. M. (1995) PAH source fingerprints for coke ovens, diesel and, gasoline engines, highway tunnels, and wood combustion emissions, *Atmos. Environ. 29*, 533–542.
2. Xu, S., Liu, W., and Tao, S. (2006) Emission of Polycyclic Aromatic Hydrocarbons in China, *Environ. Sci. Technol. 40*, 702–708.
3. Boffetta, P., Jourenkova, N., and Gustavsson, P. (1997) Cancer risk from occupational and environmental exposure to polycyclic aromatic hydrocarbons, *Cancer Causes Control CCC 8*, 444–472.
4. Straif, K., Baan, R., Grosse, Y., Secretan, B., El Ghissassi, F., and Cogliano, V. (2005) Carcinogenicity of polycyclic aromatic hydrocarbons, *Lancet Oncol. 6*, 931–932.
5. Bosetti, C., Boffetta, P., and La Vecchia, C. (2007) Occupational exposures to polycyclic aromatic hydrocarbons, and respiratory and urinary tract cancers: a quantitative review to 2005, *Ann. Oncol. Off. J. Eur. Soc. Med. Oncol. ESMO 18*, 431–446.
6. Choi, H., Jedrychowski, W., Spengler, J., Camann, D. E., Whyatt, R. M., Rauh, V., Tsai, W.-Y., and Perera, F. P. (2006) International studies of prenatal exposure to polycyclic aromatic hydrocarbons and fetal growth, *Environ. Health Perspect. 114*, 1744–1750.
7. Perera, F. P., Rauh, V., Tsai, W.-Y., Kinney, P., Camann, D., Barr, D., Bernert, T., Garfinkel, R., Tu, Y.-H., Diaz, D., Dietrich, J., and Whyatt, R. M. (2003) Effects of transplacental exposure to environmental pollutants on birth outcomes in a multiethnic population., *Environ. Health Perspect. 111*, 201–205.
8. Perera, F. P., Tang, D., Wang, S., Vishnevetsky, J., Zhang, B., Diaz, D., Camann, D., and Rauh, V. (2012) Prenatal polycyclic aromatic hydrocarbon (PAH) exposure and child behavior at age 6-7 years, *Environ. Health Perspect. 120*, 921–926.
9. Perera, F. P., Wang, S., Vishnevetsky, J., Zhang, B., Cole, K. J., Tang, D., Rauh, V., and Phillips, D. H. (2011) Polycyclic aromatic hydrocarbons-aromatic DNA adducts in cord blood and behavior scores in New York city children, *Environ. Health Perspect. 119*, 1176–1181.
10. Chung, M. K., Hu, R., Cheung, K. C., and Wong, M. H. (2007) Pollutants in Hong Kong soils: Polycyclic aromatic hydrocarbons, *Chemosphere 67*, 464–473.
11. Lodovici, M., Venturini, M., Marini, E., Grechi, D., and Dolara, P. (2003) Polycyclic aromatic hydrocarbons air levels in Florence, Italy, and their correlation with other air pollutants, *Chemosphere 50*, 377–382.
12. Whitehead, T., Metayer, C., Gunier, R. B., Ward, M. H., Nishioka, M. G., Buffler, P., and Rappaport, S. M. (2011) Determinants of polycyclic aromatic hydrocarbon levels in house dust, *J. Expo. Sci. Environ. Epidemiol. 21*, 123–132.
13. Zhou, J. ., and Maskaoui, K. (2003) Distribution of polycyclic aromatic hydrocarbons in water and surface sediments from Daya Bay, China, *Environ. Pollut. 121*, 269–281.
14. Kavouras, I. G., Koutrakis, P., Tsapakis, M., Lagoudaki, E., Stephanou, E. G., Von Baer, D., and Oyola, P. (2001) Source Apportionment of Urban Particulate Aliphatic and Polynuclear Aromatic Hydrocarbons (PAHs) Using Multivariate Methods, *Environ. Sci. Technol. 35*, 2288–2294.

15. Gelboin, H. V. (1980) Benzo[alpha]pyrene metabolism, activation and carcinogenesis: role and regulation of mixed-function oxidases and related enzymes, *Physiol. Rev. 60*, 1107–1166.
16. Liebler, D. C. (2008) Protein damage by reactive electrophiles: targets and consequences, *Chem. Res. Toxicol. 21*, 117–128.
17. Poirier, M. C., and Weston, A. (1996) Human DNA adduct measurements: state of the art, *Environ. Health Perspect. 104 Suppl 5*, 883–893.
18. Phillips, D. H., and Arlt, V. M. (2007) The 32P-postlabeling assay for DNA adducts, *Nat. Protoc. 2*, 2772–2781.
19. Godschalk, R. W., Van Schooten, F. J., and Bartsch, H. (2003) A critical evaluation of DNA adducts as biological markers for human exposure to polycyclic aromatic compounds, *J. Biochem. Mol. Biol. 36*, 1–11.
20. Knudsen, L. E., Ryder, L. P., and Wassennann, K. (1992) Induction of DNA Repair Synthesis in Human Monocytes/B-Lymphocytes Compared with T-Lymphocytes After Exposure to N-Acetoxy-N-Acetylaminofluorene and Dimethylsulfate in Vitro, *Carcinogenesis 13*, 1285–1287.
21. Beach, A. C., and Gupta, R. C. (1992) Human biomonitoring and the 32P-postlabeling assay, *Carcinogenesis 13*, 1053–1074.
22. Phillips, D. H., Hewer, A., and Arlt, V. M. (2004) 32P-Postlabeling Analysis of DNA Adducts. In *Molecular Toxicology Protocols*, pp 3 –12.
23. Phillips, D. H., and Castegnaro, M. (1993) Results of an interlaboratory trial of 32P-postlabelling, *IARC Sci. Publ.* 35–49.
24. Phillips, D. H., and Castegnaro, M. (1999) Standardization and Validation of DNA Adduct Postlabelling Methods: Report of Interlaboratory Trials and Production of Recommended Protocols, *Mutagenesis 14*, 301–315.
25. Brown, K. (2012) Methods for the Detection of DNA Adducts. In *Genetic Toxicology* (Parry, J. M., Parry, E. M., and Walker, J. M., Eds.), pp 207–230, Springer New York.
26. Hollstein, M., Sidransky, D., Vogelstein, B., and Harris, C. C. (1991) p53 mutations in human cancers, *Science 253*, 49–53.
27. Braithwaite, E., Wu, X., and Wang, Z. (1999) Repair of DNA lesions: mechanisms and relative repair efficiencies, *Mutat. Res. 424*, 207–219.
28. Day, B. W., Doxtader, M. M., Rich, R. H., Skipper, P. L., Singh, K., Dasari, R. R., and Tannenbaum, S. R. (1992) Human serum albumin-benzo[a]pyrene anti-diol epoxide adduct structure elucidation by fluorescence line narrowing spectroscopy, *Chem Res Toxicol 5*, 71–76.
29. Day, B. W., Skipper, P. L., Zaia, J., and Tannenbaum, S. R. (1991) Benzo[a]pyrene anti-diol epoxide covalently modifies human serum albumin carboxylate side chains and imidazole side chain of histidine(146), *J Am Chem Soc 113*, 8505–8509.
30. Lee, B. M., Yin, B. Y., Herbert, R., Hemminki, K., Perera, F. P., and Santella, R. M. (1991) Immunologic measurement of polycyclic aromatic hydrocarbon-albumin adducts in foundry workers and roofers, *Scand. J. Work. Environ. Health 17*, 190–194.
31. Sherson, D., Sabro, P., Sigsgaard, T., Johansen, F., and Autrup, H. (1990) Biological monitoring of foundry workers exposed to polycyclic aromatic hydrocarbons, *Br. J. Ind. Med. 47*, 448–453.

32. Käfferlein, H. U., Marczynski, B., Mensing, T., and Brüning, T. (2010) Albumin and hemoglobin adducts of benzo[a]pyrene in humans--analytical methods, exposure assessment, and recommendations for future directions, *Crit. Rev. Toxicol. 40*, 126–150.
33. Lee, B. M., and Santella, R. M. (1988) Quantitation of protein adducts as a marker of genotoxic exposure: immunologic detection of benzo[a]pyrene--globin adducts in mice, *Carcinogenesis 9*, 1773–7.
34. Tas, S., Buchet, J. P., and Lauwerys, R. (1994) Determinants of benzo[a]pyrene diol epoxide adducts to albumin in workers exposed to polycyclic aromatic hydrocarbons, *Int. Arch. Occup. Environ. Health 66*, 343–348.
35. Verma, N., Pink, M., Rettenmeier, A. W., and Schmitz-Spanke, S. (2012) Review on proteomic analyses of benzo[a]pyrene toxicity, *Proteomics 12*, 1731–1755.
36. Chung, M. K., Riby, J., Li, H., Iavarone, A. T., Williams, E. R., Zheng, Y., and Rappaport, S. M. (2010) A sandwich enzyme-linked immunosorbent assay for adducts of polycyclic aromatic hydrocarbons with human serum albumin, *Anal. Biochem. 400*, 123–129.
37. Lin, Y. S., McKelvey, W., Waidyanatha, S., and Rappaport, S. M. (2006) Variability of albumin adducts of 1,4-benzoquinone, a toxic metabolite of benzene, in human volunteers, *Biomarkers Biochem. Indic. Expo. Response Susceptibility Chem. 11*, 14–27.
38. McClean, M. D., Rinehart, R. D., Ngo, L., Eisen, E. A., Kelsey, K. T., Wiencke, J. K., and Herrick, R. F. (2004) Urinary 1-hydroxypyrene and polycyclic aromatic hydrocarbon exposure among asphalt paving workers, *Ann. Occup. Hyg. 48*, 565–578.
39. McClean, M. D., Wiencke, J. K., Kelsey, K. T., Varkonyi, A., Ngo, L., Eisen, E. A., and Herrick, R. F. (2007) DNA adducts among asphalt paving workers, *Ann. Occup. Hyg. 51*, 27–34.
40. Keller, B. O., Sui, J., Young, A. B., and Whittal, R. M. (2008) Interferences and contaminants encountered in modern mass spectrometry, *Anal. Chim. Acta 627*, 71–81.
41. Trott, O., and Olson, A. J. (2010) AutoDock Vina: improving the speed and accuracy of docking with a new scoring function, efficient optimization, and multithreading, *J. Comput. Chem. 31*, 455–461.
42. Humphrey, W., Dalke, A., and Schulten, K. (1996) VMD: visual molecular dynamics, *J. Mol. Graph. 14*, 33–38, 27–28.
43. Stone, J. E. (1998) An Efficient Library For Parallel Ray Tracing And Animation.
44. Day, B. W., Skipper, P. L., Zaia, J., Singh, K., and Tannenbaum, S. R. (1994) Enantiospecificity of Covalent Adduct Formation by Benzo[a]pyrene anti-Diol Epoxide with Human Serum Albumin, *Chem Res Toxicol 7*, 829–835.
45. Bjerner, J., Børmer, O. P., and Nustad, K. (2005) The War on Heterophilic Antibody Interference, *Clin. Chem. 51*, 9–11.
46. Fahie-Wilson, M., and Halsall, D. (2008) Polyethylene glycol precipitation: proceed with care, *Ann. Clin. Biochem. 45*, 233–235.
47. Ismail, A. A. A. (2005) A Radical Approach Is Needed to Eliminate Interference from Endogenous Antibodies in Immunoassays, *Clin. Chem. 51*, 25–26.
48. Ismail, A. A. A. (2009) Interference from endogenous antibodies in automated immunoassays: what laboratorians need to know, *J. Clin. Pathol. 62*, 673–678.
49. Chiu, Norman H.L., and Christopoulos, Theodore K. (2012) Advances in Immunoassay Technology, InTech, Rijeka, Croatia.

50. Hoofnagle, A. N., and Wener, M. H. (2009) The fundamental flaws of immunoassays and potential solutions using tandem mass spectrometry, *J. Immunol. Methods 347*, 3–11.
51. Crawford, F. G., Mayer, J., Santella, R. M., Cooper, T. B., Ottman, R., Tsai, W. Y., Simon-Cereijido, G., Wang, M., Tang, D., and Perera, F. P. (1994) Biomarkers of environmental tobacco smoke in preschool children and their mothers, *J. Natl. Cancer Inst. 86*, 1398–1402.
52. Autrup, H., Vestergaard, A. B., and Okkels, H. (1995) Transplacental transfer of environmental genotoxins: polycyclic aromatic hydrocarbon-albumin in non-smoking women, and the effect of maternal GSTM1 genotype, *Carcinogenesis 16*, 1305–1309.
53. Alexandrov, K., Cascorbi, I., Rojas, M., Bouvier, G., Kriek, E., and Bartsch, H. (2002) CYP1A1 and GSTM1 genotypes affect benzo[a]pyrene DNA adducts in smokers' lung: comparison with aromatic/hydrophobic adduct formation, *Carcinogenesis 23*, 1969–1977.
54. Uppstad, H., Osnes, G. H., Cole, K. J., Phillips, D. H., Haugen, A., and Mollerup, S. (2011) Sex differences in susceptibility to PAHs is an intrinsic property of human lung adenocarcinoma cells, *Lung Cancer Amst. Neth. 71*, 264–270.
55. Mollerup, S., Berge, G., Baera, R., Skaug, V., Hewer, A., Phillips, D. H., Stangeland, L., and Haugen, A. (2006) Sex differences in risk of lung cancer: Expression of genes in the PAH bioactivation pathway in relation to smoking and bulky DNA adducts, *Int. J. Cancer J. Int. Cancer 119*, 741–744.
56. Cheng, Y.-W., Hsieh, L.-L., Lin, P.-P., Chen, C.-P., Chen, C.-Y., Lin, T.-S., Su, J.-M., and Lee, H. (2001) Gender difference in DNA adduct levels among nonsmoking lung cancer patients, *Environ. Mol. Mutagen. 37*, 304–310.
57. Shinozaki, R., Inoue, S., Choi, K. S., and Tatsuno, T. (1999) Association of benzo[a]pyrene-diol-epoxide-deoxyribonucleic acid (BPDE-DNA) adduct level with aging in male smokers and nonsmokers, *Arch. Environ. Health 54*, 79–85.
58. Ramdahl, T., Becher, G., and Bjoerseth, A. (1982) Nitrated polycyclic aromatic hydrocarbons in urban air particles, *Environ. Sci. Technol. 16*, 861–865.
59. Shen, H., Huang, Y., Wang, R., Zhu, D., Li, W., Shen, G., Wang, B., Zhang, Y., Chen, Y., Lu, Y., Chen, H., Li, T., Sun, K., Li, B., Liu, W., Liu, J., and Tao, S. (2013) Global atmospheric emissions of polycyclic aromatic hydrocarbons from 1960 to 2008 and future predictions, *Environ. Sci. Technol.*

Tables

Table 1. Accuracy and precision of the revised ELISA (paired measurement with SSC) with different amounts of BPDE-HSA.

	BPDE-HSA added		
	0.4 ng	**2 ng**	**10 ng**
Absorbance			
BPDE tetrols added	0.175	0.341	0.786
BPDE tetrols not added	0.222	0.583	1.679
Recovery (%)			
With SSC	103	104	115
Without SSC	164	176	177
CV[a] (%)			
Intraday	17.2	5.05	7.55
Interday	7.50	6.37	14.4

Three sets of triplicate experimental/background pairs of spiked plasma were analyzed on 13 different days.

[a] Calculated from the data calibrated by SSC

Table 2. ELISA measurements of BPDE-HSA in smokers and nonsmokers.

Characteristic	No. of Samples[b]	No. excluded[d]	BPDE-HSA (ng/mg HSA)[a] Geo. mean	Min.	Max.
Male					
Nonsmokers	8	0	0.529	0.280	1.08
Smokers	10	0	0.941	0.356	2.88
Total	18	0	Fold change = 1.78[c]		
Female					
Nonsmokers	7	1	0.710	0.412	1.20
Smokers	10	2	0.577	0.335	1.25
Total	17	3	Fold change = 0.813		

Archive specimens from (*37*).

[a] Note that 1 ng BPDE-HSA is equivalent to 14.96 fmol of BPDE, assuming the molecular weight of BPDE-HSA is 66863 and 100% 1:1 binding ratio in BPDE-HSA.

[b] Each sample represents plasma pooled from 4 or 5 subjects.

[c] *p*-value = 0.035.

[d] All samples are excluded because measurements had *min > y* absorbance readings.

Table 3. ELISA measurements of BPDE-HSA in highway workers.

Characteristic	No. of samples	No. excluded[e]	BPDE-HSA (ng/mg HSA)[a] Geo. mean	Min.	Max.
Job					
Paving	56	4	1.55	0.475	13.9
Construction	24	8	1.53	0.346	6.08
Total	80	12	Fold change= 1.01		
Season					
Spring	8	0	1.15	0.620	2.15
Summer	31	5	1.37	0.475	5.99
Fall	15	7	1.29	0.346	4.56
Winter	26	0	2.39	0.556	13.9
Total	80	12	Fold change = 2.08[b]		
Task[d]					
Construction	16	4	1.18	0.346	5.99
Paver operator	6	1	1.20	0.475	2.15
Raker	21	0	1.29	0.525	4.56
Screedman	11	0	1.55	0.538	3.36
Total	54	5	Fold change = 1.31[c]		

Archive specimens from (*38*, *39*).

[a] Note that 1 ng BPDE-HSA is equivalent to 14.96 fmol of BPDE, assuming the molecular weight of BPDE-HSA is 66863 and 100% 1:1 binding ratio in BPDE-HSA.

[b] *p*-value = 0.041.

[c] *p*-value = 0.037.

[d] Excluding winter samples.

[e] 9/12 samples are excluded because BPDE-HSA levels differed by more than 10-fold across quadruplicate measurements

Figures

Figure 1. Sandwich ELISA for direct measurement of BPDE-HSA in plasma. After centrifugation, plasma is mixed with reagents and loaded into pairs of wells in a precoated plate. Because the anti-HSA detection antibody responds to both BPDE-HSA (about 1 nM in plasma) and unadducted HSA (about 1 mM in plasma), a high background signal is created from amplification of nonspecifically bound HSA on well surfaces. To overcome this problem, paired measurements (''background'' and ''sample'') are obtained for each plasma sample in quadruplicate and the signals are deconvoluted and calibrated by a sample-specific calibration procedure (SSC) (Figure 3). Background wells are treated with BPDE tetrols to deactivate the capture antibody (8E11) and thereby to produce matched controls. To minimize measurement errors, each result is screened for validity using predetermined rules. Valid samples are used for statistical analyses and invalid samples are treated as missing observations.

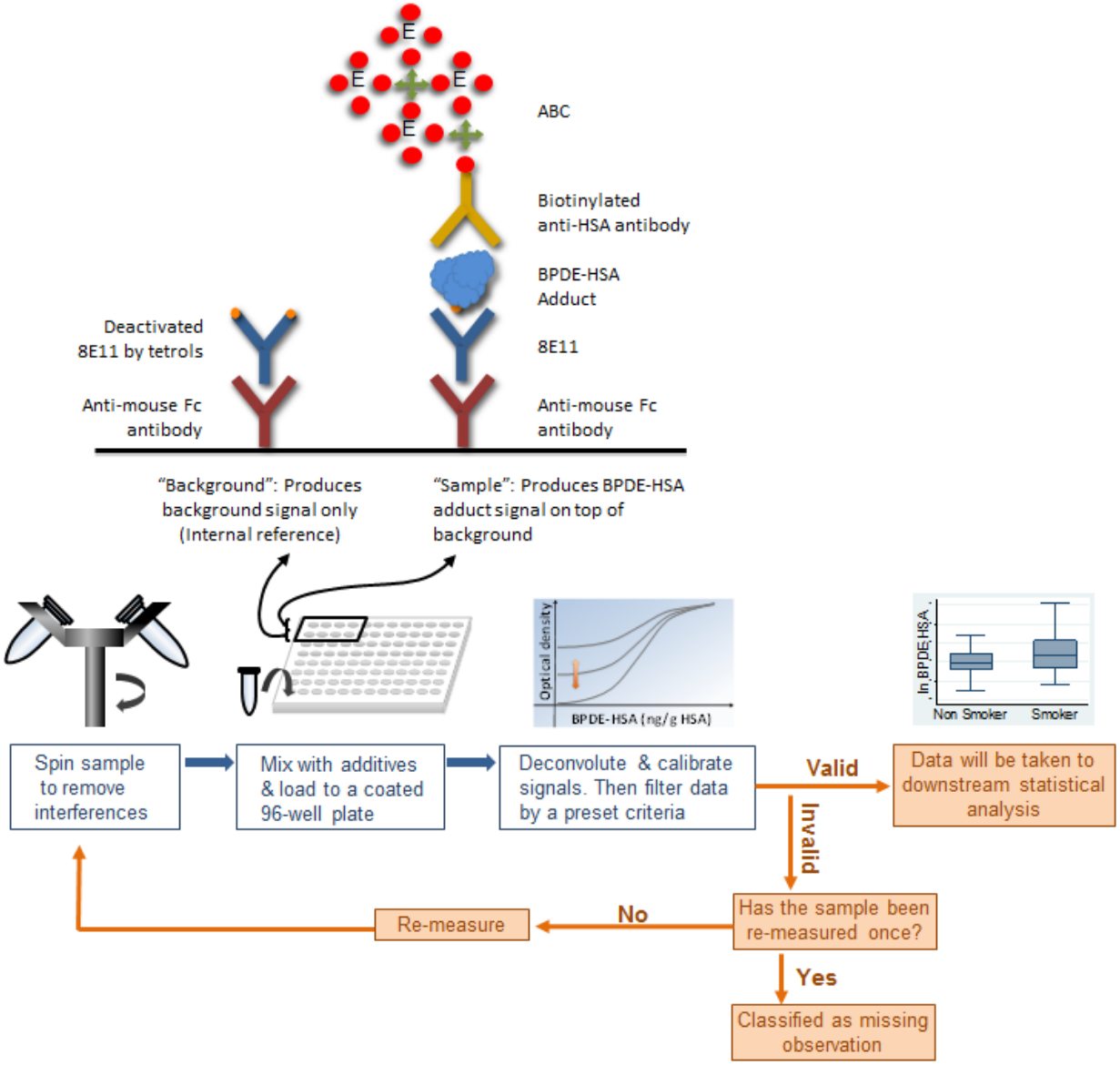

Figure 2. Molecular model of BPDE-HSA. A) View of BPDE-HSA showing the side with Asp187, Glu188, Lys195 (in blue). B) View of BPDE-HSA showing the side with His146 (In blue but hidden). BPDE adducts at His146 and Lys195 are shown in red and those to Asp187 and Glu188 are in green. The inset figures show the corresponding HSA domains in color. Domain I, II and III are represented in red, brownish orange and light green, respectively. All potential modification sites are located on domain I (residues 1-195) and BPDE is likely to occupy the space in the interfaces between domains. According to the shotgun proteomics results, BPDE likely occupies a shared space when modifying Asp187, Glu188 or Lys195.

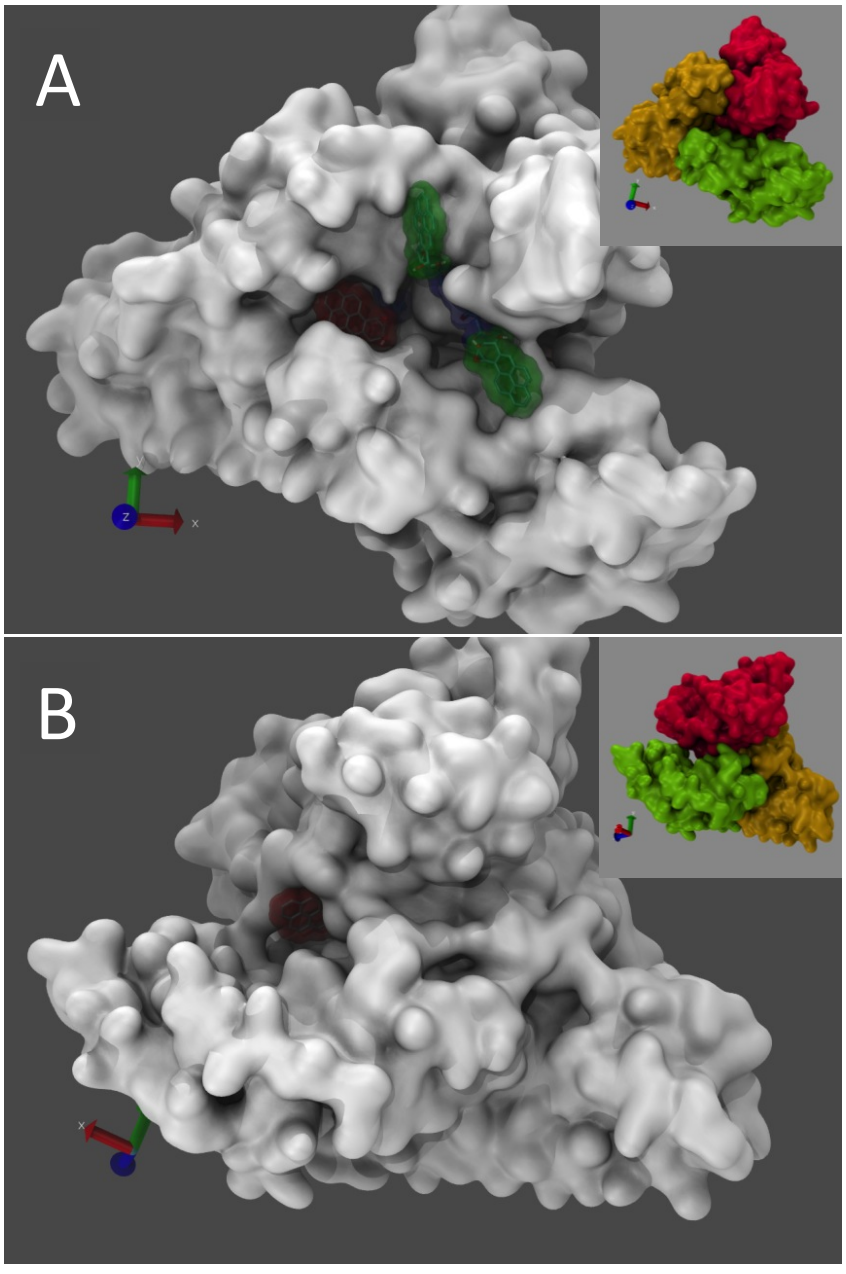

Figure 3. Sample-specific calibration (SSC). In any non-linear calibration curve, the relationship between the signal and concentration of an analyte is dynamic. The concentration information is encoded into the 1) signal difference between "signal" and "background" and also 2) the level of the background signal. Traditional calibration approaches simplify the procedure by matching the background level between the standard curve and the samples. In contrast, SSC provides an unbiased estimation of analyte concentration in a background-varying scenario, thereby creating a calibration curve for each sample. To begin, each standard or plasma sample is split into pairs of wells to determine 'background' (*min*) and 'sample' (*y*) absorbance readings (see Figure 1). A set of BPDE-HSA standards is used to develop a sigmoid standard curve [Eq. (1)], the shape of which is influenced by the particular background reading (*min*) as well as the *Hillslope* variable. The solid curve represents a standard curve obtained from BPDE-HSA standards (in buffer) where *min* = 0.026 absorbance units, *max* = 2.7 absorbance units, log(*IC50*) = 2.53 and *Hillslope* = 0.5. Having established the standard curve with buffer solution, the value of *min* for each plasma specimen is substituted into the sigmoid function to solve for 10^x, representing the concentration of BPDE-HSA (ng/mg HSA) in that plasma specimen. The three dashed curves in the figure represent background plasma readings where *min* = 0.26, 0.76 and 1.1 absorbance units, respectively.

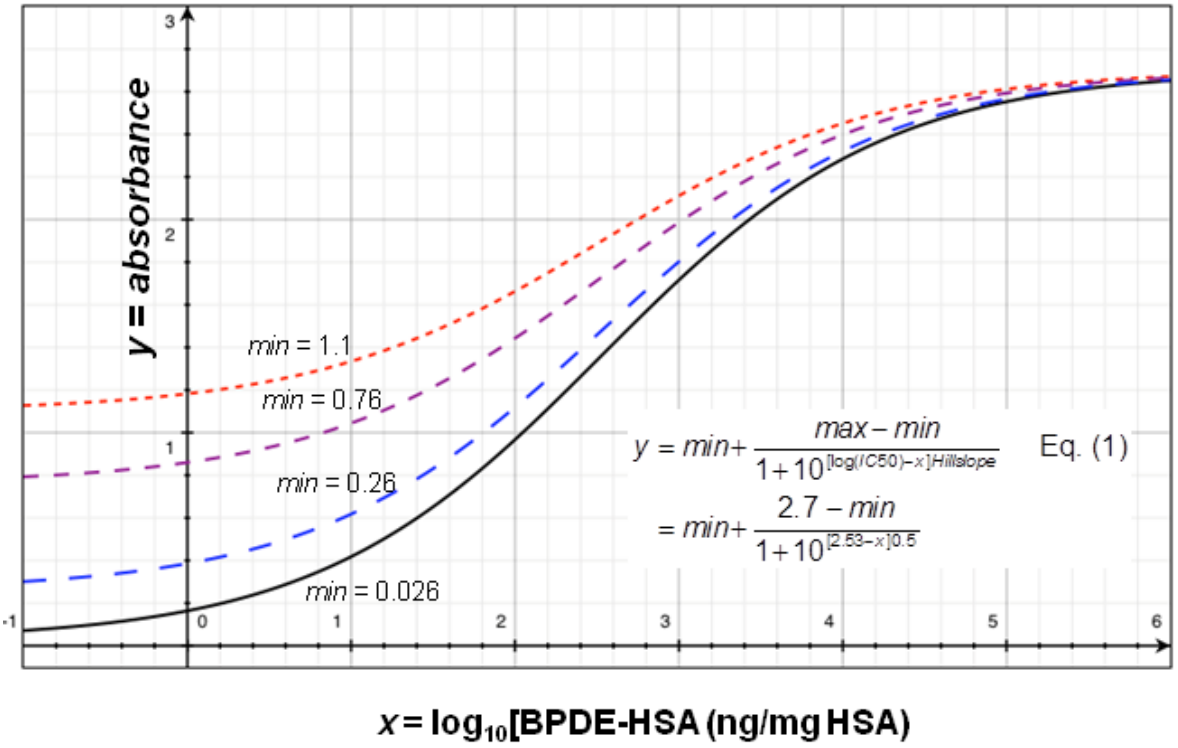

Figure 4. Tandem mass spectra of the triply charged precursor ion at *m/z* 734.70 (BPDE adduct of peptide RHPYFYAPELLFFAK) obtained by ETD activation (a) or CID activation (c) and tandem mass spectra of the doubly charged precursor ion at *m/z* 525.25 (BPDE adduct of peptide ASSAKQR) obtained by ETD activation (b) or CID activation (d).

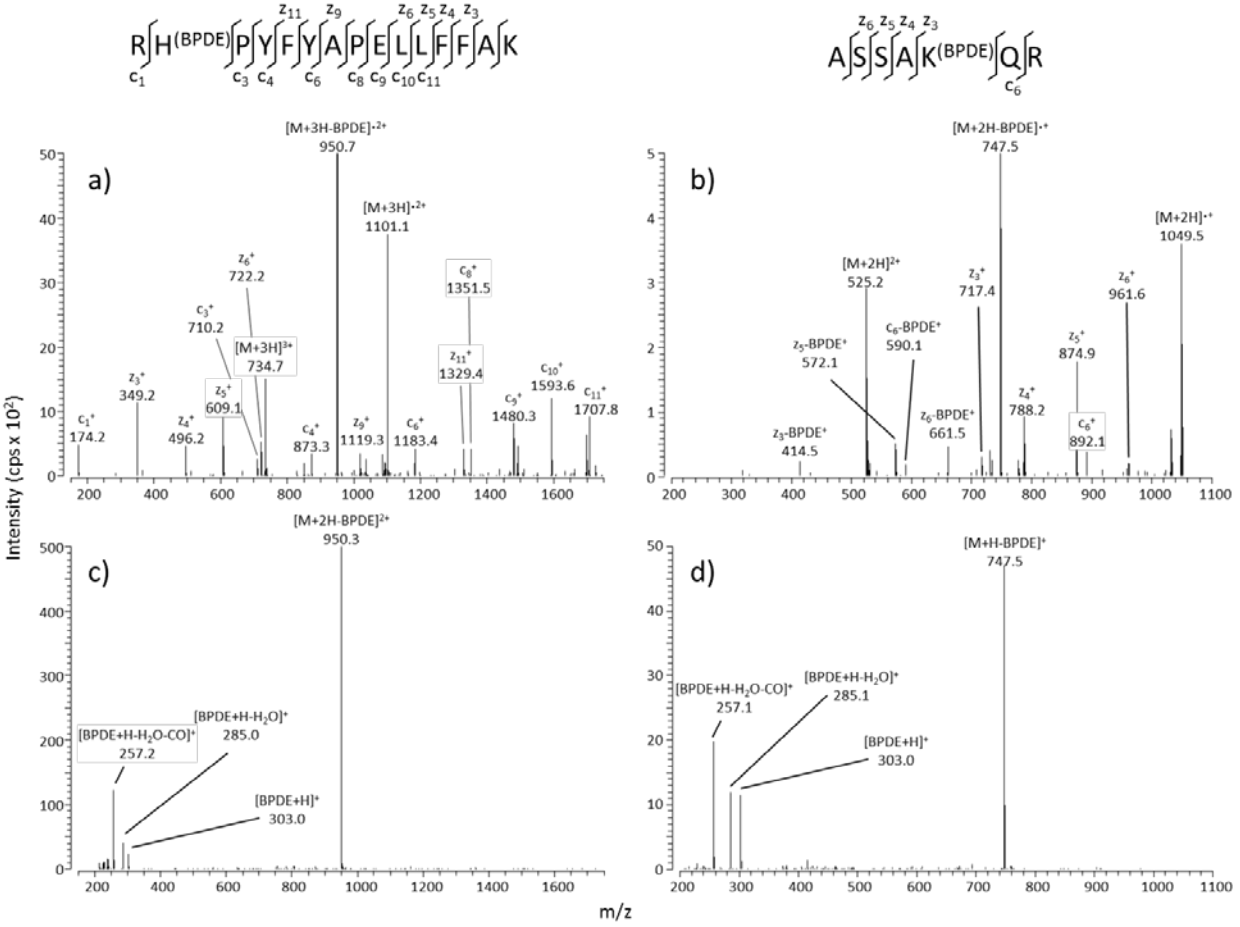

Figure 5. Box-plot comparing the ln BPDE-HSA level (ng/mg HSA) between pooled samples of plasma from smokers (n = 18) and nonsmokers (n = 14).

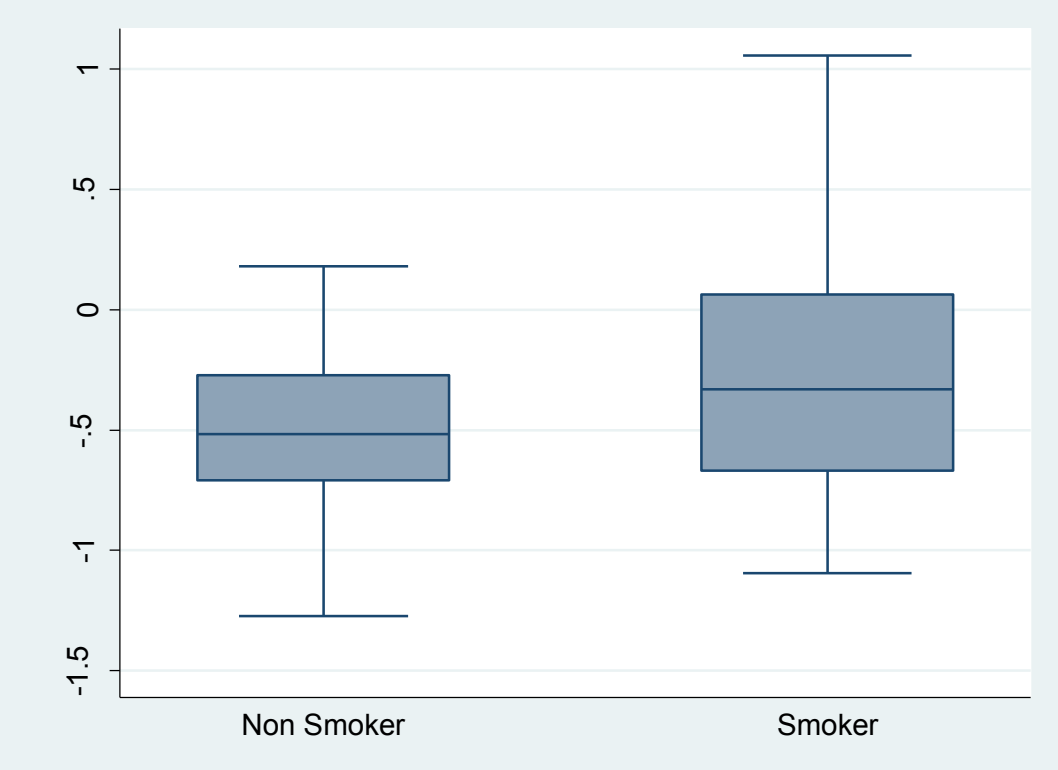

Figure 6. Scatter plot of ln BPDE-HSA (ng/mg HSA) shows against the average number of cigarette smoked per day in pooled plasma samples.

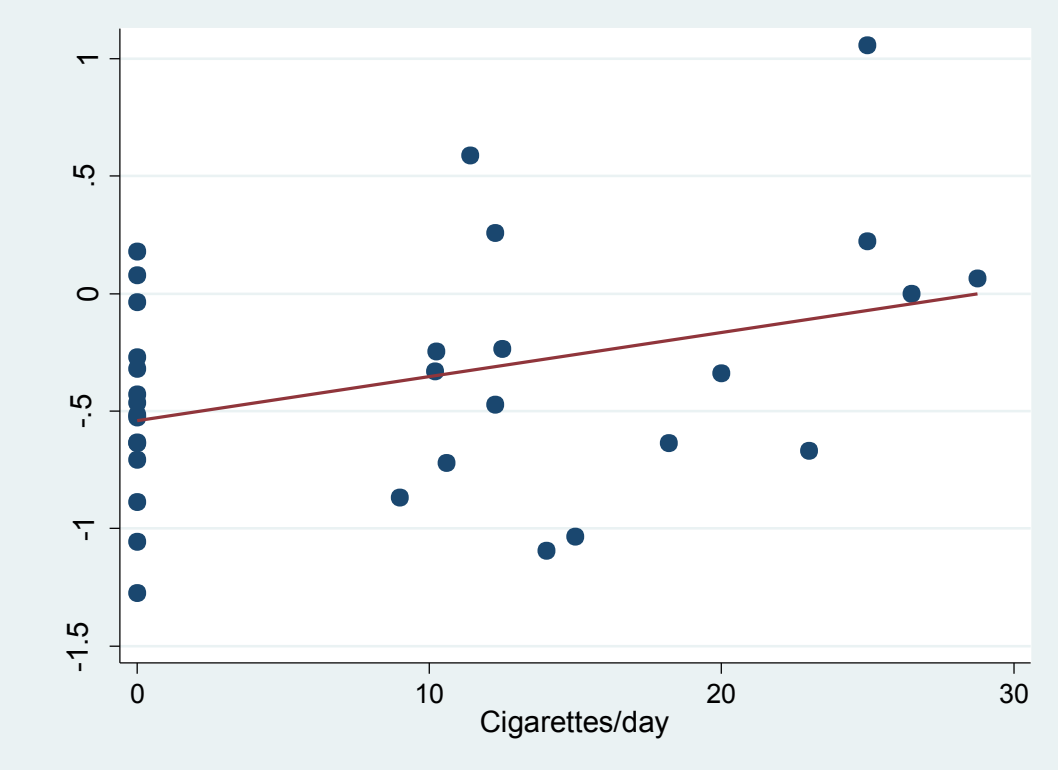

Figure 7. Box-plot comparing the ln BPDE-HSA level (ng/mg HSA) of asphalt paving workers working in different seasons. Samples are come from the original study by McClean *et al.* (2004).

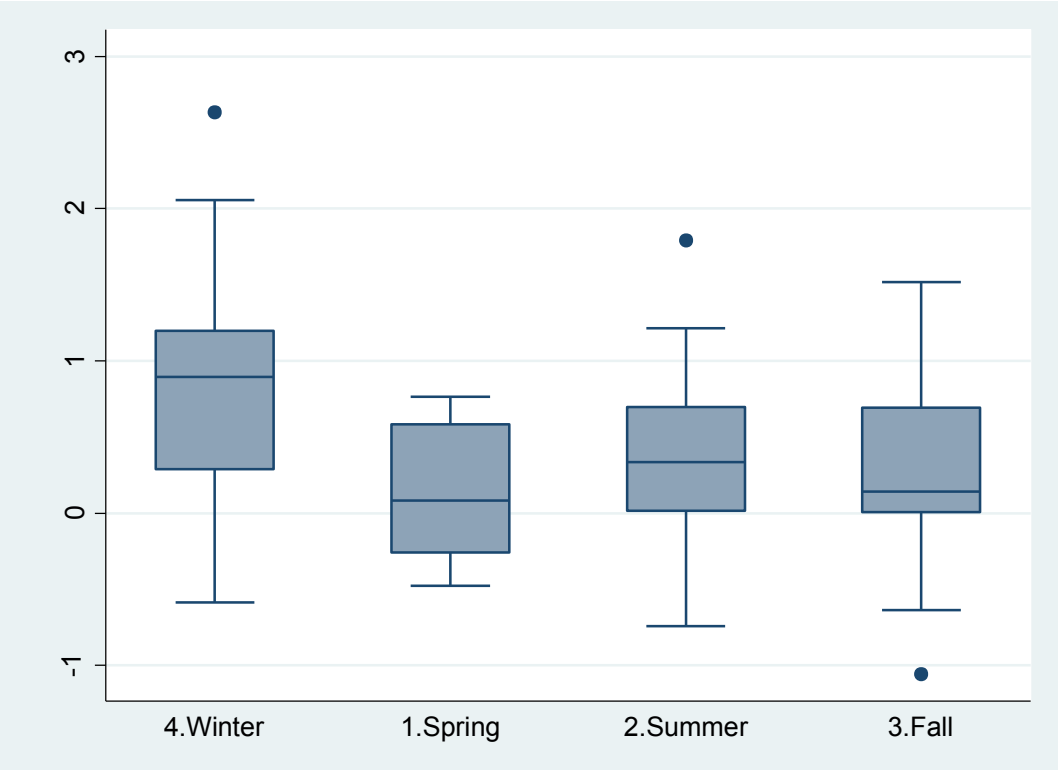

Figure 8. Box-plot comparing the ln BPDE-HSA level (ng/mg HSA) of asphalt paving workers with different tasks (excluding winter season). Samples are come from the original study by McClean *et al.* (2004).

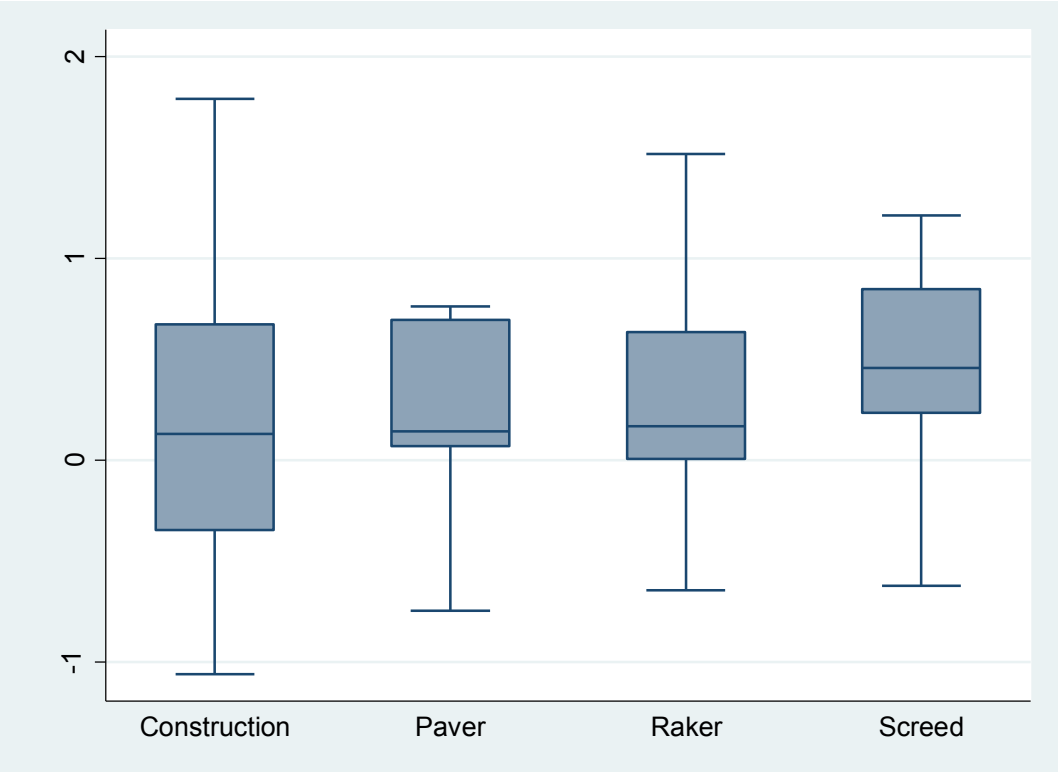

Chapter 4

A Semi-Targeting Immunomagnetic Enrichment Method for Measuring the Albumin Cys34 Adductome by Mass Spectrometry

Introduction

Electrophilic species are inherently toxic because of their ability to react with functional nucleophilic sites in DNA and proteins, thereby damaging organs, initiating and promoting tumor development, and contributing to chronic diseases (*1*–*3*). Because electrophiles are generally too reactive to measure directly in biological systems, investigators have identified and quantified adducts, resulting from reactions between electrophilic species and target nucleophiles in blood, cells or tissues (*4*–*6*). For investigating human exposures to targeted electrophiles, adducts of hemoglobin and human serum albumin (HSA) have been extensively investigated because of the abundance and relatively long residence times (1 - 2 months) of hemoglobin and HSA in human blood (*7*). Recent interest in untargeted analysis of adducts (adductomics) for investigating causes of human diseases has focused upon Cys34 of HSA, which is the most active and abundant nucleophile in serum (*8*).

Rappaport *et al.* defined the adductome as the totality of covalent adducts present in a biospecimen (*8*) and have developed a proteomics method for investigating the HSA-Cys34 adductome (*9*–*12*) in human serum or plasma. In brief, HSA is isolated from serum or plasma, enriched for Cys34 by thiol-affinity chromatography, and digested with trypsin. The tryptic peptides are fractionated by off-line high performance liquid chromatography (HPLC) and the Cys34-containing peptides (T3 peptides) are detected *en masse* by a novel application of selected-reaction monitoring - called fixed-step SRM - involving triple-quadrupole mass spectrometry (TSQ MS). Quantitation is based upon an isotopically-labeled T3, which is added to the tryptic digest. Adducts are visualized in a heat map showing hits in *m/z* bins for HSA specimens from different human samples of interest. The identities of particular adduct hits can be explored with follow-up experiments involving high resolution MS, adduct database searches, and comparisons with synthetic T3 adducts (*9*).

Not surprisingly, the above analytical scheme is lengthy and has drawbacks that limit detection and identification of unknown HSA-Cys34 adducts. First, human serum or plasma is a complex matrix containing as many as 20,000 proteins (*13*). Although HSA is the most abundant serum protein, there is no simple, non-denaturing method for isolating and recovering HSA in high purity. Second, because only about 5% of HSA contains covalent Cys34 adducts of interest (*14*), enrichment of Cys34 adducts is necessary to achieve sufficient sensitivity to detect minor constituents. The current enrichment method uses thiol-affinity resins to remove mercaptalbumin (i.e. unadducted HSA-Cys34) and requires overnight incubation and tedious buffer exchange prior to digestion. Third, because enzymatic digestion increases the complexity of the matrix, chromatographic fractionation is necessary prior to MS

but is not sufficient to eliminate co-eluting peptides that can suppress ionization of the T3 adducts, increase background noise, reduce adduct detection rates, and contribute to false positives.

As an alternative strategy for detecting and identifying HSA-Cys34 adducts, Anderson *et al.* used anti-peptide antibodies to enrich peptide analytes about 1000-fold in a protein digest (*15*–*17*). Similar enrichment methods have also been used in applications of proteomics, which focus on post translational modifications such as phosphoproteomics, employing phospho-site specific antibodies (*18*), immobilized metal affinity chromatography (IMAC) (*19*) and titanium dioxide chromatography (*20*). Though promising, these targeted methods have limited applicability to discovery-based adductomics where the goal is to detect all peptides containing unknown modifications at a given locus.

Here, a semi-targeted, immuno-enrichment method employing a polyclonal anti-T3 antibody is described. The basic design principle is to focus upon the modified side-chain of Cys34 while regarding the flank sequences on both the C and N termini as conserved structural epitopes. As shown in Figure 1, in this chapter, 1) the anti-T3 antibody design is described and cross-reactivit y of the antibody to 4 T3-quinone adducts is tested; 2) the immune-enrichment method is characterized with 4 different magnetic beads; and 3) a hybrid analytical platform (immuno-enrichment + LC-MS) is established and validated for adductomic studies with plasma samples from healthy volunteers.

Materials & Methods

Chemicals & Reagents

The following chemicals and reagents were purchased from the corresponding vendors: Fisher Scientific (Pittsburgh, PA): ThermalSeal® adhesive films, Tris-buffered saline (TBS, 10x), acetonitrile (Optima grade, 99.9%), formic acid (Optima®, LC-MS Grade), iodoacetamide (IAA), dimethylsulfoxide (DMSO), ammonium sulfate, methanol (LC-MS grade), TCEP, acetic acid (LC-MS grade), Tris Base (≥ 99.9 %); Sigma-Aldrich (St. Louis, MO): Carbonate-bicarbonate buffer, Tween 20, 1,4-benzoquinone (1,4-BQ), 1,4-naphtoquinone (1,4-NQ), 4-hydroxyestradiol (4-OH-E_2) and silver(I) oxide, porcine trypsin, ammonium bicarbonate, HSA (lyophilized powder, 97-99%), soybean trypsin inhibitor (Type I-S, lyophilized powder); Bethyl Lab, Inc. (Montgomery, TX): TMB peroxidase substrate; Thermo Scientific (Rockford, IL): SuperBlock®, ABC Peroxidase kits.

The followings chemicals were custom synthesized: Midwest Research Institute (MRI, Camp LeJeune, NC): 1,2-phenanthrenequinone (1,2-PQ); Biomatik (Wilmington, DE): T3 peptide (ALVLIAFAQYLQQCPFEDHVK); BioMer Technology (Pleasanton, CA): Isotopically-modified T3 (iT3) with sequence AL-[^{15}N, ^{13}C-Val]-LIAFAQYLQQCPFEDH-[^{15}N, ^{13}C-Val]-K.

Synthesis of Internal Standard and T3 Adducts

Stock solutions of T3 and iT3 were prepared in DMSO at 5 mM and then diluted with water or methanol to a final concentration of 100 μM. A Cys34 adduct of iT3 (iT3-IAA) was used as an internal standard. Individual T3 adducts (modified at Cys34) of diol and quinone forms of 1,4-BQ, 1,4-NQ and 1,2-PQ and iT3-IAA were prepared as described (*21*). To prepare reduced and oxidized forms of T3-EQ, 3,4-estrogen quinone (3,4-EQ) was first synthesized by dissolving

1 mg of 4-OH-E_2 in 500 μl methanol and incubating with a 7-fold molar excess of silver(I) oxide at room temperature for 40 min. After precipitating the silver(I) oxide by spinning, 30 μl of supernatant was incubated with 100 μl T3 stock in the dark for 6 h at room temperature.

The internal standard and T3 adducts were subsequently purified by HPLC using a C18 column (5 μm, 250 mm x 4.6 mm, 300 Å pore size) and the yields were determined by TSQ MS in selected ion monitoring (SIM) mode. Final stock solutions of adducts were in 30-45% acetonitrile, 0.1% formic acid with a concentration of around 20 μM (iT3-IAA) and 100 μM (T3 adducts, reported as a sum of oxidized and reduced quinione forms) and were stored at -80°C prior to use. Full preparation details are reported in Li *et al.* and Grigoryan *et al.* (*21*, *22*).

Predicting the 3D Structure of the T3 peptide

A 3D model of the T3 peptide in aqueous solution was constructed to assist the design of the immunogen preparation strategy for anti-T3 antibody. To begin, T3 amino acid sequence (ALVLIAFAQYLQQCPFEDHVK, from Ala21 to Lys41) was obtained from *in silico* digestion of HSA (UniProt identifier: P02768) with trypsin using ProteinProspector (prospector.ucsf.edu). Other than removing all the variable modifications and setting the maximum missed cleavages to 0, default settings were used. Next, the T3 sequence was input to the I-TASSER (*23*) and PEP-FOLD (*24*) servers with the default settings and leaving additional restraints or exclusion blank. Finally, Visual Molecular Dynamics (VMD, v.1.9.1) (*25*) was used to create molecular representations of predicted 3D structures and the images were rendered with Tachyon (Figure 2).

Aligning the N- and C- Terminal T3 sequence

To determine the effects of truncating the T3 sequence, the homologous protein and overlapping sequences were searched with the BLAST server (blast.ncbi.nlm.nih.gov). The N terminal (ALVLIAFAQYLQQ) and C terminal (PFEDHVK) sequences were used and aligned with the human proteins (taxid:9606) curated in the NCBI reference protein database. Short query automatic adjustment was selected and the blastp algorithm (*26*) was then applied with all the default parameters unchanged. Parts of the alignment results are shown in Table 1 and Table 2.

Production of Anti-T3 Antibody

The polyclonal anti-T3 antibody was prepared to the specifications under contract by Genscript (Piscataway, NJ). In brief, T3 peptide (2433 Da) was synthesized by Genscript to 92% purity. Then, Genscript prepared the immunogen by coupling the sulfhydryl group from the endogenous Cys34 residue on T3 to keyhole limpet hemocyanin (KLH) with a maleimide hetero-bifunctional crosslinker. Then, Genscript mixed the immunogen with with adjuvant and injected into 3 rabbits; immunizations were repeated twice over the course of 8 weeks. After immunization, Genscript screened rabbit antisera for titer quality by ELISA. Because the immunogen was a KLH conjugate instead of multiple antigen peptides, antibody clones responded to KLH and the Genscript removed the crosslinker from antisera by peptide affinity purification, using an affinity resin conjugated to the Cys34 residue of the T3 peptide. Genscript the purified anti-T3 antibody which was then biotinylated and characterized by ELISA. The final product was lyophilized and stored at -80°C prior to shipment to the laboratory. Prior to use, the anti-T3 antibody was dissolved in water at mg/ml.

Cross-Reactivity of the Anti-T3 Antibody

A direct ELISA was used to characterize the cross-reactivity of the anti-T3 antibody. Unless otherwise specified: the loading volume was 100 µl/well; plates were rinsed with TBS-T (0.05% Tween) 3 times at 200 µl/well between incubation steps; and incubations were performed for 45 min at 37°C. In brief, T3, reduced and oxidized forms of T3-BQ, T3-NQ, T3-PQ, T3-EQ and solvent controls were serially diluted 2x and coated onto a 96-well MaxiSorp™ plate (with 0.1 M carbonate-bicarbonate buffer, starting from 60 nM/well). After overnight incubation at 4°C, the plate was blocked with SuperBlock® at 200 µl/well and (biotinylated) anti-T3 antibody (0.5 µl/ml) was transferred to the wells. Then, ABC was added and the plate was incubated at room temperature for 30 min. Finally, TMB was loaded and the plate was incubated for another 30 min, in the dark. Color intensity was measured at 652 nm with a microplate spectrophotometer (ELx800, Bio-Tek, Winooski, VT). Results from direct ELISA were plotted by Qtiplot (v. 0.9.8.3, ProIndep Serv SRL) (*27*) (Figure 3).

Binding Affinities of the Anti-T3 Antibody

Binding affinities of the anti-T3 antibody to various T3-quinone adducts were estimated via their dissociation constant (Kd) according to the method of Friguet *et al*. (*28*), with minor modifications. A 96-well plate (BD Falcon™) was blocked with SuperBlock® overnight (at room temperature, 250 µl/well). Then, T3 and T3 quinones were loaded and serially diluted 2x with SuperBlock® (from 0.6 µM/well, 100 µl/well) and the anti-T3 antibody was added (4 nM, 50 µl/well) with a final volume of 150 µl/well. The mixture was incubated overnight in the dark at room temperature. Another 96-well MaxiSorp™ plate was coated with T3 and T3 quinones dissolved in 0.1 M carbonate-bicarbonate buffer (20 nM, 100 µl/well). After being incubated overnight at 4°C, the MaxiSorp™ plate was washed and blocked, and 100 µl of the anti-T3 antibody mixtures were transferred to the wells coated with the corresponding antigens. After incubation for 1 h at room temperature, ABC was loaded, followed by TBM (both with 30 min incubation). The color intensity was measured at 652 nm with a microplate spectrophotometer. Dissociation constants (Kd) for T3 and T3 quinones were calculated with Excel (v. 14, Microsoft).

Human Plasma Samples

Fresh human plasma samples were collected from three volunteer subjects and prepared as described by Grigoryan *et al.* (*22*). Briefly, HSA was partially purified by precipitation with saturated ammonium sulfate by mixing with plasma samples at a ratio of 2:3 (v:v). The supernatant was buffer exchanged and free Cys34-HSA containing molecules were removed by mixing with a thiol affinity Sepharose 4B resin in a 0.45 µm pore size centrifuge-filter tube. After overnight incubation at room temperature, the flow-through fraction was collected, buffer exchanged with digestion buffer (50 mM ammonium bicarbonate, 1 mM EDTA, pH 8) and the total protein content was measured by a Nanodrop spectrophotometer (ND-1000, Thermo Scientific).

Prior to digestion, enriched HSA from plasma, described above, or commercial HSA was diluted to 1 mg/ml in digestion buffer containing 10% methanol and 5 mM TCEP. Samples were incubated for 15 min at 37^{o}C to reduce disulfide bonds Trypsin was added at a ratio of 1:10 (trypsin to peptide, w:w) and the mixture was digested in a barocycler (Barocycler NEP2320, Pressure Biosciences Inc.) cycling between ambient pressure (15 s) and 20,000 psi (45 s) at 37°C

for 30 min. The digest was transferred to a glass vial with addition of trypsin inhibitor (1:3, trypsin to inhibitor, w:w) and stored at -80°C prior to immuno-enrichment.

Immunomagnetic Enrichment of T3 Adducts

Digested samples of HSA were diluted 10x with 10 mM Tris buffer (pH 7) to a final volume of 200 μl in a 1.5 ml tube. For each treatment, a selected volume of stock solution containing anti-T3 antibody was added and incubated for 1 h in 37°C. Dynabeads® (M270, M280, C1 or T1, Invitrogen Life Technologies, Grand Island, NY) were washed 3 times with TBS before mixing with the incubated digest at a ratio suggested by the bead manufacturer. The tube was mounted on a rotor (Labquake Rotisserie, Thermo Scientific) and incubated for 30 min at room temperature. After the bead-anti-T3-adduct complexes were formed, beads were washed twice with 10 mM Tris (pH 7) and then twice with deionized water. The T3 adducts were released from the complexes by eluting with 1% acetic acid (3 times, 21.34 μl each) and then diluting to 80 μl with acetonitrile. Finally, all samples were spiked with iT3-IAA to a concentration of 0.2 pmol/μl.

Mass Spectrometry

The instrumental settings described in Grigoryan *et al.* were employed with minor modifications (*22*). Samples were analyzed using an Agilent 1200 HPLC (Santa Clara, CA) that was connected in-line with an LTQ Orbitrap XL hybrid MS equipped with an Ion Max electrospray ionization source (ESI; Thermo Fisher Scientific, Waltham, MA).

The HPLC employed a reverse-phase, C8 analytical column (300SB Zorbax, 1.0 × 150 mm, 3.5-μm particles, 300Å pore size, Agilent) with a flow rate of 80 μl/min. Solvent A was H_2O/0.1% FA (v/v) and solvent B was ACN/0.1% FA (v/v). An injection volume of 40 μl (partial loop injection mode) was used. The elution program consisted of a linear gradient from 2 % to 25 % B over 5 min, an isocratic hold for 5 min, a linear gradient to 60 % B over 40 min, and then a rapid increase to 98 % B over 0.5 min followed by an isocratic hold for 15 min and re-equilibrium of the system at 2% B for 25 min.

Mass spectra were acquired in the positive ion mode over the range m/z = 750 to 1000 using the Orbitrap mass analyzer, in profile format, with a resolution setting of 6×10^4 (at m/z = 400, measured at full width at half maximum peak height). In the data-dependent mode, the six most intense precursor ions exceeding an intensity threshold of 10,000 counts were selected from each full mass spectrum for further MS/MS analysis using collision-induced dissociation (CID). MS/MS spectra were acquired in the positive ion mode using the linear ion trap, in profile format, with the following parameters: precursor ion mass range for data-dependent MS/MS m/z = 750 to 1000, isolation width 3 m/z units, normalized collision energy 28 %, activation time 30 ms, activation Q 0.25, and default charge state +3. Only triply charged precursor ions were allowed for CID fragmentation from data-dependent MS/MS analysis. To avoid the occurrence of redundant MS/MS measurements, real-time dynamic exclusion was enabled to preclude re-selection of previously analyzed precursor ions, using the following parameters: repeat count 2, repeat duration 10 s, exclusion list size 500, exclusion duration 50 s, and exclusion width 20 ppm. LC-HRMS data were analyzed using Xcalibur software (version 2.0.7, Thermo Fisher Scientific).

Putative T3 Adducts

The list of precursor ions related to putative T3 adducts was generated by screening the MS/MS spectra acquired during the data dependent analysis. A set of seven singly charged *b*-series fragment ions was selected in the Ion Map view in the Xcalibur Qual Browser window. The mass tolerance for each fragment ion was set to ± 0.5 *m/z*. The list of precursor ions was exported to Excel and a VLOOKUP function was used to identify arrays of precursor ions, containing at least five singly charged *b*-series fragment ions out of a possible seven. These arrays were then filtered and arranged by retention times (RT). The monoisotopic masses of the corresponding 3^+-charged precursor ions were extracted from the Total Ion Chromatograms (TICs) within a 10-ppm mass accuracy by an in-house MatLab algorithm. Each extracted precursor ion was then manually extracted from the TICs to confirm or reject the presence of a putative T3 adduct.

Added masses of putative T3 adducts were calculated by subtracting the monoisotopic mass of unmodified T3 from the monoisotopic masses of modified T3 peptides and multiplied by three (only 3^+-charged peptides were screened). Elemental compositions of the unknown adducts were inferred from the measured accurate masses and searches of the UNIMOD protein-modifications database for mass spectrometry (www.unimod.org), the Molecular Weight Calculator algorithm (v. 6.48, created by Matthew Monroe in 2010) and the Elemental composition search algorithm built into the Xcalibur software (version 2.0.7, Thermo Fisher Scientific). The isotope distribution of the identified T3 adducts was simulated using Xcalibur and mass accuracy was calculated based on the theoretical monoisotopic masses of the isotope distribution after isotope simulation.

Results & Discussion

3D Structural Model of T3 the Peptide

Two different modeling methods, namely I-TASSER and PEP-FOLD, were used to predict the 3D structure of T3 from its amino acid sequence. I-TASSER takes a composite approach that involves multiple threading alignments from a library and iterative structural assemblies. PEP-FOLD includes a complete *de novo* solution, utilizing structural alphabets (e.g. helixes and strands) that are derived from iterative simulations based upon a hidden Markov model. Since predictions returned multiple models, models with the highest c-score from I-TASSER and with lowest energy from PEP-FOLD were selected (Figures 2A & 2B). The T3-peptide models from the two methods are strikingly similar, thus the predicted 3D structure is considered as a good representation of the T3 peptide in an aqueous environment. For simplicity, the rest of the discussion will focus on the I-TASSER model.

Given a peptide with only 21 amino acids and no elements for a disulfide bridge, the rich structural conformation of the T3 peptide was a surprise. Instead of a simple linear structure, the T3 peptide displays folds representing an alpha helix (ALVLIAFAQYLQQ), a 180-degree turn of the backbone around Cys34 and Pro35, and a random coil in the tail (FEDHVK). The predicted turn is suspected to be largely influenced by Pro35, because proline is the only amino acid that can adopt the necessary *cis*-amide bond formation for inducing such a turn. To test this, the T3 sequence was run without Pro35 (ALVLIAFAQYLQQCFEDHVK) in I-TASSER and PEP-FOLD, and best models were simple linear helical conformations.

Design of the Immunogen for Anti-T3 Antibody

The basic idea in semi-targeting enrichment is to make a polyclonal antibody that would cross-react with a wide range of unknown T3 adducts. To achieve such an antibody, it is necessary to minimize the role that Cys34 modifications might play in antigen recognition and offer binding only to the effective structural motifs (i.e. epitopes accessible by the antibody) that are conserved from the T3 peptide and shared with a high degree of similarity by all T3 adducts.

The first factor to consider is the length of the peptide immunogen. Since an epitope is typically comprised of 5 to 8 amino acids, after excluding Cys34, the antigenic sequence would have to be either the N-terminal peptide (ALVLIAFAQYLQQ) or the C-terminal peptide (PFEDHVK) or both. This is equivalent to making a choice between antibody specificity and affinity to T3 adducts. That is, the shorter immunogenic sequence (C-terminal peptide) would lead to a polyclonal antibody that is more specific to T3 adducts than that from the longer sequence (N-terminal peptide). However, more than 1 epitope can be found on a longer sequence and hence a higher affinity and avidity is expected.

Because the intended sample matrix is derived from human plasma, the specificity of the antibody in a plasma digest was explored by aligning either the N- or C- terminal sequence to the human proteome through the BLAST server. Tables 1 and 2 show those proteins found with a 100% identity match to the N-terminal peptide (29 hits) and the C-terminal peptide (32 hits). Other than HSA, only one match could be classified as a blood protein (Table 1, Angiomotin-like protein). Thus, taking the full T3 sequence (i.e. the N- plus C-terminal peptides) for the immunogen should not significantly affect the final purity of T3 adducts given the lack of overlapping T3 epitopes from other plasma proteins.

The second factor to consider in designing the antibody is adding terminal truncations or additions, which further optimizes the antibody specificity while preserving the affinity to T3 adducts. Interestingly, alignment results show that most of the overlapping sequence to N- and C-terminal peptides are away from the termini (Tables 1 and 2), suggesting that truncations to the full T3 sequence would offer little advantage. Terminal modifications to a peptide, such as acetylation and amidation, are commonly employed to remove terminal charges when preparing an immunogen. These modifications are unnecessary because the T3 adducts in the digest are naturally charged at the termini and the native charged termini are close to each other and could be part of a discontinuous epitope (epitope not made up with a linear primary sequence), a unique structural motif that would be shared only by the T3 related peptides (Figures 2C and 2D).

The last factor is the conjugation strategy. Typically, a Cys is tagged to either the N- or C- terminus to allow crosslinking to the carrier protein. However, because Cys34 is occupying a strategic locus and conjugation using the endogenous Cys provides two major benefits. First, without tagging an extra terminal Cys, the possibility to form a cyclic peptide is eliminated. Second, modifications at Cys34 have the potential to alter torsional angles in the T3 backbone due to a change in the energy state of the final adduct. The direct steric hindrance and indirect changes to structural motifs could significantly compromise the affinity of the anti-T3 antibody to T3 adducts. Unexpectedly, an immunogen with the greatest degree of mimicry to T3 adducts

is achieved by coupling the crosslinker to Cys34, which conserves all the effective orientation of structural motifs and partial hindrance caused by Cys adducts.

In summary of these design considerations, the full T3 sequence, without any terminal modification, was used as the immunogen.

Cross-Reactivity of the Anti-T3 Antibody to T3 Quinones

By estimating the cross-reactivity of the anti-T3 antibody towards some synthetic T3 adducts, it is possible to investigate the affinity characteristics of this antibody. To gauge the affinity of anti-T3 over a range of adduct sizes, four synthetic T3 adducts of quinones with increasing molecular weights (BQ=108.09 Da, NQ=158.15 Da, PQ=208.21 Da and EQ=284.35 Da) were tested. As expected, because of a lack of partial epitope blocking, none of these T3 adducts had a higher affinity to the anti-T3 antibody than the free T3 peptide (Figure 3). Using the T3 peptide as a reference, the following trend was observed in the order of binding strength: T3 > T3-BQ > T3-NQ > T3-EQ > T3-PQ. Thus, the greater the molecular weight of the modifying species, the lower the affinity of the resulting T3 adduct to anti-T3. The only exception to this rule was T3-EQ, which showed a higher affinity for anti-T3 than that of T3-PQ despite having a higher molecular weight. This could be due to a higher water solubility of EQ than PQ (0.57 g/l vs. 0.054 g/l). Because binding occurs in an aqueous medium, solvation would logically encourage the quinone of T3-EQ to move away from the peptide backbone while encouraging the quinone of T3-PQ to compress towards the peptide backbone, potentially blocking some epitopes. The order of affinities of T3-quinone adducts was also found to be consistent with the estimated dissociation constants (Kd; T3: 3.9871×10^{-7} M; T3-BQ: 3.9872×10^{-7} M; T3-NQ: 3.9876×10^{-7} M; T3-EQ: 3.9877×10^{-7} M; T3-PQ: 3.9880×10^{-7} M). These results indicate that the immunogen design was successful in the sense that anti-T3 captured a range of adducts with good affinity.

Immunomagnetic Enrichment with Sigma HSA

To assess the effects of various magnetic beads to the enrichment method, Sigma HSA was used with 2 treatments (3 and 24 μg anti-T3 antibody) and a control sample prepared by carrying a paired plasma sample through the procedure without the anti-T3 antibody. Preliminary studies showed that some non-T3 peptides were also detected in the anti-T3-enriched peptide mixture, probably due to non-specific binding of peptides to the magnetic beads. To facilitate comparisons and characterization of the purity of the anti-T3-enriched solution, the following discussion focuses on three other HSA peptides produced by tryptic digestion, namely T3, T4 (MPCAEDYLSVVLNQLCVLHEK) and a miscleaved T4 (RMPCAEDYLSVVLNQLCVLHEK). Since the majority (>95%) of T3 peptides has a free Cys34 after digestion (*14*), the level of this unadducted T3 peptide is used as a proxy for total T3 peptides, including T3 adducts. Because T4 and miscleaved T4 have very similar physiochemical properties to T3, there is always co-elution of T4/miss-cleaved T4 with T3 in LC (Figure 4). Thus, the level of T4s (sum of T4 and miss-cleaved T4) provides another useful indicator of purity.

In general, a decrease of concentrations of T4s and an increase of the T3 concentration and the T3:T4s ratio of the treatments over the controls is observed across all 4 kinds of beads (Table 3), suggesting the compatibility of using anti-T3-enrichment in the adductomics workflow. The slight increases of T4 concentrations in controls are probably due to an

enhanced non-specific binding on the bead surface (by not adding anti-T3 antibody and hence exposing a larger bead area). This may also explain why m270, the only unblocked bead (i.e. no BSA in the storage buffer), shows the highest level of T4s. To simplify purity comparison, the T3:T4s ratio is used as a summarizing metric, which can be interpreted as the higher the better. Clearly, the T1 magnetic bead had the best performance of the 4 tested types, with a value of T3:T4s that is two to three times those of the other bead types.

A few unexpected drops of T3:T4s were seen when comparing the 3 µg and 24 µg antibody treatments. After carefully inspecting spectra, these drops appear to reflect a noisier background with the 24 µg treatment and thus a lower signal to noise ratio. This suggests that there is an optimal set of concentrations of antigen, antibody and magnetic-bead substrate for maximizing signals of T3 adducts.

Immunomagnetic Enrichment (IME) with Human Plasma

Plasma samples obtained from three healthy volunteer subjects were tested using the IME-LC-HRMS platform. Controls and samples treated with 12 µg anti-T3 antibody were analyzed by LTQ Orbitrap HRMS. Data-dependent MS/MS spectra were screened to detect T3 and its related precursor ions. A set of seven singly charged *b series* fragment ions (b_3 − 284.19, b_4 − 397.28, b_5 −510.36, b_6− 581.40, b_{11} – 1203.42, b_{12} − 1331.77, and b_{13}− 1459.83 m/z) were chosen for the screening process to confirm that no other amino acid residue had been modified at positions prior to Cys34. As shown in Table 4, at least a 4-fold increase in T3:T4s was observed following IME across the three samples. A closer look at the T3 and T4s levels reveals that increases in T3:T4s are mainly driven by a decrease of concentrations of T4s in the treatment groups rather than an increase in T3 concentrations.

Putative T3 Adducts in Plasma Samples

The precursor ions found to be related to T3 peptide and detected in all control and IME treated samples were combined and manually extracted from the acquired TICs. Table 5 summarizes the list of T3 related precursor ions that were observed in all samples and represents the list of putative T3 adducts. The observed monoisotopic masses of the peptides are reported as means of the observed monoisotopic masses. The standard deviation was within 0.2 – 6 ppm for these masses. Three of the modifications at 848.09460 *m/z*, 851.42705 *m/z* and 858.75447 *m/z* found in IME treated samples were not detected in control samples. Overall, 14 and 17 (excluding the IAA-iT3) T3 related modifications were detected in control and IME treated samples, respectively.

To identify unknown modifications of T3 peptides, the monoisotopic masses of each peptide were identified from single-ion chromatograms (SICs) and the molecular masses of the putative adducts were calculated. Table 5 shows the list of putative T3 adducts with observed and theoretical monoisotopic *m/z* values of 3^+-charged peptides as well as retention times, calculated added masses and the elemental composition of each adduct. All but two of the modified T3 peptides were unambiguously identified within <3 ppm mass accuracy. The oxidation products of Cys34 were detected in all analyzed samples, namely a sulfinamide formed by an intramolecular reaction (+O, −H2, 816.41911 *m/z*) (*29*), the sulfinic acid (+O2, 822.42263 *m/z*) and the sulfonic acid (+O3, 827.75427 *m/z*). Modifications with single metal ions (Na, 21.97987 Da, K, 37.94070 Da and Fe, 53.90971 Da) or a combination of metal ions

(2Na, 43.95616 Da, (Na + K), 59.92251 Da) were detected in all samples. The 3^{+}-charged peptide (829.74991 *m/z*) with a retention time of 34 min was identified as a sodiated adduct of the sulfinic acid of Cys34.

Two modifications detected only in IME treated samples were unambiguously identified as cysteinylated Cys34 (851.42705 *m/z*) and its sodiated adduct (858.75447 m/z) within <1 ppm mass accuracy. Detection of Cys-Cys34 adducts might be due to incomplete reduction of disulfide bonds with TCEP or to disulfide scrambling during sample preparation (*30*, *31*).

Two putative T3 adducts were unable to identify with monoisotopic masses of 814.71186 m/z and 848.09460 m/z and with an average RT of 36.84 and 38.21 min, respectively.

Implications

The preliminary experiment with human plasma was carried out under the conditions that 1) there are still lots of free T3 in the plasma HSA digest and 2) the injected T3 concentrations of control and IME treatment to LC-MS are similar (assuming 1 mole of antibody captures 2 moles of antigens, with only 12 μg of capture antibody, the final T3 concentration in treatment will be only about 86% of that in control), the performance metrics are still good and there is even a slight increase in the concentration of individual adducts and the numbers of detected adducts. These improvements could be due to a cleaner matrix and hence lower ion suppression effect during the ionization process in MS.

The complexity to identify adducts manually is directly proportional to the sample size in a study. Ultimately, parameter-based bioinformatics method has to be developed to substitute the manually work. Since vast amount of unwanted peptides are removed with the immunomagnetic enrichment, the false positive identification rate of T3 adducts would be greatly reduced in any bioinformatics approaches.

Finally, the preliminary experiment was demonstrated at low anti-T3 antibody level. Hence, the sensitivity to the detect T3 adducts has ample room to scale up.

Summary

Because *targeted* enrichment methods that focus only on known peptide modifications cannot be successfully applied to *untargeted* adductomics, a semi-targeting assay was developed and tested with human plasma samples. A polyclonal anti-T3 antibody was designed for capturing Cys34 adducts in HSA. To minimize influence of modified Cys34 residues, epitopes were selected from sequences at both C- and N-termini based on the 3D structure of the T3 peptide. Immuno-enrichment of Cys34 adducts was simplified by attaching magnetic beads to the anti-T3 antibody. The IME method was applied to HSA samples from healthy human subjects and analyzed by LC-HRMS. Initial screening of the raw data showed more hits of T3 like peptides in IME-treated samples compared to control samples. Overall, 17 putative T3 adducts were detected and 15 were identified with < 4 ppm mass accuracy.

References

1. Liebler, D. C. (2008) Protein Damage by Reactive Electrophiles: Targets and Consequences, *Chem. Res. Toxicol. 21*, 117–128.
2. Brodie, B. B., Reid, W. D., Cho, A. K., Sipes, G., Krishna, G., and Gillette, J. R. (1971) Possible mechanism of liver necrosis caused by aromatic organic compounds, *Proc. Natl. Acad. Sci. U. S. A. 68*, 160–164.
3. Miller, E. C., and Miller, J. A. (1981) Searches for ultimate chemical carcinogens and their reactions with cellular macromolecules, *Cancer 47*, 2327–2345.
4. Nair, U., Bartsch, H., and Nair, J. (2007) Lipid peroxidation-induced DNA damage in cancer-prone inflammatory diseases: A review of published adduct types and levels in humans, *Free Radic. Biol. Med. 43*, 1109–1120.
5. Dipple, A., Khan, Q. A., Page, J. E., Pontén, I., and Szeliga, J. (1999) DNA reactions, mutagenic action and stealth properties of polycyclic aromatic hydrocarbon carcinogens (review), *Int. J. Oncol. 14*, 103–111.
6. Xue, W., and Warshawsky, D. (2005) Metabolic activation of polycyclic and heterocyclic aromatic hydrocarbons and DNA damage: A review, *Toxicol. Appl. Pharmacol. 206*, 73–93.
7. Rubino, F. M., Pitton, M., Di Fabio, D., and Colombi, A. (2009) Toward an "omic" physiopathology of reactive chemicals: thirty years of mass spectrometric study of the protein adducts with endogenous and xenobiotic compounds., *Mass Spectrom Rev 28*, 725–84.
8. Rappaport, S. M., Li, H., Grigoryan, H., Funk, W. E., and Williams, E. R. (2012) Adductomics: Characterizing exposures to reactive electrophiles, *Toxicol. Lett. 213*, 83–90.
9. Grigoryan, H., Li, H., Iavarone, A. T., Williams, E. R., and Rappaport, S. M. (2012) Cys34 adducts of reactive oxygen species in human serum albumin, *Chem. Res. Toxicol. 25*, 1633–1642.
10. Li, H., Grigoryan, H., Funk, W. E., Lu, S. S., Rose, S., Williams, E. R., and Rappaport, S. M. (2011) Profiling Cys34 adducts of human serum albumin by fixed-step selected reaction monitoring, *Mol. Cell. Proteomics Mcp 10*, M110.004606.
11. Hoos, J. S., Damsten, M. C., de Vlieger, J. S. B., Commandeur, J. N. M., Vermeulen, N. P. E., Niessen, W. M. A., Lingeman, H., and Irth, H. (2007) Automated detection of covalent adducts to human serum albumin by immunoaffinity chromatography, on-line solution phase digestion and liquid chromatography–mass spectrometry, *J. Chromatogr. B 859*, 147–156.
12. Aldini, G., Regazzoni, L., Orioli, M., Rimoldi, I., Facino, R. M., and Carini, M. (2008) A tandem MS precursor-ion scan approach to identify variable covalent modification of albumin Cys34: a new tool for studying vascular carbonylation, *J. Mass Spectrom. Jms 43*, 1470–1481.
13. Anderson, N. L., Anderson, N. G., Pearson, T. W., Borchers, C. H., Paulovich, A. G., Patterson, S. D., Gillette, M., Aebersold, R., and Carr, S. A. (2009) A human proteome detection and quantitation project, *Mol. Cell. Proteomics Mcp 8*, 883–886.
14. Funk, W. E., Li, H., Iavarone, A. T., Williams, E. R., Riby, J., and Rappaport, S. M. (2010) Enrichment of cysteinyl adducts of human serum albumin, *Anal. Biochem. 400*, 61–68.

15. Anderson, N. L., Anderson, N. G., Haines, L. R., Hardie, D. B., Olafson, R. W., and Pearson, T. W. (2004) Mass Spectrometric Quantitation of Peptides and Proteins Using Stable Isotope Standards and Capture by Anti-Peptide Antibodies (SISCAPA), *J. Proteome Res. 3*, 235–244.
16. Whiteaker, J. R., Zhao, L., Anderson, L., and Paulovich, A. G. (2010) An automated and multiplexed method for high throughput peptide immunoaffinity enrichment and multiple reaction monitoring mass spectrometry-based quantification of protein biomarkers, *Mol. Cell. Proteomics Mcp 9*, 184–196.
17. Whiteaker, J. R., Zhao, L., Zhang, H. Y., Feng, L.-C., Piening, B. D., Anderson, L., and Paulovich, A. G. (2007) Antibody-based enrichment of peptides on magnetic beads for mass-spectrometry-based quantification of serum biomarkers, *Anal. Biochem. 362*, 44–54.
18. Rush, J., Moritz, A., Lee, K. A., Guo, A., Goss, V. L., Spek, E. J., Zhang, H., Zha, X.-M., Polakiewicz, R. D., and Comb, M. J. (2005) Immunoaffinity profiling of tyrosine phosphorylation in cancer cells, *Nat. Biotechnol. 23*, 94–101.
19. Villén, J., and Gygi, S. P. (2008) The SCX/IMAC enrichment approach for global phosphorylation analysis by mass spectrometry, *Nat. Protoc. 3*, 1630–1638.
20. Larsen, M. R., Thingholm, T. E., Jensen, O. N., Roepstorff, P., and Jørgensen, T. J. D. (2005) Highly Selective Enrichment of Phosphorylated Peptides from Peptide Mixtures Using Titanium Dioxide Microcolumns, *Mol. Cell. Proteomics 4*, 873–886.
21. Li, H., Grigoryan, H., Funk, W. E., Lu, S. S., Rose, S., Williams, E. R., and Rappaport, S. M. (2011) Profiling Cys34 Adducts of Human Serum Albumin by Fixed-Step Selected Reaction Monitoring, *Mol. Cell. Proteomics Mcp 10*.
22. Grigoryan, H., Li, H., Iavarone, A. T., Williams, E. R., and Rappaport, S. M. (2012) Cys34 Adducts of Reactive Oxygen Species in Human Serum Albumin, *Chem. Res. Toxicol. 25*, 1633–1642.
23. Zhang, Y. (2008) I-TASSER server for protein 3D structure prediction, *BMC Bioinformatics 9*, 40.
24. Maupetit, J., Derreumaux, P., and Tuffery, P. (2009) PEP-FOLD: an online resource for de novo peptide structure prediction, *Nucleic Acids Res. 37*, W498–503.
25. Humphrey, W., Dalke, A., and Schulten, K. (1996) VMD: visual molecular dynamics, *J. Mol. Graph. 14*, 33–38, 27–28.
26. Altschul, S. F., Gish, W., Miller, W., Myers, E. W., and Lipman, D. J. (1990) Basic local alignment search tool, *J. Mol. Biol. 215*, 403–410.
27. Chung, M. K., Riby, J., Li, H., Iavarone, A. T., Williams, E. R., Zheng, Y., and Rappaport, S. M. (2010) A sandwich enzyme-linked immunosorbent assay for adducts of polycyclic aromatic hydrocarbons with human serum albumin, *Anal. Biochem.*
28. Friguet, B., Chaffotte, A. F., Djavadi-Ohaniance, L., and Goldberg, M. E. (1985) Measurements of the true affinity constant in solution of antigen-antibody complexes by enzyme-linked immunosorbent assay, *J. Immunol. Methods 77*, 305–319.
29. Grigoryan, H., Li, H., Iavarone, A. T., Williams, E. R., and Rappaport, S. M. (2012) Cys34 adducts of reactive oxygen species in human serum albumin, *Chem. Res. Toxicol. 25*, 1633–1642.
30. Wang, Z., Rejtar, T., Zhou, Z. S., and Karger, B. L. (2010) Desulfurization of cysteine-containing peptides resulting from sample preparation for protein characterization by mass spectrometry, *Rapid Commun. Mass Spectrom. Rcm 24*, 267–275.

31. Liu, H., Gaza-Bulseco, G., Chumsae, C., and Newby-Kew, A. (2007) Characterization of lower molecular weight artifact bands of recombinant monoclonal IgG1 antibodies on non-reducing SDS-PAGE, *Biotechnol. Lett. 29*, 1611–1622.

Tables

Table 1. Summary of the BLAST result. Search was carried out with input sequence ALVLIAFAQYLQQ against human reference protein database. Only those with 100% identity match are shown.

No.	Description	Kind of Protein	Matching Seq.
1	Serum albumin preproprotein	Blood protein	**ALVLIAFAQYLQQ**
2	Ceramide glucosyltransferase	Cell protein	**LIAFAQY**
3	Macrosialin isoform B precursor	Transmembrane glycoprotein in monocytes and tissue macrophages	**ALVLIAF**
4	Macrosialin isoform A precursor	Transmembrane glycoprotein in monocytes and tissue macrophages	**ALVLIAF**
5	Forkhead box protein B1	Cell protein	**AQYLQQ**
6	Protein misato homolog 1 isoform c	Cell protein	**AQYLQQ**
7	Protein misato homolog 1 isoform b	Cell protein	**AQYLQQ**
8	Protein misato homolog 1 isoform a	Cell protein	**AQYLQQ**
9	Polyhomeotic-like protein 2 isoform a	Cell protein	**AQYLQQ**
10	Polyhomeotic-like protein 3	Cell protein	**AQYLQQ**
11	Tetratricopeptide repeat protein 23-like	Structural motif for cell proteins	**QYLQQ**
12	Ubiquitin carboxyl-terminal hydrolase 14 isoform b	Cell protein	**QYLQQ**
13	tRNA guanosine-2'-O-methyltransferase TRM13 homolog	Cell protein	**QYLQQ**
14	Ubiquitin carboxyl-terminal hydrolase 14 isoform a	Cell protein	**QYLQQ**
15	Angiomotin-like protein 2	*Blood protein*	**QYLQQ**
16	BRCA1-associated ATM activator 1	Cell protein	**QYLQQ**
17	Gamma-tubulin complex component 2 isoform 2	Cell protein	**QYLQQ**
18	Gamma-tubulin complex component 2 isoform 1	Cell protein	**QYLQQ**
19	Exportin-T	Cell protein	**QYLQQ**
20	Kv channel-interacting protein 4 isoform 5	Cell protein	**FAQYL**
21	Sister chromatid cohesion protein PDS5 homolog a isoform 3	Cell protein	**FAQYL**
22	Sister chromatid cohesion protein PDS5 homolog a isoform 1	Cell protein	**FAQYL**
23	F-actin-capping protein subunit alpha-1	Cell protein	**AFAQY**
24	Coiled-coil domain-containing protein 166	Not annotated	**AQYLQ**
25	Zinc finger protein 561	Cell protein	**AFAQY**
26	Potassium voltage-gated channel subfamily A member 2 isoform a	Cell protein	**AQYLQ**
27	Signal peptide peptidase-like 3	Cell protein	**LVLI**
28	Iduronate 2-sulfatase isoform a precursor	Cell protein	**AFAQ**
29	Mucolipin-3 isoform 1	Cell protein	**YL**

Table 2. Summary of the BLAST result. Search was carried out with input sequence PFEDHVK against human reference protein database. Only those with 100% identity match are shown.

No.	Description	Kind	Matching Seq.
1	Serum albumin preproprotein	Blood protein	**PFEDHVK**
2	Phosphatidylinositol 3,4,5-trisphosphate 3-phosphatase and dual-specificity protein phosphatase PTEN	Cell protein	**PFEDH**
3	Calcium-binding and coiled-coil domain-containing protein 2 isoform 5	Cell protein	**FEDHV**
4	Calcium-binding and coiled-coil domain-containing protein 2 isoform 4	Cell protein	**FEDHV**
5	Calcium-binding and coiled-coil domain-containing protein 2 isoform 3	Cell protein	**FEDHV**
6	Calcium-binding and coiled-coil domain-containing protein 2 isoform 2	Cell protein	**FEDHV**
7	Calcium-binding and coiled-coil domain-containing protein 2 isoform 1	Cell protein	**FEDHV**
8	Coiled-coil domain-containing protein 3 precursor	Cell protein components	**EDHVK**
9	Solute carrier family 12 member 1 isoform F	Cell membrane protein	**EDHVK**
10	Solute carrier family 12 member 1 isoform A	Cell membrane protein	**EDHVK**
11	Solute carrier family 12 member 2 isoform 2	Cell membrane protein	**EDHVK**
12	Solute carrier family 12 member 2 isoform 1	Cell membrane protein	**EDHVK**
13	Suppressor APC domain-containing protein 1	Not annotated	**FEDH**
14	Psychosine receptor	Transmembrane protein	**FEDH**
15	F-box/WD repeat-containing protein 12 isoform 2	Cell protein	**FEDH**
16	TBC1 domain family member 13	Cell protein	**FEDH**
17	Epidermal growth factor receptor isoform c precursor	Transmembrane glycoprotein	**FEDH**
18	Zinc finger CCCH domain-containing protein 10	Structural motif for cell proteins	**FEDH**
19	F-box/WD repeat-containing protein 12 isoform 3	Cell protein	**FEDH**
20	Wd repeat-containing protein 41	Structural motif for cell proteins	**FEDH**
21	F-box/wd repeat-containing protein 12 isoform 1	Cell protein	**FEDH**
22	Glioma tumor suppressor candidate region gene 2 protein	Cell protein	**FEDH**
23	Armadillo repeat-containing x-linked protein 5	Repeating sequence for proteins	**FEDH**
24	Epidermal growth factor receptor isoform b precursor	Transmembrane glycoprotein	**FEDH**
25	Ras-associated and pleckstrin homology domains-containing protein 1 isoform 3	Cell protein	**FEDH**
26	Amyloid beta A4 precursor protein-binding family B member 1-interacting protein	Transmembrane glycoprotein	**FEDH**
27	Epidermal growth factor receptor isoform d precursor	Transmembrane glycoprotein	**FEDH**
28	Cysteine--tRNA ligase, cytoplasmic isoform a	Cell protein	**FEDH**
29	Cysteine--tRNA ligase, cytoplasmic isoform b	Cell protein	**FEDH**
30	Cysteine--tRNA ligase, cytoplasmic isoform e	Cell protein	**FEDH**
31	Cysteine--tRNA ligase, cytoplasmic isoform c	Cell protein	**FEDH**
32	Protein Shroom1 isoform 2	Cell protein	**FEDH**

Table 3. Sample purity metrics for 4 different kinds of magnetic beads obtained using Sigma HSA.

Bead Type	M270				M280			
	Controls[d]		Treatments		Controls[d]		Treatments	
Amount of Anti-T3 antibody (μg)	3[d]	24[d]	3	24	3[d]	24[d]	3	24
A: T4s (pmol/μl)[a]	0.26	0.14	0.03	0.02	0.11	0.11	0.05	0.13
B: T3 (pmol/μl)[b]	0.01	0.01	0.37	0.21	0.01	0.04	0.82	1.42
C: T3:T4s[c]	0.06	0.05	11.5	13.4	0.09	0.32	16.1	11.2

Bead Type	C1				T1			
	Controls[d]		Treatments		Controls[d]		Treatments	
Amount of Anti-T3 antibody (μg)	3[d]	24[d]	3	24	3[d]	24[d]	3	24
A: T4s (pmol/μl)[a]	0.11	0.11	0.03	0.03	0.08	0.04	0.02	0.02
B: T3 (pmol/μl)[b]	0.01	0.01	0.46	0.18	0.01	0.01	0.52	0.82
C: T3:T4s[c]	0.08	0.06	15.1	7.06	0.08	0.30	30.4	41.2

[a] T4s are unwanted co-eluating peptides. Lower value represents better performance.

[b] T3 is used as a proxy to T3 adducts. Higher value represents better performance.

[c] Higher value represents better performance.

[d] Controls were plasma samples prepared without addition of anti-T3 antibody but using the corresponding amount of magnetic beads.

Table 4. Sample purity metrics and counts of T3 peptides using plasma samples collected from 3 healthy volunteers.

	Plasma 1		Plasma 2		Plasma 3	
	Control[d]	Treatment	Control[d]	Treatment	Control[d]	Treatment
A: T4s (pmol/μl)[a]	1.26	0.32	1.11	0.25	1.02	0.18
B: T3 (pmol/μl)[b]	0.65	0.69	0.54	0.77	0.56	0.53
C: T3:T4s[c]	0.51	2.17	0.49	3.13	0.55	2.99

[a] T4s are unwanted co-eluating peptides. Lower value represents better performance.

[b] T3 is used as a proxy to T3 adducts. Higher value represents better performance.

[c] Higher value represents better performance.

[d] Controls are HSA digests that were not treated with anti-T3.

Table 5. The list of T3 putative adducts detected in the control and IME treated human plasma samples.

Observed Monoisotopic Mass[a] (+3, m/z)	Plasma A, RT		Plasma B, RT		Plasma C, RT		Calculated Adduct Mass	Theoretically calculated monoisotopic mass (+3, m/z)[c]	Mass accuracy in ppm[b]	T3 Putative Adducts
	Control	IME treated	Control	IME treated	Control	IME treated				
769.06267	38.52	38.48	38.53	38.49	38.51	38.47	-128.09629	769.06102	2.15	Loss of Lys AA from C terminus
805.75770	36.44	36.36	36.35	36.4	36.45	36.35	-18.01148	805.75583	2.32	Loss H_2O molecule
811.76139	36.29	36.23	36.27	36.22	36.21	36.24	0.00000	811.75933	2.53	T3
814.71186	36.89	36.79	36.86	36.78	36.85	36.86	8.84862			*unknown*
816.41934	34.17	34.1	34.18	34.19	34.21	34.16	13.97243	816.41911	0.28	O, $-H_2$
819.08660	36.26	36.25	36.27	36.22	36.21	36.21	21.97987	819.08667	-0.09	Na
822.42294	34.15	34.16	34.18	34.19	34.14	34.19	31.98313	822.42263	0.38	O_2
824.40864	36.26	36.25	36.3	36.22	36.21	36.21	37.94070	824.41132	-3.25	K
826.41353	36.26	36.38	36.35	36.22	36.21	36.19	43.95616	826.41399	-0.56	2Na
827.75469	34.42	34.39	34.42	34.36	34.35	34.39	47.97889	827.75427	0.50	O_3
829.73125	36.29	36.23	36.3	36.2	36.21	36.21	53.90971	829.73245	-1.45	Fe
829.74991	34.11	34.13	34.14	34.19	34.1	34.19	53.96443	829.74995	-0.05	O_2, Na
831.73576	36.29	36.33	36.19	36.22	36.37	36.19	59.92251	831.73863	-3.45	Na, K
834.77660	34.62	34.62	34.65	34.62	34.64	34.62	57.02424	834.77568	1.10	IS
848.09460		38.21		38.21		38.2	108.99412			*unknown*
851.42705		33.16		33.19		33.21	118.99147	851.42739	-0.40	$C_3H_5NO_2S_1$
858.75447		33.16		33.19		33.19	140.97374	858.75470	-0.27	$C_3H_5NO_2S_1$, Na
863.79283	34.76	34.78	34.77	34.81	34.78	34.79	156.09514	863.79306	-0.26	Arg transpeptidation from C terminus

[a] Average of observed monoisotopic masses in each analyzed sample (standard deviation was in within 0.2 -6ppm).
[b] Mass accuracies of T3 putative adducts were calculated based on theoretical monoisotopic masses of triply charged peptides calculated from isotope distribution simulation algorithm using the defined empirical formulas.
[c] Theoretical monoisotopic masses of triply charged peptides were calculated from the isotope distribution simulation algorithm using the defined empirical formulas.

Figures

Figure 1. An overview of the study. A) To produce a semi-targeting anti-T3-adducts antibody, the immunogen was designed based on the predicted 3D structure of the T3 peptide. The affinity and cross reactivity of anti-T3 antibody were tested and confirmed by ELISAs with 4 different T3 quinone adducts. B) Using commercial human serum albumin (HSA) and the antibody produced, the immunomagnetic enrichment method was optimized and was tested with 4 different kinds of magnetic beads using different purity metrics. C) The best configuration of the enrichment step was incorporated into the LC-MS platform and the compatibility of this platform with an adductomic study was validated using human plasma samples. The workflow started with isolation of HSA from plasma using ammonium sulfate precipitation and then removal of free-Cys34 HSA by incubating with thiol affinity Sepharose resin. The supernatant was collected and digested with trypsin and then enrichment for T3 and T3 adducts using the anti-T3 antibody. The T3-adduct-enriched sample was characterized by LC-MS and the adducts were extracted.

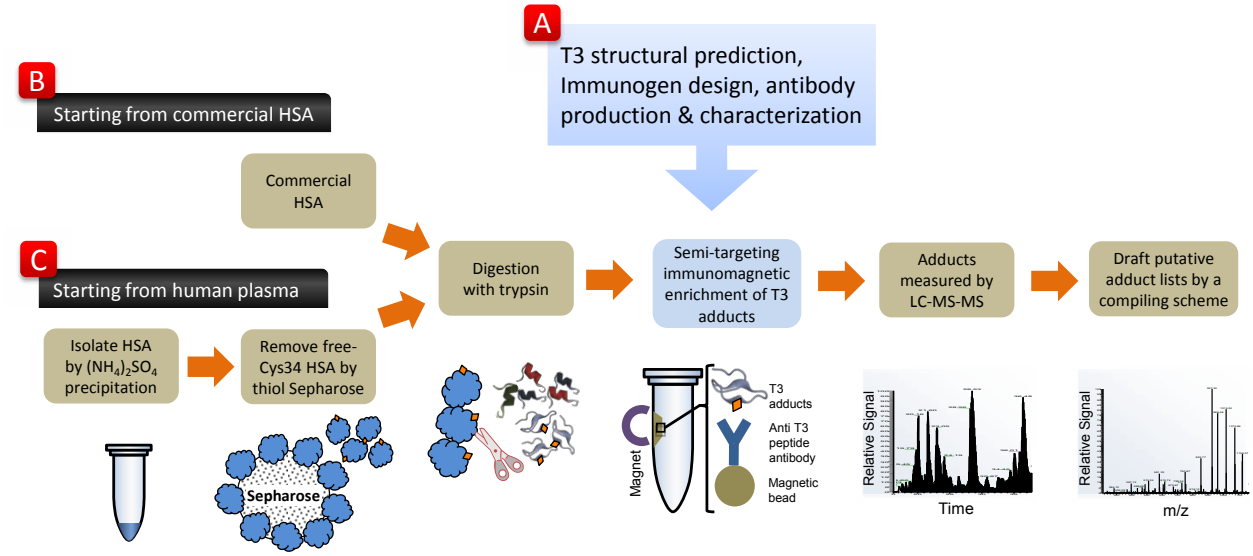

Figure 2. The predicted 3D structures of the T3 peptide (ALVLIAFAQYLQQCPFEDHVK). A) Model predicted by I-TASSER, Cys34 is shown in yellow. B) Model predicted by PEP-FOLD, Cys34 is shown in yellow. There is a high degree of similarity of the 3D structure estimated by the 2 methods, including a bend of backbone around Cys34 and the alpha helix found between Cys34 and the N-terminus. C) A elaborated I-TASSER model. Cys34 is represented by "Licorice style" and the sulfhydryl group is shown in yellow and white. The isosurface is created from the volumetric density map in VMD. It is observed the sulfhydryl group is pointing outward around the bend, suggesting the structural stress caused by the modification on Cys34 is minimal. Also, the close proximity between the alpha helix and the random coil might allow for the formation of discontinuous epitopes. D) Side view of the elaborated I-TASSER model.

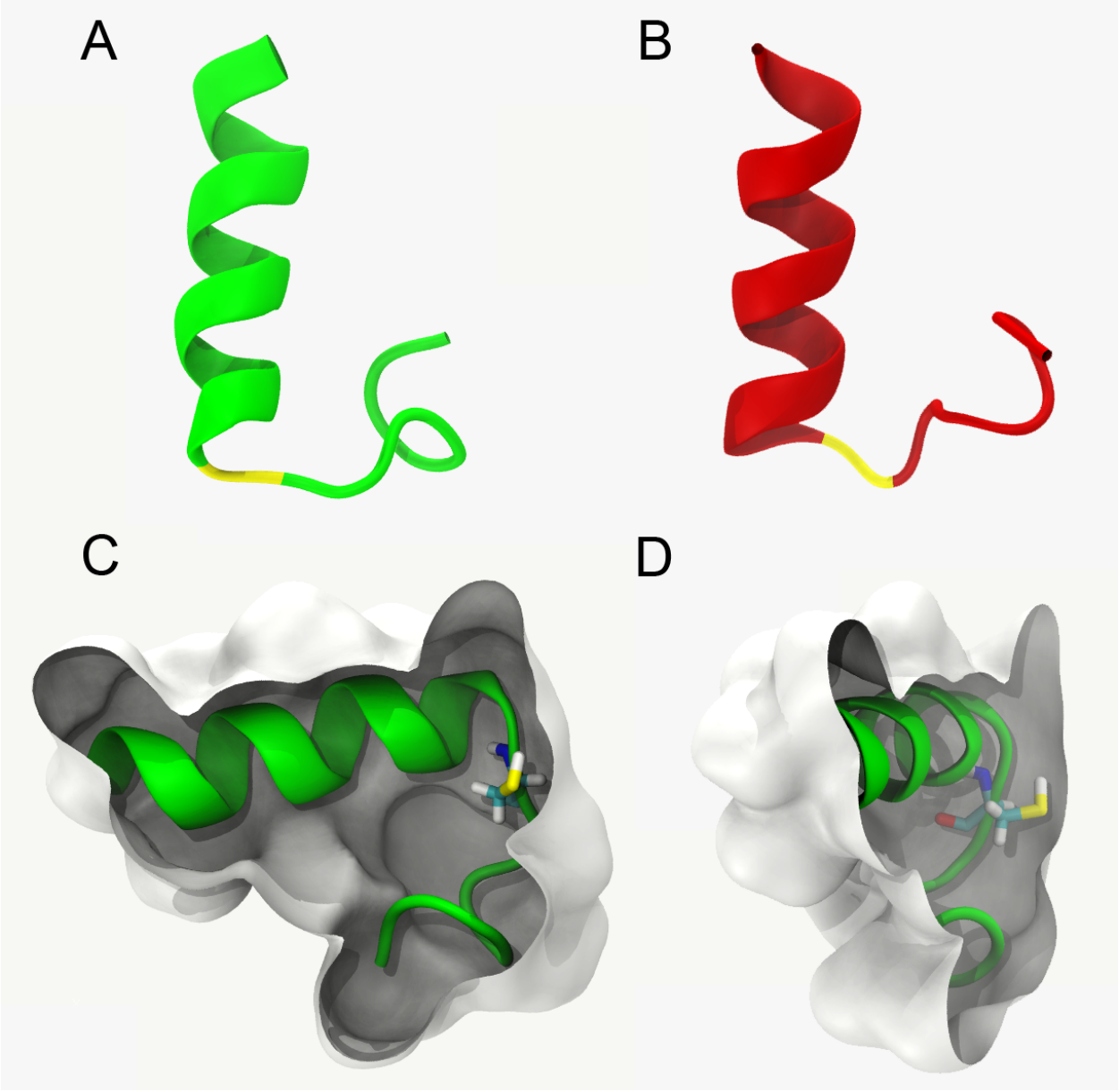

Figure 3. Plot of the reactivities between the anti-T3 antibody and various antigens. The reactivity to the unmodifiedT3 peptide was the greatest (●). Reactivity decreased in the order: T3-BQ (■) > T3-NQ (▲)> T3-EQ (⤫) > T3-PQ (▼). This order of reactivity is inversely related to the masses of the adducting species except for the pair T3-EQs (EQ: 284.35 Da) and T3-PQs (PQ: 208.21 Da), where the aqueous solubility may have played a role (EQ: 0.57 g/l; PQ: 0.054 g/l). Methanol and 30% acetonitrile were solvent controls.

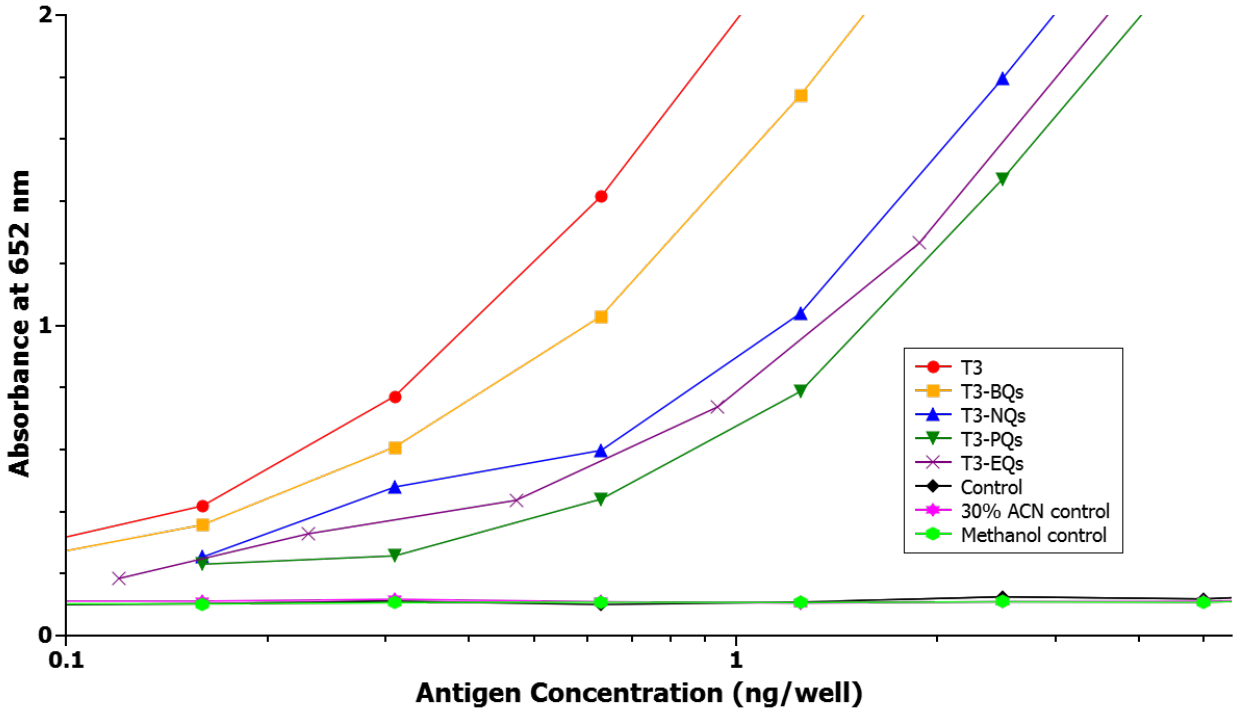

Figure 4. Total ion chromatograms (TICs) of a plasma sample. A) TIC from the control sample. B) TIC from the 12 μg anti-T3 treatment. The inset windows show the corresponding selected extracted ion chromatograms (EICs) of T3 (m/z: 811.7593), T4 (m/z: 802.0618) and the miscleaved T4 peptides (m/z: 854.0955). The retention time (RT) and the integrated area (AA) for each EIC is shown. The TICs demonstrate that immunomagnetic enrichment of T3 adducts removed most of the unwanted HSA peptides eluting before 35 min. In (B), the most intense peak is T3 while a significant drop of co-eluting T4 and miscleaved T4 are observed.

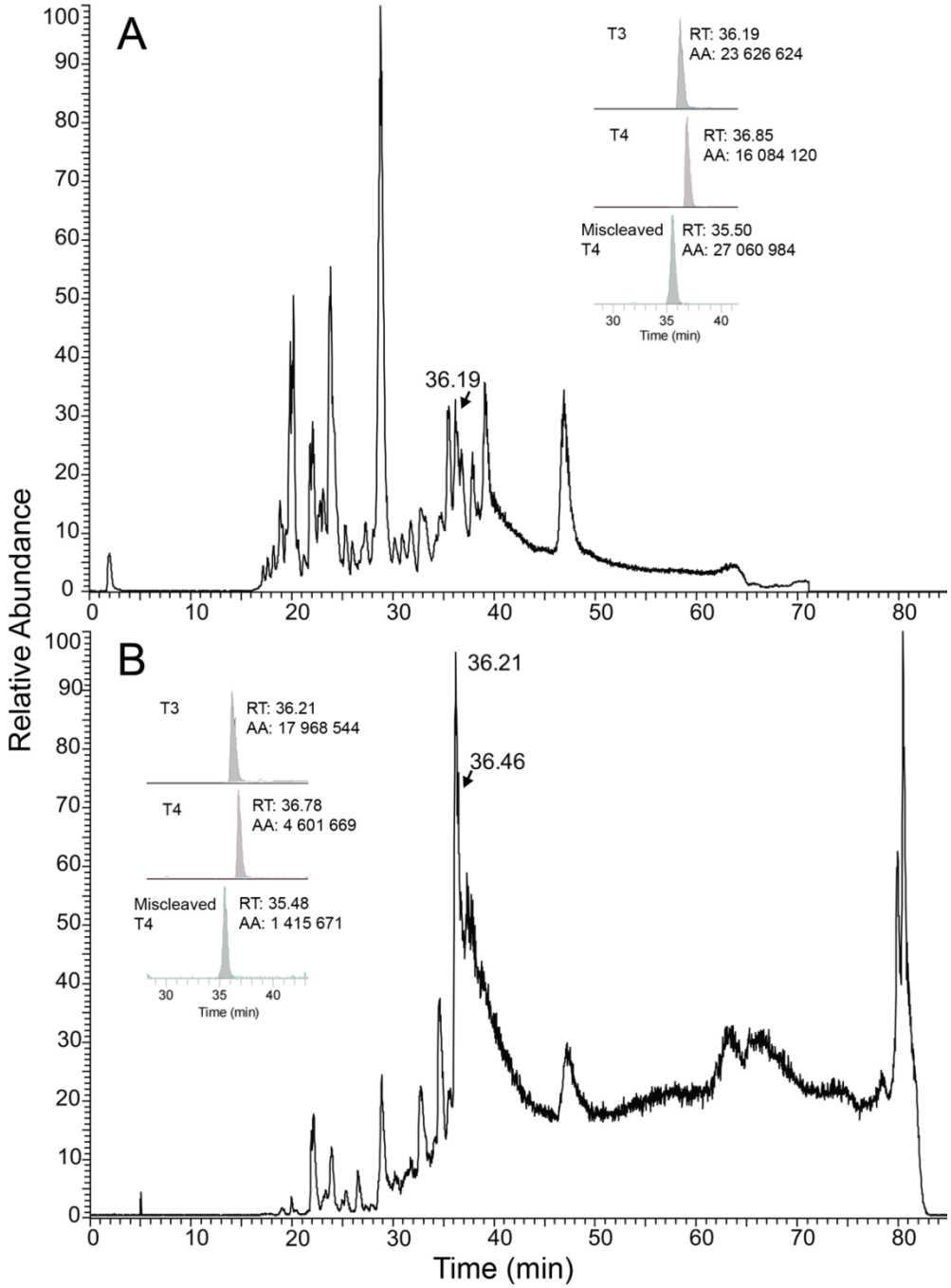

Chapter 5

Summary and Conclusions

Summary

Aromatic hydrocarbons are ubiquitous pollutants, exposures to which are commonly monitored for health surveillance and epidemiologic studies. The mutagenicity of an important PAH, benzo[*a*]pyrene (BaP), results in the formation of (+)-anti-benzo[a]pyrene-7,8-diol-9,10-epoxide (BPDE-I) adduct (BPDE-albumin), which also binds to HSA. Thus BPDE-HSA adducts possess desirable properties as biomarkers of exposure (details discussed in chapter 1). A competitive ELISA has been used for more than 20 years to measure BPDE-HSA adducts. This assay has marginal sensitivity for applications involving populations with ambient PAH exposures and also involves tedious preparation steps that inflate the assay error. In chapter 2, a sandwich ELISA is described that overcomes the disadvantages of the competitive ELISA for measuring BPDE-HSA adducts isolated from serum or plasma. The sandwich design is much simpler and has about 10-fold greater sensitivity than the competitive ELISA (1 vs. 10 ng BPDE-HSA/mg HSA). This sandwich ELISA was validated with HSA from populations with high PAH exposures (steel-factory workers) and is appropriate for use in assessing BPDE-HSA levels in heavily exposed subjects.

In chapter 3, the sandwich ELISA described in chapter 2 was improved to further increase sensitivity about 5-fold (to 0.2 ng BPDE-HSA/mg HSA) and can be used directly with serum or plasma, thereby eliminating the need for prior isolation of HSA. The improved sandwich ELISA was validated with plasma from smoking subjects and from highway workers exposed to PAHs outdoors. Results indicated that BPDE-HSA levels were significantly associated with smoking intensity. Regarding the highway workers, levels of BPDE-HSA were higher during the winter season when, paradoxically, these subjects were not working and thus were exposed to PAHs primarily indoors. The same conclusion had been drawn from the original study that provided the samples, using PAH-DNA adducts as a biomarker (*1*). Our results also confirmed those from the earlier study, which used urinary 1-hydroxypyrene as the endpoint to characterize PAH exposures (*2*), namely, that the PAH exposures in the highway workers increased in the order: construction worker < paver operator < raker < screedman.

The ELISAs developed in chapters 2 and 3 can detect only a single analyte, namely BPDE-HSA. To assess exposures to multiple HSA adducts, instrumental platforms such as LC-MS can be used. The major benefits of MS analyses are unambiguous identification of analytes and exceptional sensitivity, which can be 100 times better than ELISA. Samples are first fractionated by LC and then ionized to permit mass resolution and detection (MS actually measures the mass-to-charge rather than the mass). Since ionization is a competitive process, abundant non-target molecules suppress the co-eluting target analytes thereby reducing the sensitivity of detection. The method described in chapter 4 reduces this hurdle by customizing a semi-targeting antibody for enriching HSA-Cys34 adducts (i.e. adducts bound to the sulfhydryl group of Cys34), which following tryptic digestion, exist on the T3 peptide as

ALVLIAFAQYLQQC$^{\Sigma R}$PFEDHVK. In essence, the semi-targeting antibody works by recognizing the shared epitopes of the T3 adducts. The cross-reactivity of the antibody was tested with four synthetic adducts of benzoquinone (BQ), naphthoquinone (NQ), phenanthrenequinone (PQ) and estrogen quinone (EQ) (molecular masses in the oxidized form are: BQ: 108.09 Da; NQ: 158.15 Da; PQ: 208.21 Da; EQ: 284.35 Da). The results showed that the antibody was able to bind these adducts with high and similar affinity values (Kd: T3-BQs: 3.9872×10^{-7} M; T3-NQs: 3.9876×10^{-7} M; T3-EQs: 3.9877×10^{-7} M; T3-PQs: 3.9880×10^{-7} M). Then, the antibody was applied as the core component of an immunomagnetic enrichment step that preceded application of LC-MS. Results from the tests with three plasma samples from volunteer subjects demonstrated that the concentrations of co-eluting peptides were significantly lower than those of the T3 peptide and its adducts. Thus, it was concluded that the sensitivity of the LC-MS platform to detect T3 adducts can be increased by incorporating the newly developed antibody-enrichment step.

Benefits

The new sandwich ELISA has many advantageous over the competitive version. First, the precision is higher. This gain is mainly due to the absence of the lengthy sample preparation steps, which include isolation, purification and release of stable analytes from the adducts. Second, sensitivity of the new assay is about 50 times greater than the competitive ELISA due to use of the latest colorimetric signaling technology. Third, although both sandwich and competitive ELISA employ a monoclonal antibody, 8E11, to capture BPDE-albumin, the specificity is higher in the sandwich design because an extra HSA-detection antibody is used. Compounds cross-reactive to 8E11 [particularly those with four or more rings and structurally similar to BaP (*3*)] are more likely to produce a signal in competitive ELISA, leading to an overestimation of BaP exposure. Fourth, the new assay takes less time to complete because of the simplified sample preparation steps (basically involving only centrifugation and addition of reagents). Also, it is easier to interpret the ELISA signal because it is directly proportional to the concentration of analytes, as opposed to being inversely proportional to concentration in competitive ELISA. Fifth, the cost per assay is lower, owing to the nearly 5-fold reduction of reagent volumes. Finally, the assay employs a paired measurement design (i.e. each measurement has an internal reference) and a sample-specific calibration method. Thus, the accuracy of the measurement is increased by removing the biasing signal caused by the interferences in the plasma matrix. When applying the assay in epidemiological studies, these advantages can be translated into increased power to detect exposure-related effects because of the higher sensitivity (lower the number of non-detected samples), increased accuracy and precision, and higher sample size at a given cost and personnel effort. .

The incorporation of the immunomagnetic enrichment step to the LC-MS analysis provides other advantages. First, the sensitivity to detect target analytes is increased by lowering the ion-suppression effects. Since the enrichment gives a cleaner matrix for measurement, a reduction in false positive identification rate can also be expected. Finally, traditional immuno-enrichment approaches use a single antibody to capture a specific analyte (*4*). With a semi-targeting antibody, the cost of antibodies per target can be greatly reduced.

Also, the immuno-enrichment approach is compatible with omic applications, where untargeted analysis of adduct populations (i.e. adductomics) is desired.

Further Improvements

A simple comparison on the adduct detection rate can be used to gauge the performance of the new assay. The detection rate of BPDE-HSA using competitive ELISA (as a sum of tetrols equivalent) in a general population was found to be 63% (*5*). In contrast, the average detection rate from the new assay was found to be 72%, using the controls described in chapter 3. Although the sandwich ELISA is ~50 times more sensitive to the competitive ELISA, the detection rate suggests that there is still room for improvement. For example, fluorescent detection can be used to replace the optical system used in the current assay, and the avidin–biotinylated enzyme amplification system can be replaced with a tyramide-signal amplification system, which could increase sensitivity by another 100 fold (*6*).

A sandwich ELISA that incorporates an adduct-specific capture antibody can be applied to advanced platforms for automation. For example, a lab-on-a-chip microfluidic device with automated loading and mixing of reagents would vastly increase the throughput of ELISA for HSA adducts.

Using the semi-targeting enrichment method developed in chapter 4, the immunomagnetic bead was used only once and then discarded. It is well-known that an immobilized antibody on a solid substrate can be reused several times without any degradation in performance. Thus, reuse of antibodies should be explored as a means to further reduce costs.

The magnetic beads have the characteristics of ease of handling and low non-specific binding. However, the antibody binding capacity is only about $1/20^{th}$ of that of agarose beads which are porous. Use of agarose beads, therefore, should be explored for further refinement of the method.

The Kd values of four structurally different AH quinone adducts were found to be very similar (see chapter 4). This suggests that differential binding to the semi-targeting antibody should trap T3 adducts with roughly equal strength and is, therefore, unlikely to bias adductomic features in untargeted applications. This idea should also be explored.

It is important to add that the methodological improvements on ELISA and LC-MS are not specific to the tested analytes described in chapters 2-4. For example, the sandwich ELISA can be modified and extended to detect other HSA adducts associated with different chemical exposures, such as formaldehyde (*7*), aflatoxin (*8*), mycotoxins (*9*), and other PAHs as long as a capture antibody is available. Likewise, when another protein locus of biological and environmental significance is considered, an equivalent semi-targeting antibody could be produced using the immunogen design principles described in chapter 4.

References

1. McClean, M. D., Wiencke, J. K., Kelsey, K. T., Varkonyi, A., Ngo, L., Eisen, E. A., and Herrick, R. F. (2007) DNA adducts among asphalt paving workers, *Ann. Occup. Hyg. 51*, 27–34.
2. McClean, M. D., Rinehart, R. D., Ngo, L., Eisen, E. A., Kelsey, K. T., Wiencke, J. K., and Herrick, R. F. (2004) Urinary 1-hydroxypyrene and polycyclic aromatic hydrocarbon exposure among asphalt paving workers, *Ann. Occup. Hyg. 48*, 565–578.
3. Lee, B. M., Yin, B. Y., Herbert, R., Hemminki, K., Perera, F. P., and Santella, R. M. (1991) Immunologic measurement of polycyclic aromatic hydrocarbon-albumin adducts in foundry workers and roofers, *Scand. J. Work. Environ. Health 17*, 190–194.
4. Anderson, N. L., Anderson, N. G., Haines, L. R., Hardie, D. B., Olafson, R. W., and Pearson, T. W. (2004) Mass Spectrometric Quantitation of Peptides and Proteins Using Stable Isotope Standards and Capture by Anti-Peptide Antibodies (SISCAPA), *J. Proteome Res. 3*, 235–244.
5. Wu, H. C., Wang, Q., Wang, L. W., Yang, H. I., Ahsan, H., Tsai, W. Y., Wang, L. Y., Chen, S. Y., Chen, C. J., and Santella, R. M. (2007) Polycyclic aromatic hydrocarbon- and aflatoxin-albumin adducts, hepatitis B virus infection and hepatocellular carcinoma in Taiwan, *Cancer Lett. 252*, 104–114.
6. Speel, E. J., Hopman, A. H., and Komminoth, P. (1999) Amplification methods to increase the sensitivity of in situ hybridization: play card(s), *J. Histochem. Cytochem. Off. J. Histochem. Soc. 47*, 281–288.
7. Li, H., Wang, J., König, R., Ansari, G. A. S., and Khan, M. F. (2007) Formaldehyde-protein conjugate-specific antibodies in rats exposed to formaldehyde, *J. Toxicol. Environ. Health A 70*, 1071–1075.
8. Wu, H. C., Wang, Q., Yang, H. I., Ahsan, H., Tsai, W. Y., Wang, L. Y., Chen, S. Y., Chen, C. J., and Santella, R. M. (2009) Aflatoxin B1 exposure, hepatitis B virus infection, and hepatocellular carcinoma in Taiwan, *Cancer Epidemiol. Biomarkers Prev. Publ. Am. Assoc. Cancer Res. Cosponsored Am. Soc. Prev. Oncol. 18*, 846–853.
9. Hooper, D. G., Bolton, V. E., Guilford, F. T., and Straus, D. C. (2009) Mycotoxin detection in human samples from patients exposed to environmental molds, *Int. J. Mol. Sci. 10*, 1465–1475.